TBM Performance Study: Influence of the Rock Properties on the Failure Occurrence

by

Edward Khokhlovich

Submitted to the Department of Civil and Environmental Engineering in partial fulfillment of the requirements for the degree of

Master of Science in Civil and Environmental Engineering

at the

MASSACHUSETTS INSTITUTE OF TECHNOLOGY

May 9, 1997

Author .....
Department of Civil and Environmental Engineering
Submitted on May 9, 1997

Certified by .....
Herbert Einstein
Professor of Civil and Environmental Engineering
Thesis Supervisor

Certified by .....
Daniel Veneziano
Professor of Civil and Environmental Engineering
Thesis Co-Supervisor

Accepted by .....
Joseph M. Sussman
Chairman,
Departmental Committee on Graduate Studies

TBM Performance Study: Influence of the Rock Properties on the Failure Occurrence

by

Edward Khokhlovich

Submitted to the Department of Civil and Environmental Engineering on May 9, 1997, in partial fulfillment of the requirements for the degree of Master of Science in Civil and Environmental Engineering

Abstract

Tunnel Boring Machine (TBM) performance depends on a number of factors. The TBM can be viewed as a complex mechanical system. Each component of the system may be critical i.e., the component failure causes the system failure. The research reported here investigates influence of rock properties on the failure occurrence, and attempts to derive quantitative characteristics of that influence. Another problem addressed in this study is the likelihood of the failure occurrence in different geologic conditions. The research is based on the data collected during the construction of the 9.5-mile Outfall Tunnel, which is part of the Boston Harbor Project.

Thesis Supervisor: Herbert Einstein
Title: Professor of Civil and Environmental Engineering

Thesis Supervisor: Daniel Veneziano
Title: Professor of Civil and Environmental Engineering

Table of Contents

List of Figures

List of Tables

Chapter 1

Introduction

1.1 Purpose and Scope

Tunneling is subject to a variety of uncertainties. Driving a long tunnel with a Tunnel Boring Machine (TBM) produces an even greater variety of things that "might go wrong". The main player in this game is geology. Before construction, the geologic conditions on the tunnel level are unknown. Even during construction, the parameters affecting excavation are only known to a limited extent. On the other hand, the Tunnel Boring Machine, a man-made product, is subject to failures related or unrelated to ground conditions. By definition, failure is an event whose occurrence results in the loss of ability to perform (Knezevic et al, 1993)[1]. Ideally, a TBM operating twenty four hours a day, advances with a certain rate depending on a number of factors, such as:

- rock properties: rebound hardness, abrasion hardness, total hardness, uniaxial compressive strength, resistance to cutter penetration;
- mechanical and operational variables of the TBM: cutter load, cutterhead rotational rate, available torque, muck cleaning efficiency;
- TBM operator skills;
- downtime occurrence and duration, where downtime is defined as any time when TBM is not cutting rock.

Most of the above mentioned parameters can be estimated during design. The expected performance parameters are estimated on the basis of the exploration data, case histories and engineering judgement. The discussion of the TBM performance parameters will be presented later in this thesis, but the essence of the question one asks when defining all those parameters is how fast can the TBM accomplish the excavation. It is in answering this question, that understanding of downtime occurrences is of great impor-

1. For references see Appendix B

tance. The works of Priscilla Nelson ("TBM Performance in Sedimentary Rock", 1983) and Peter Tarkoy ("Predicting TBM penetration rates in selected rock types", 1973) addressed this issue by looking at the effects of geologic conditions on penetration rate, advance rate and utilization, which are the major parameters defining a TBM performance. A TBM downtime is a major component of these parameters.

The purpose of this research is to analyze the data collected during the excavation of the Boston Harbor Project Outfall Tunnel, and to produce a probabilistic answer to the question of what influence, if any, the physical properties of the surrounding rock mass have on the downtime frequency. The data collected by the construction management personnel contain a complete shift-based record of the TBM performance, including the information on each downtime occurrence, and its cause. The idea behind this research is look at the tunnel boring machine as a system of components each of which being essential to the whole system contributes to downtime, and causes the whole system to shut down. To find correlation between of each of these components and total hardness is the main task of this research.

1.2 Thesis Organization

The scope of work leads to the following thesis organization. Chapter 2 will familiarize the reader with the project, site geology, equipment technology, as well as the data used for analysis. Chapter 3 will discuss the mathematical tools employed in qualitative analyses. Chapter 4 will present the results of the analysis performed using the post-excavation rock testing data. Chapter 5 will present the results of the analysis performed on the pre-excavation data along with a comparison of these results with the ones obtained using the post-excavation data. The practical consequences and the possibilities for data extrapolation and prognosis will be discussed in Chapter 6.

Chapter 2

Site Description and Data Structure

2.1 Outfall Tunnel: Design and Construction

The outfall tunnel will transport treated effluent from the new Deer Island wastewater facilities to a location approximately 9.5 miles offshore in Massachusetts Bay. The outfall tunnel is an important element of the Boston Harbor Project. (see Figure 2.1)

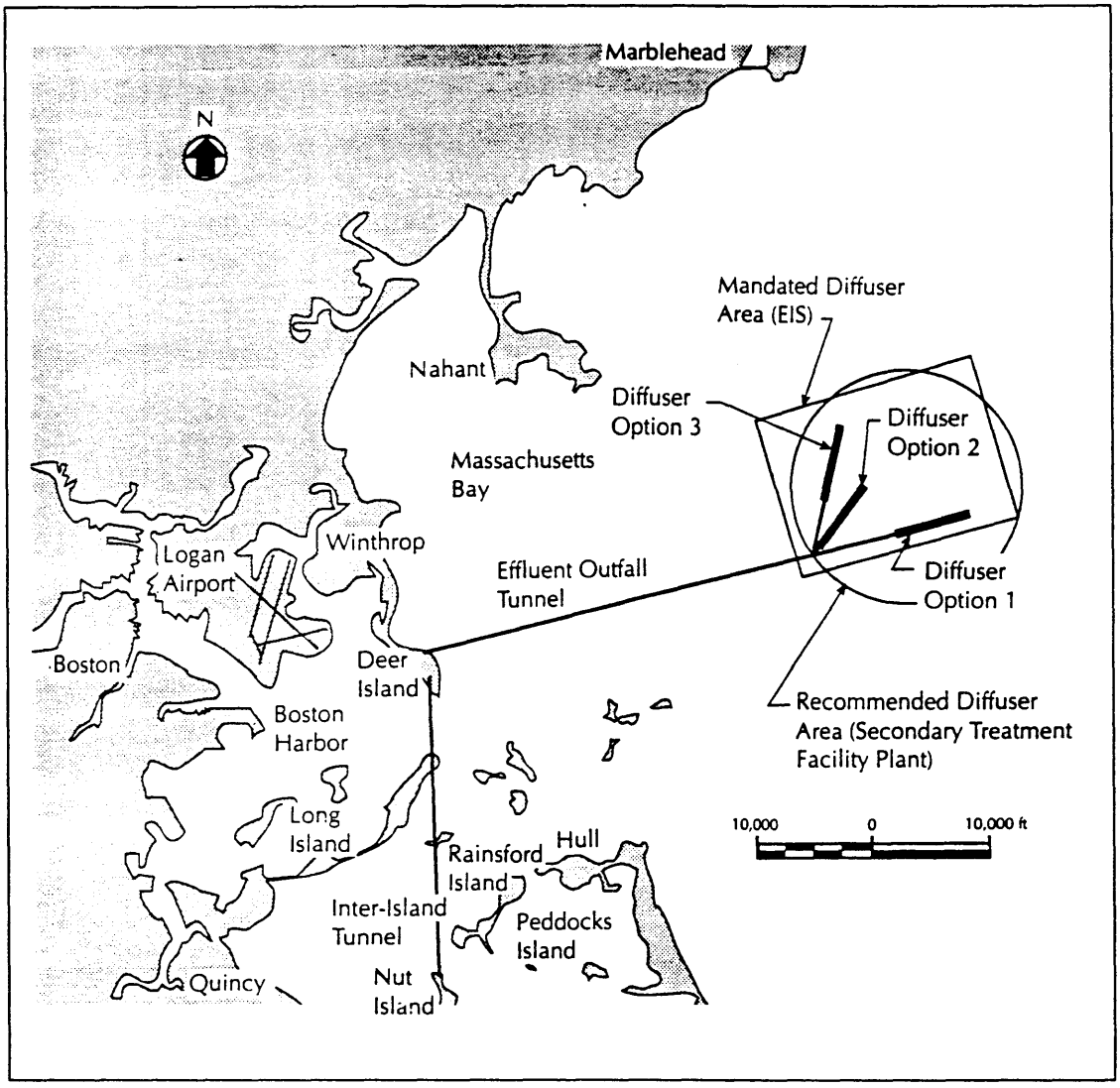

Figure 2.1: Plan of the Boston Harbor showing Effluent Outfall Tunnel

The outfall tunnel consists of the following principal components, listed in the order of direction of effluent flow:

- The outfall conduit, an underground concrete box structure carrying effluent from the disinfection facility to the shaft, constructed by the cut and cover method using diaphragm walls for temporary retaining walls.
- The outfall shaft, 30 ft. in diameter and approximately 430 ft. deep, sunk through soil and rock, using diaphragm walls for initial support and lined with concrete.
- The main outfall tunnel, 24.25 ft. finished diameter, 43,026.5 ft. (8.15 miles) long to the beginning of the diffuser area.
- Diffuser area tunnel, 6,600 ft. (1.25 miles) long, mined through and then backfilled with grout to get a gradually diminishing cross sectional area for maintaining effluent velocity.
- 55 riser offtakes connecting from the diffuser tunnel to risers.
- 55 riser pipes, 2.5 ft. in diameter, furnished with diffuser heads above the sea floor, to carry the effluent from the tunnel to dispersal in the ocean (see Figure 2.2)

The upper part of the shaft through glacial till is lined with fiber reinforced concrete. Through rock, the shaft is lined with unreinforced concrete. The depth of the tunnel was determined such that the crown of the tunnel would be at least 100 feet below the top of rock. This is equivalent to approximately three times the excavated tunnel diameter plus a margin of about 20 feet. The tunnel is given a small up-slope grade of 0.05%, providing a small advantage in control of water inflow.

The contractor was given two options for the final lining, a precast segmental concrete lining erected under a shield, and a cast-in-place lining with a precast invert segment. The contractor chose a fully precast lining using six tapered precast segments

The risers and diffusers were in place before the diffuser area tunnel was constructed. Offtake adits were being excavated horizontally from the tunnel to the installed risers (Parsons Brinckerhoff Summary Report, 1990).

The outfall tunnel was mined using a Robbins Tunnel Boring Machine, made for this project. The predominant rock was Cambridge Argillite.

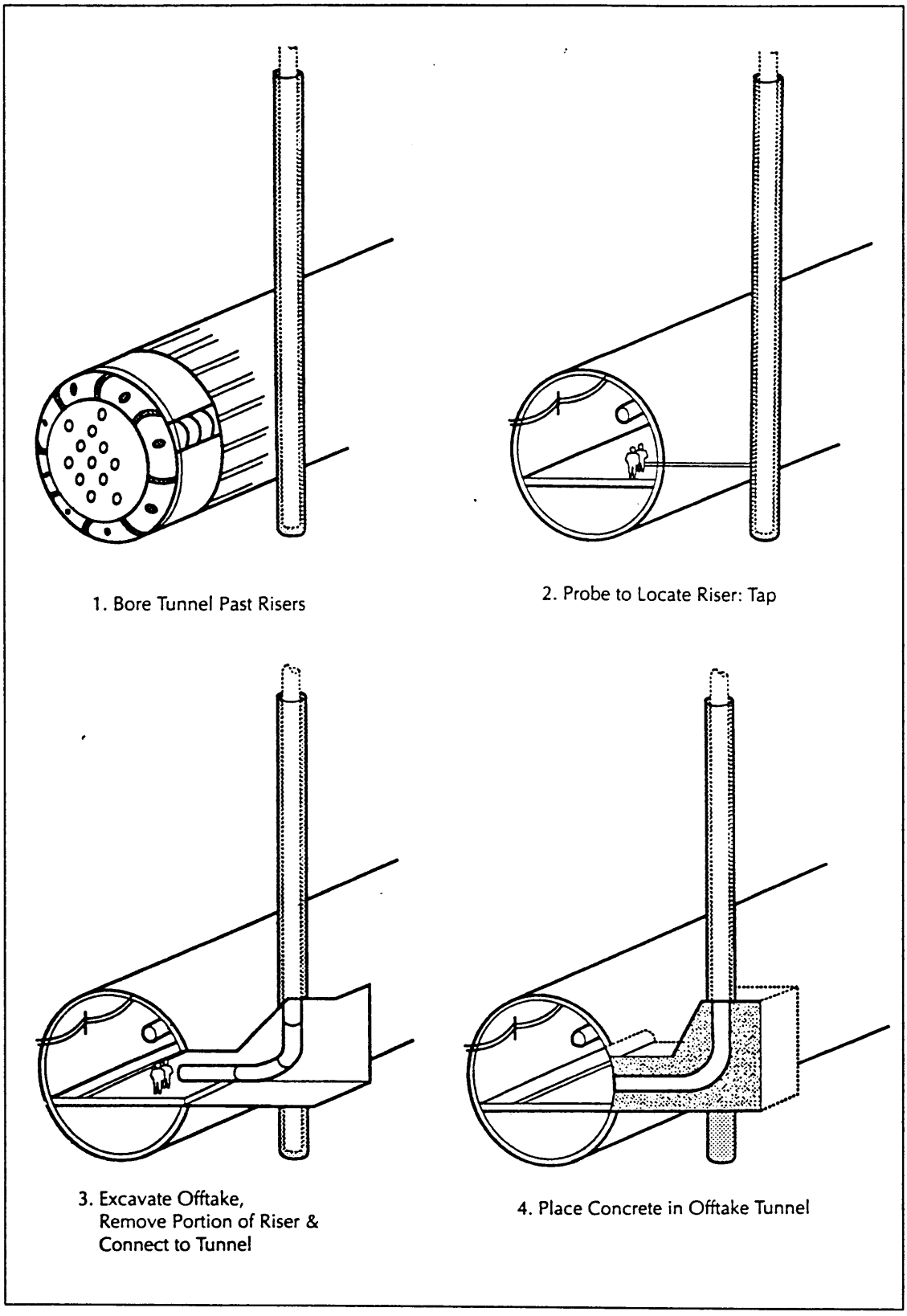

Figure 2.2: Diffuser Construction Sequence

2.2 Site Geology

2.2.1 Regional Geology

Cambridge Argillite is one of the rocks that constitute the Boston Basin. The Boston Basin is an east-northeast-trending, wedge-shaped, down-faulted body of sedimentary and volcanic rock. Onshore, the basin is widest along the coast, where it measures about 15 miles north to south. Offshore, it extends to the east under Massachusetts Bay, where it appears to widen still more (Barosh et al, 1989) (see Figure 2.3).

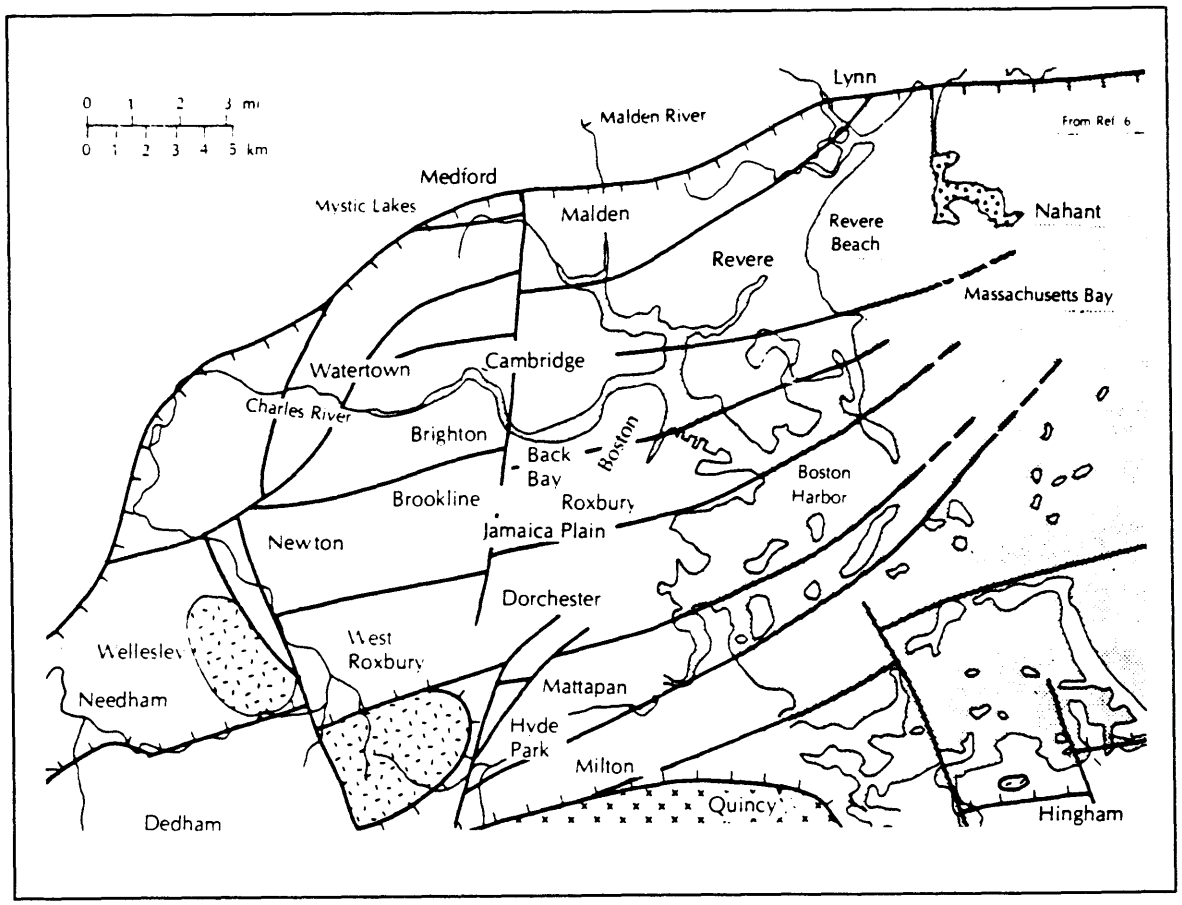

Figure 2.3: Map of Boston showing the limits of the Boston Basin (ticked line)

The Boston Basin sedimentary rocks were formed during the Late PreCambrian and were subjected to folding and faulting during the collision between the North American

and Eurasian/African Plates in the Late Palezoic. During the Triassic separation of the continents, the bedrock was rifted at high angles and intruded by numerous diabase dikes. The lightest relief and source areas lay to the south and west of the basin. The sedimentary rocks consist of detritus that has been eroded from the surrounding highlands and fault scarps and that has been deposited as interfingering lithofacies (Barosh et al, 1989). A map of the major tectonic provinces of southeastern New England appears in Figure 2.4.

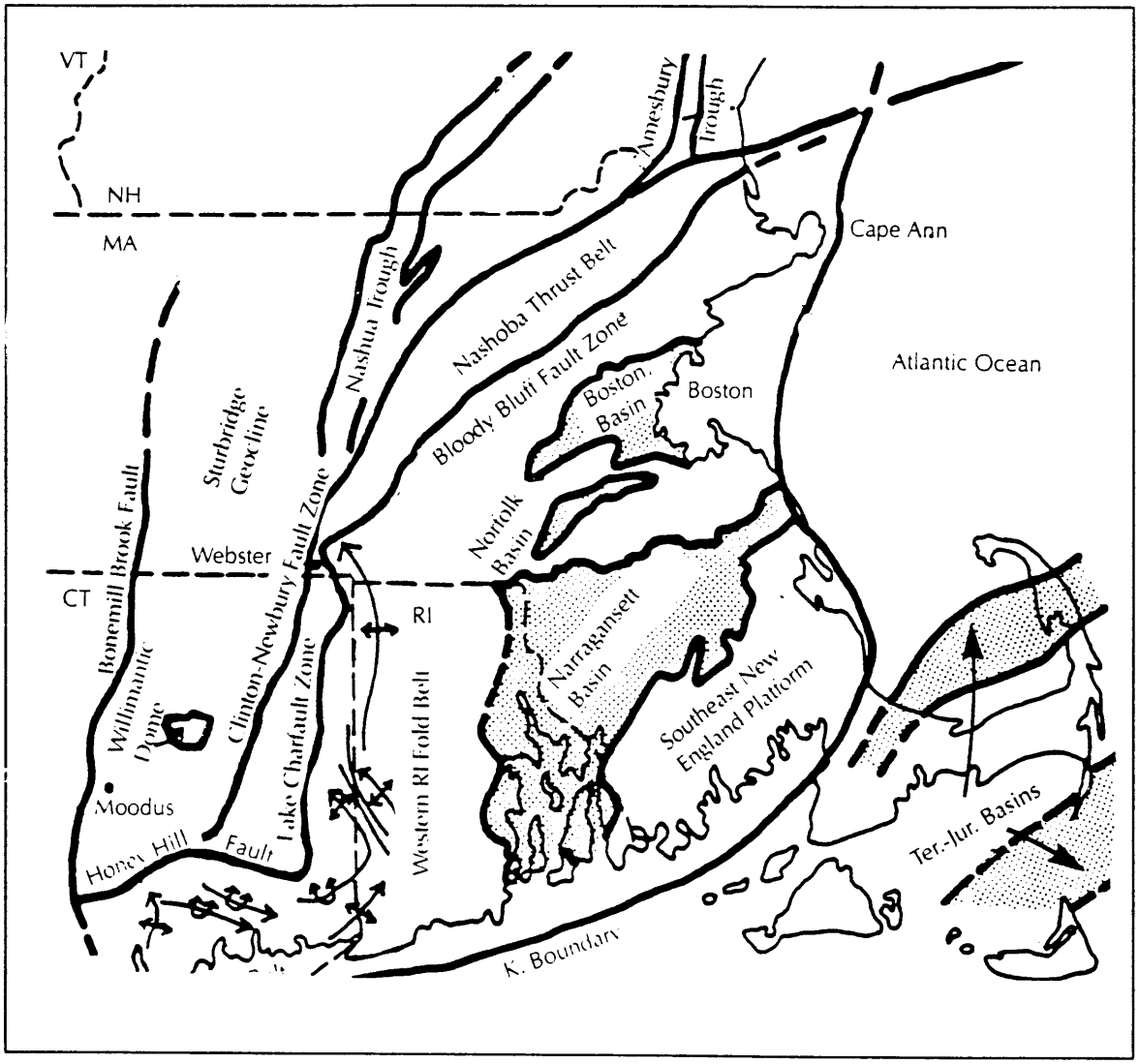

Figure 2.4: Map of tectonic provinces of Southeastern New England

Of the rock formations making up the Boston Basin Group, the Cambridge Argillite is the only one observed along the tunnel alignment. The Cambridge Argillite is a grey, lay-

ered, slightly calcareous rock with bed thicknesses generally ranging from 0.05 to 3 inches and occasionally up to 5 feet. Volcanic flows of ash fall tuffs, with an average thickness of 0.05 inch to about 1 foot, are occasionally interbedded with the argillite. Intruding the Cambridge argillite are igneous dikes and sills, predominantly of diabase, with minor amounts of basalt and/or andesite, and felsite (Parsons Brinckerhoff Interpretive Report, 1989).

2.2.2 Bedrock Geology Along the Outfall Tunnel

The bedrock geology along the alignment was evaluated from rock core samples. Twenty five borings in 1988 and thirty one test borings in 1989 were drilled by Metcalf & Eddy for this project. The lithologic percentages in the 1989 cores agree well with those in the 1988 program and are as follows:

- sandy argillite and tuffaceous argillite - 31%;
- argillite - 56%;
- diabase, felsite, or andesite - 7.4%.

The principal structural feature observed in the argillite is bedding, which varies from laminated to thick. In general, the bedding strikes northeast and dips 15-40 degrees south-east.

The primary intrusive rock is diabase. The diabase occurs in either dikes or sills. Most of the observed contacts are either gradational or fractured.

2.3 Tunneling in Argillite

Eight tunnels have been constructed through rock in the Boston area; all of them encountered at least some argillite. The argillite crossed by these tunnels does not neces-

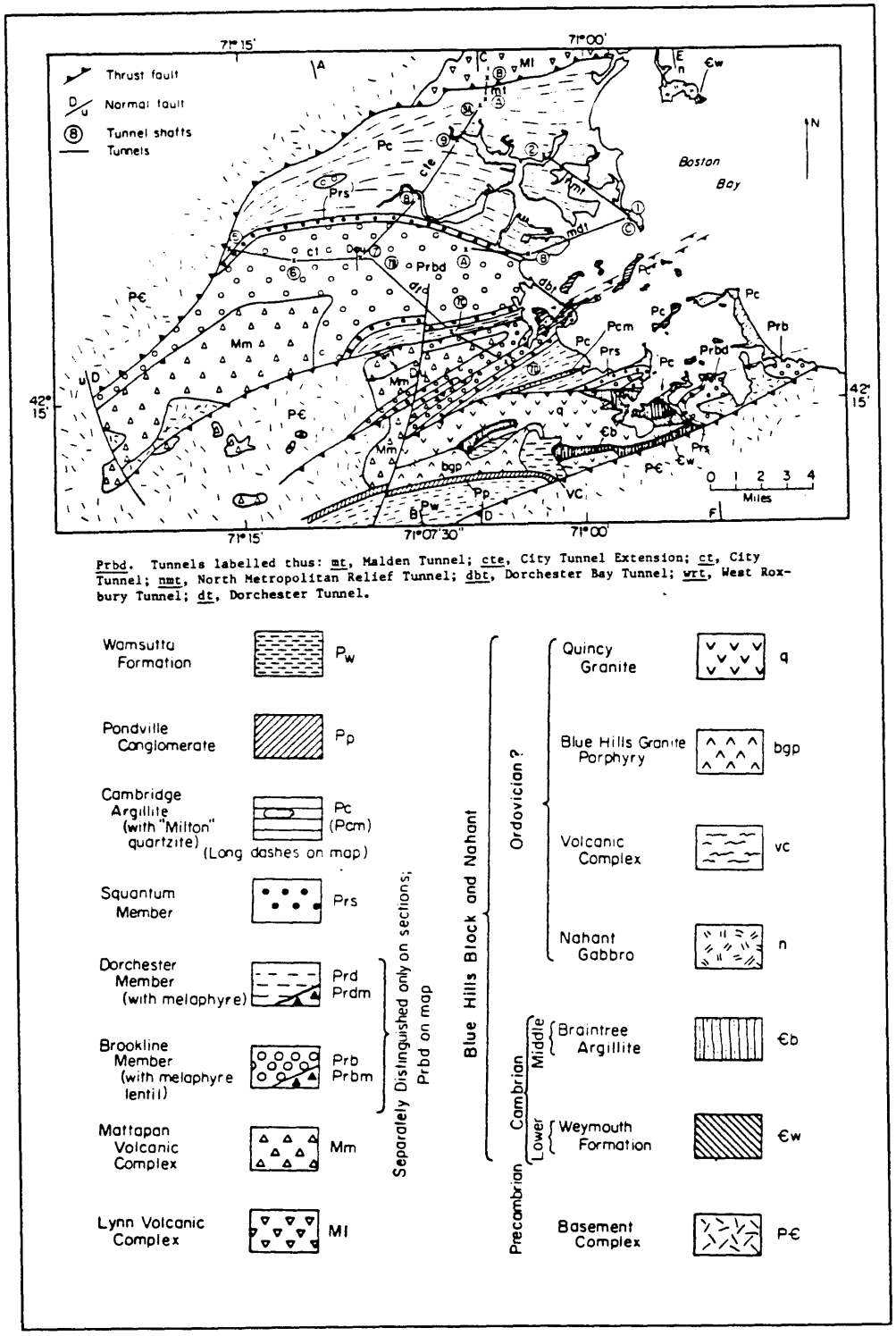

Figure 2.5: Geologic map of the Boston Area showing tunnels location

sarily represent the argillite encountered in the outfall tunnel, but some similarities can be observed.

Water Supply and Drainage Tunnels: Water Supply and Drainage tunnels have been constructed in the region at various times. These tunnels were constructed largely in argillite. Igneous intrusions, mostly diabase dikes, were encountered extensively; three tunnels with extensive geologic mapping (City Tunnel Extension (cte), City Tunnel (ct), Malden Tunnel (mt)) (see Figure 2.5) encountered such intrusions at a rate of 3 to 6 per 1000 ft. on the average. The intrusions were typically 5-10 ft. thick, the diabase in the dikes was often fractured, and adjacent rock was often altered and fractured. The number of faults encountered in these tunnels was typically about 3 per 1000 ft. Almost all of them were thin and remineralized (Parsons Brinckerhoff Geotechnical Interpretive Report, 1989).

Red Line Extension: The 3.1 miles Northwest Extension of the MBTA Red Line beyond Harvard Square (see Figure 2.6) consists of two deep tunnel sections and a cut-and-cover section. The primary rock type along the tunnel alignment is Cambridge Argillite with lesser amounts of intrusive rocks that penetrate the country rock. Bedding characteristics showed extreme variability, although the bedding generally dipped gently to moderately (20 to 45 degrees) to the south. The bedrock varied from a massive dark to medium gray fine-grained argillite to an argillite that exhibited rhythmic bands of light gray layers alternating with medium to dark gray layers. The coarser grained and generally lighter colored layers had well developed bedding structures. These structures included graded sequences, cross bedding and ripple marks. The major joint set along the alignment, other than bedding plane joints, generally strikes north-northeast, with nearly vertical dips. Jointing parallel to bedding was commonly developed striking nearly east-west with gentle to moderate dips (Parsons Brinckerhoff Geotechnical Interpretive Report, 1989).

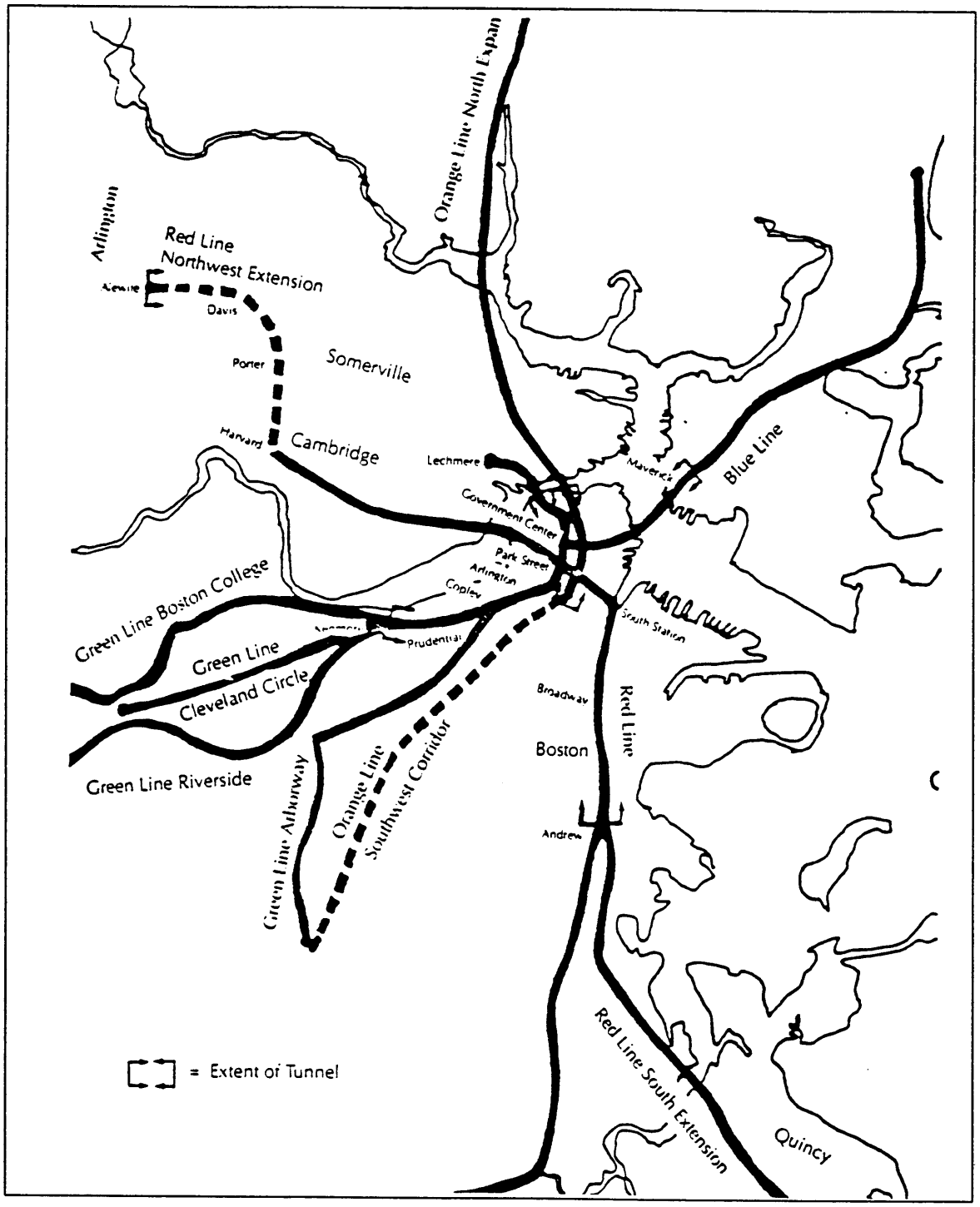

Figure 2.6: Map of MBTA Subway Lines

2.4 Pre-excavation Exploration Program

As mentioned above, in addition to the "tunnelling experience in argillite" study, the designer conducted its own exploration program, that was implemented by the Metcalf & Eddy in 1988 and 1989. The program yielded a set of the rock properties which along with the data already available became a basis for the preliminary design recommendations. The following figures (Figures 2.7 through 2.16) show a complete geological profile constructed as a result of the pre-bid exploration. The figures also show the relative location of the borings and the tunnel alignment. The offset of the borings from the alignment is quite significant which points to one of the major limitations of the pre-excavation boring program. The analysis of some of the limitations will be presented later in the thesis. The comparison of the pre-excavation and the post-excavation data will also be addressed later in the thesis.

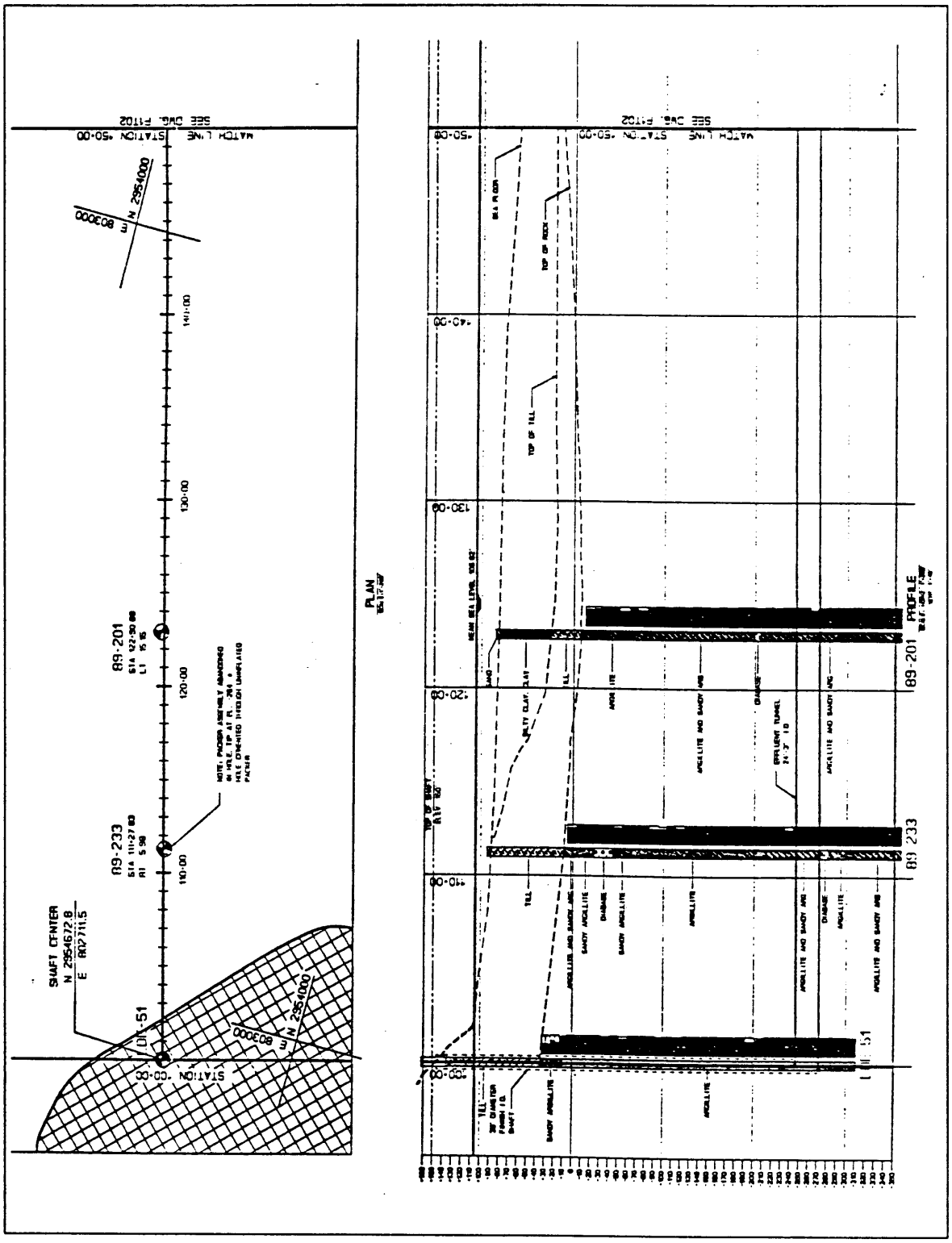

Figure 2.7: Geological Profile: Sta 100+00 to Sta 150+00

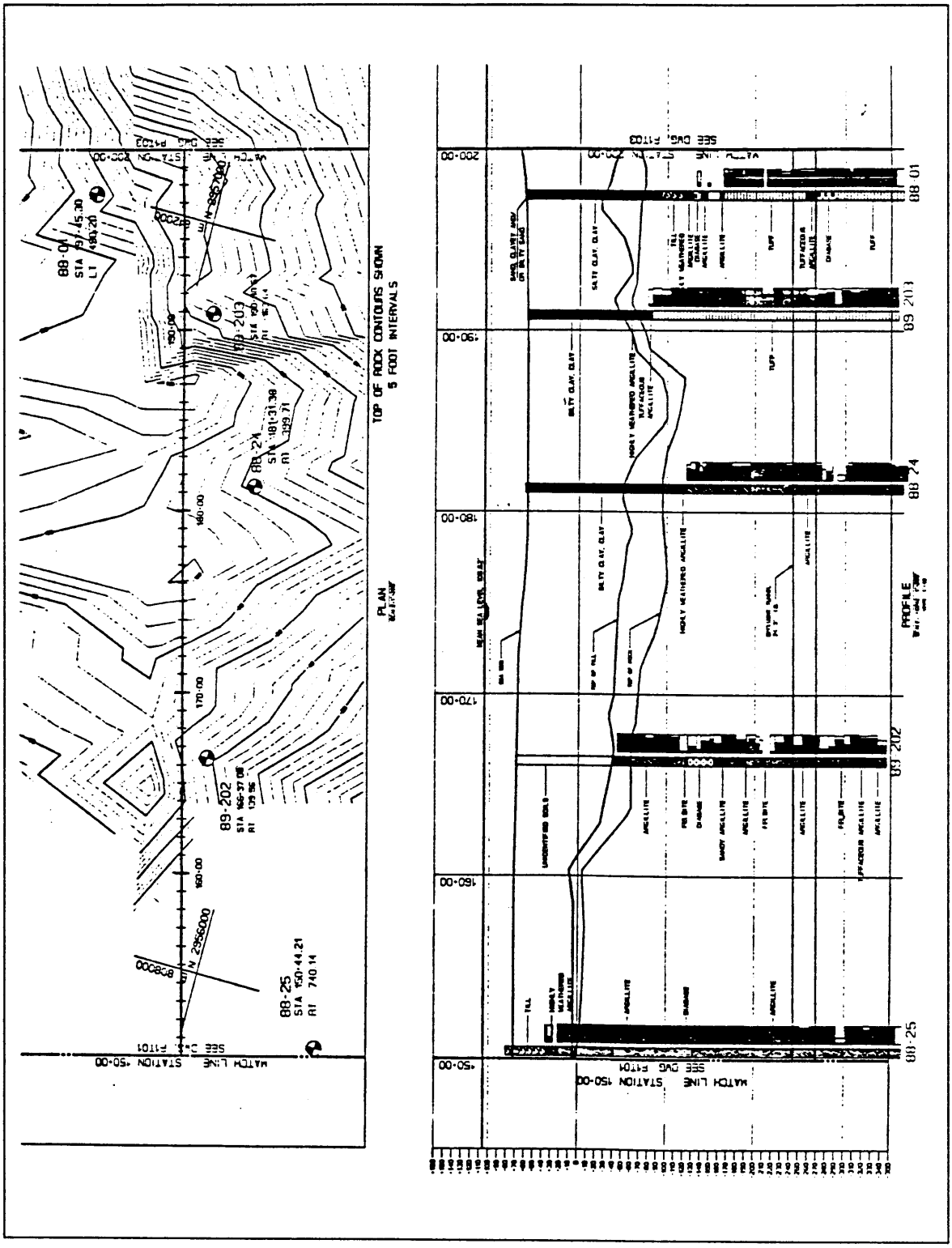

Figure 2.8: Geological Profile: Sta 150+00 to Sta 200+00

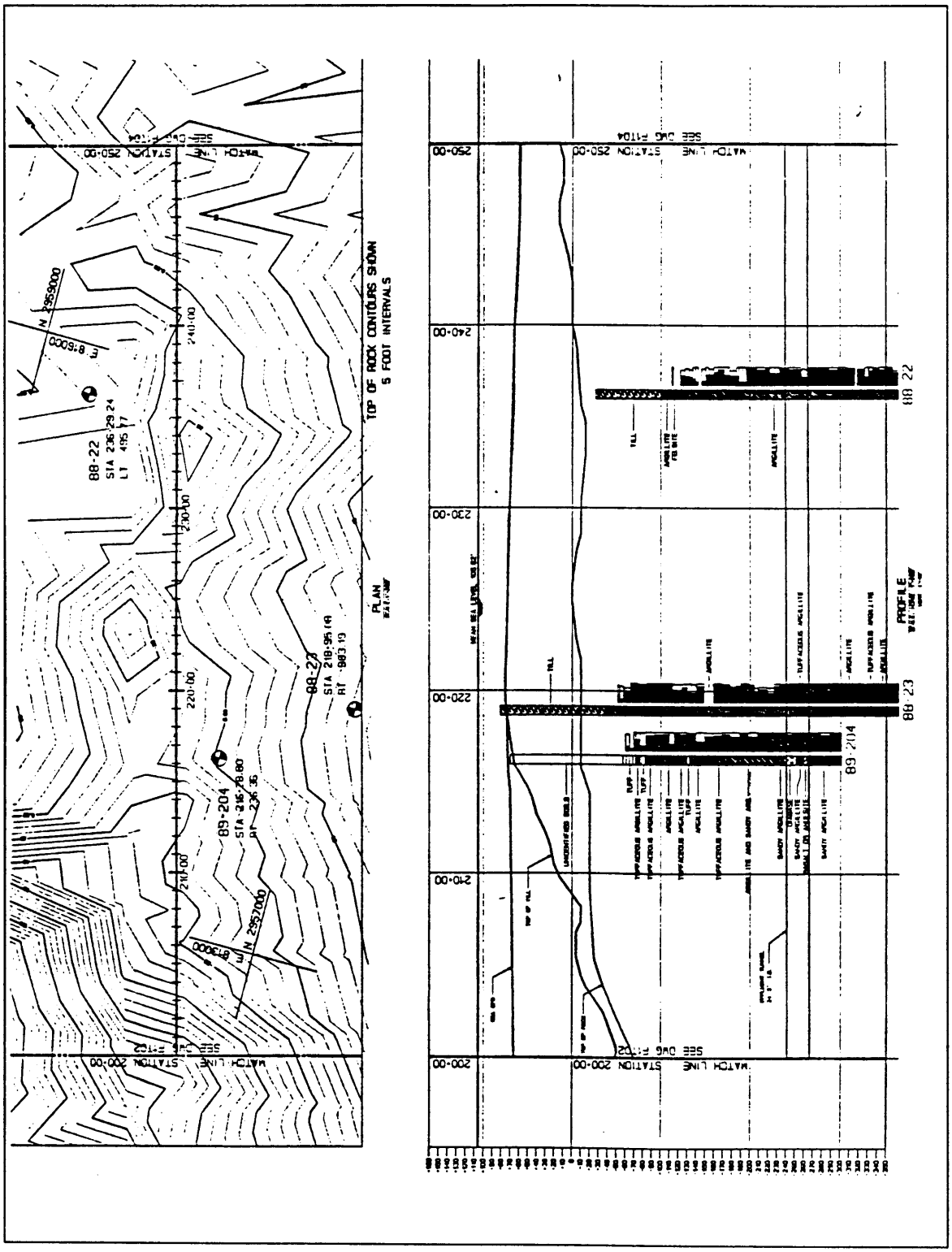

Figure 2.9: Geological Profile: Sta 200+00 to Sta 250+00

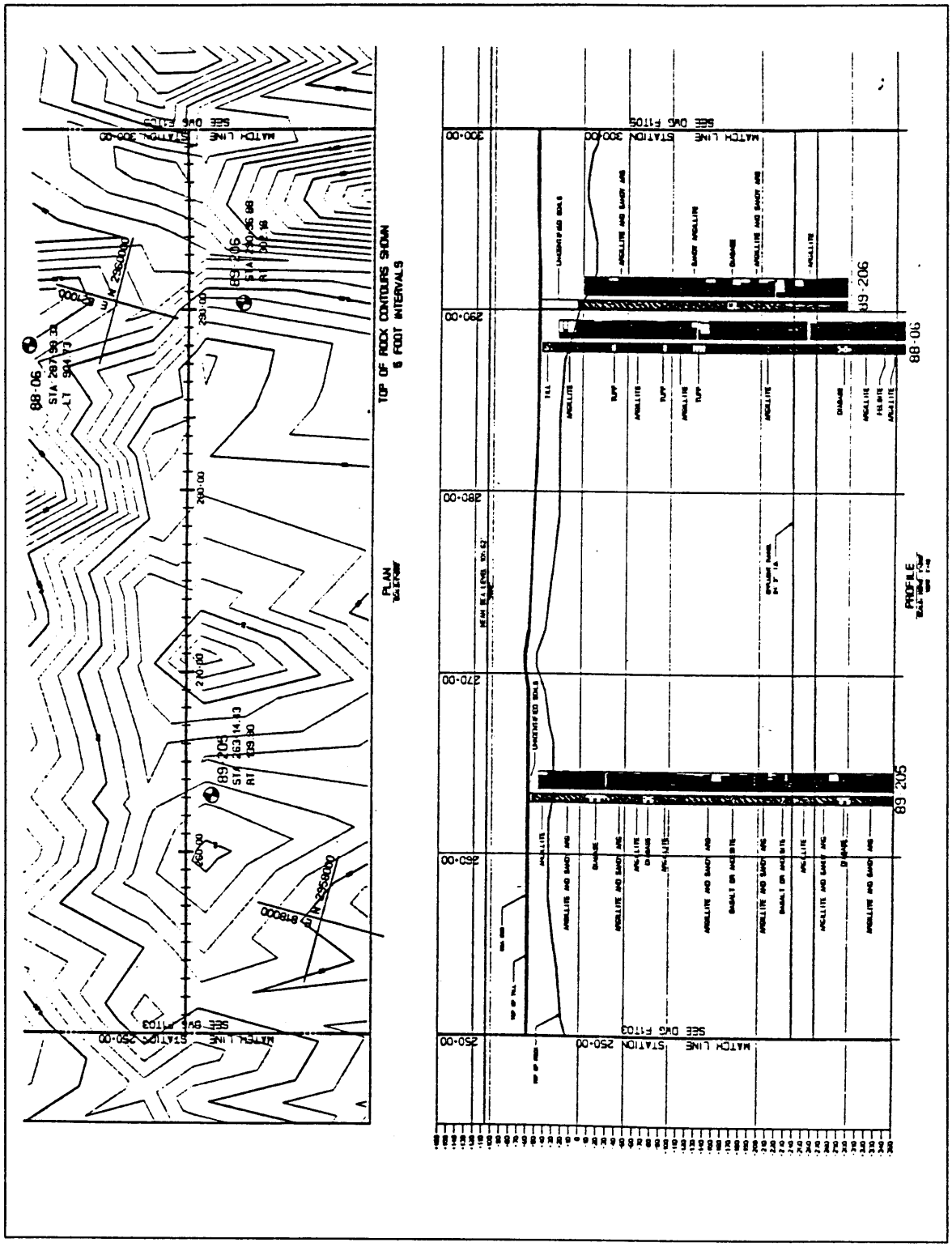

Figure 2.10: Geological Profile: Sta 250+00 to Sta 300+00

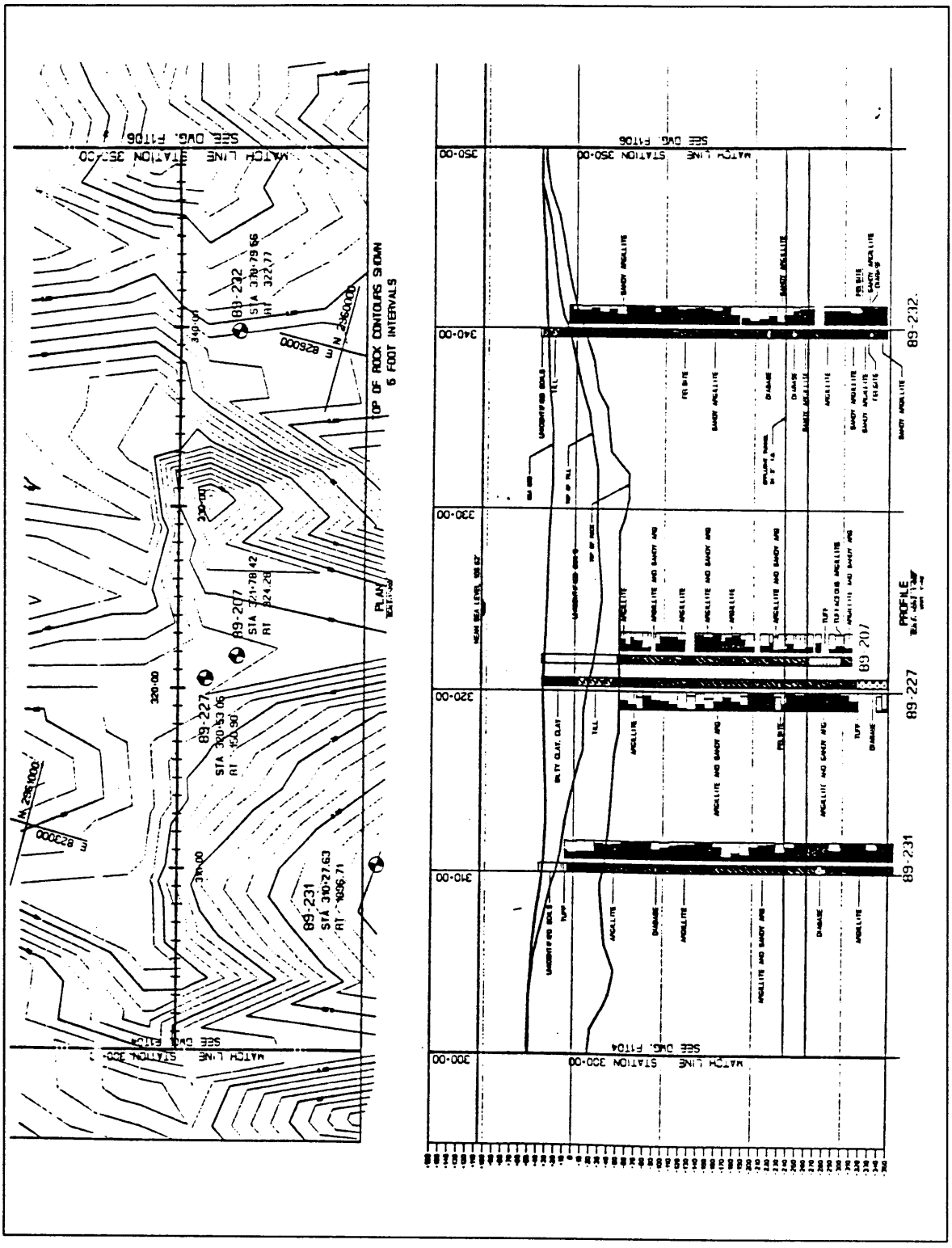

Figure 2.11: Geological Profile: Sta 300+00 to 350+00

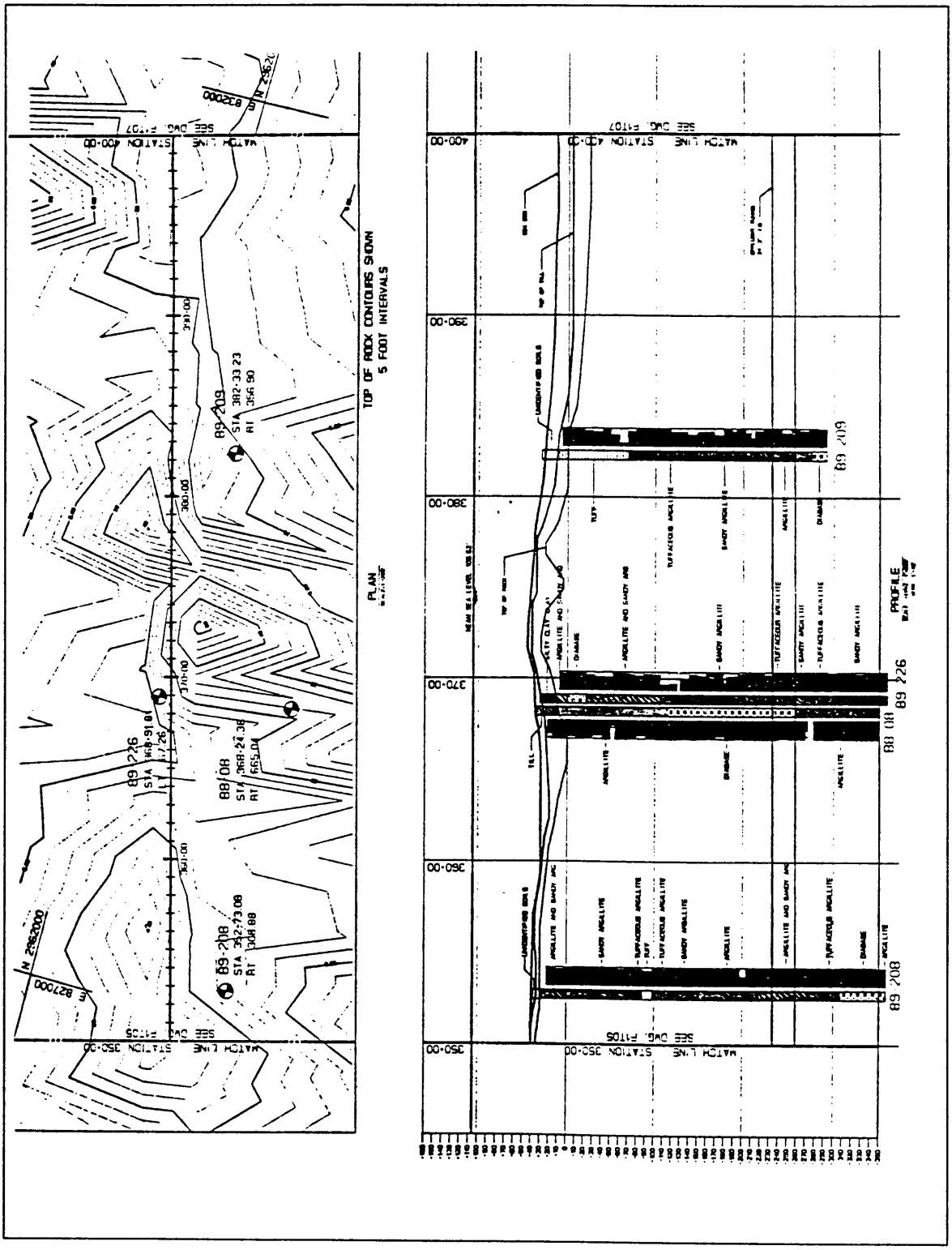

Figure 2.12: Geological Profile: Sta 350+00 to Sta 400+00

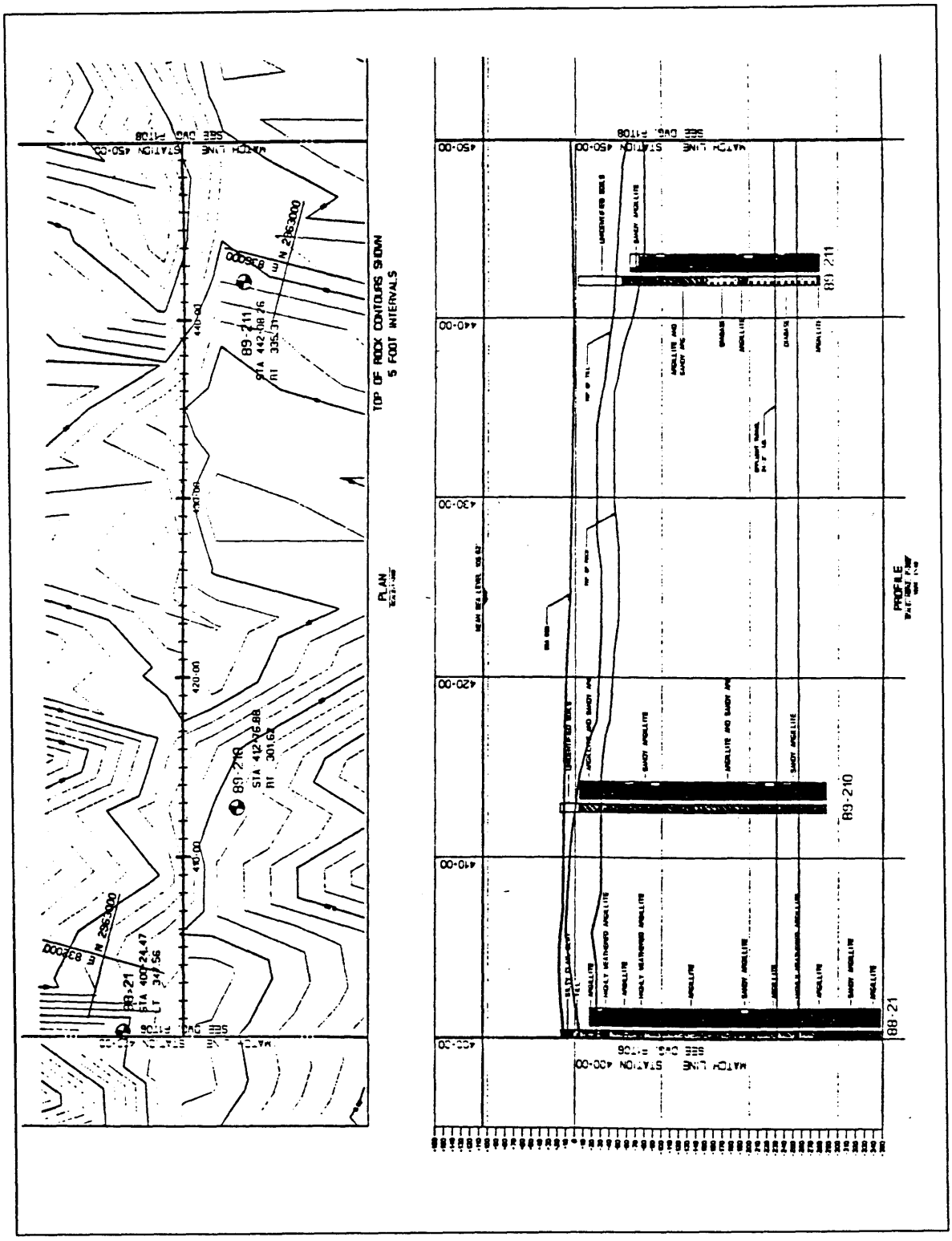

Figure 2.13: Geological Profile: Sta 400+00 to Sta 450+00

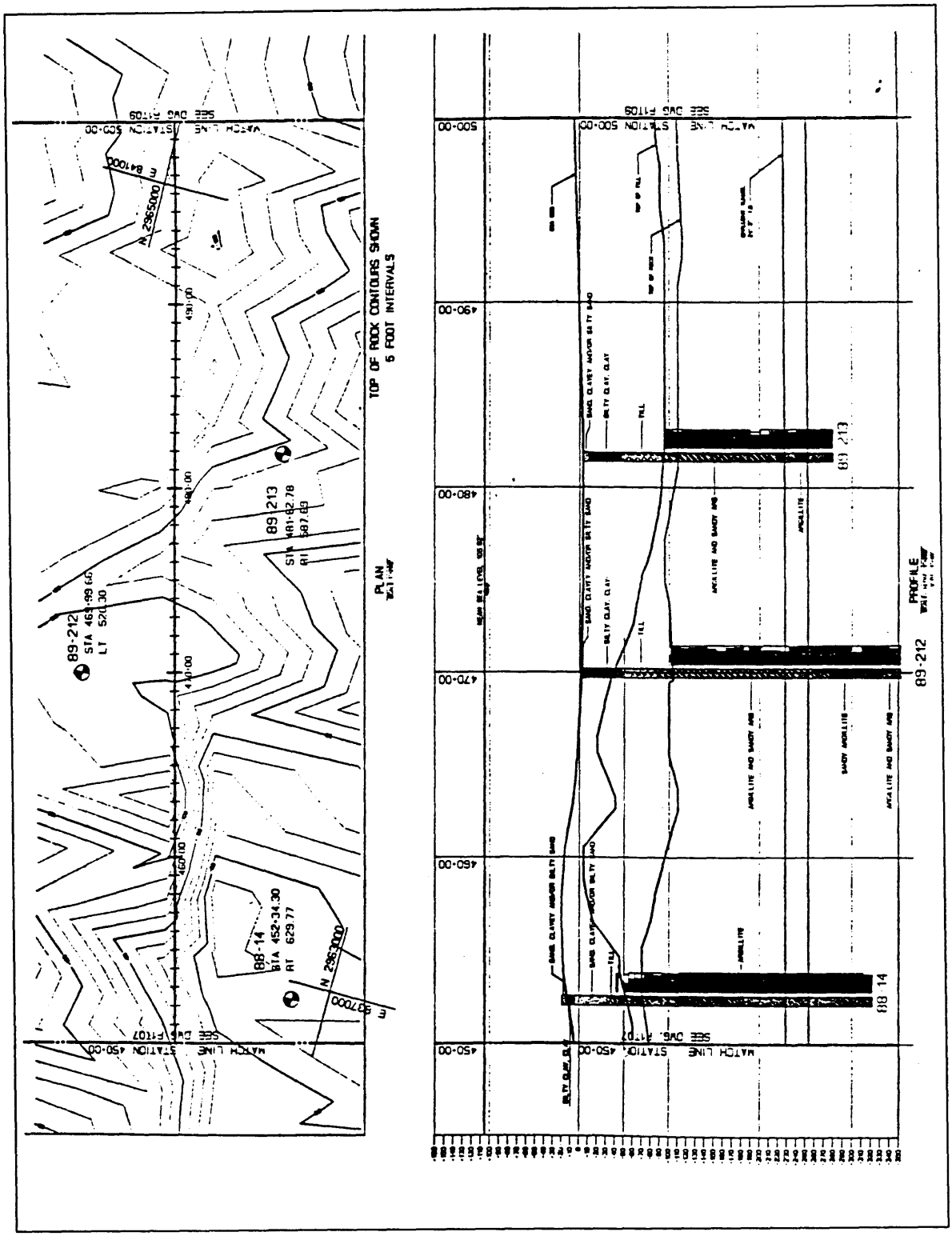

Figure 2.14: Geological Profile: Sta 450+00 to 500+00

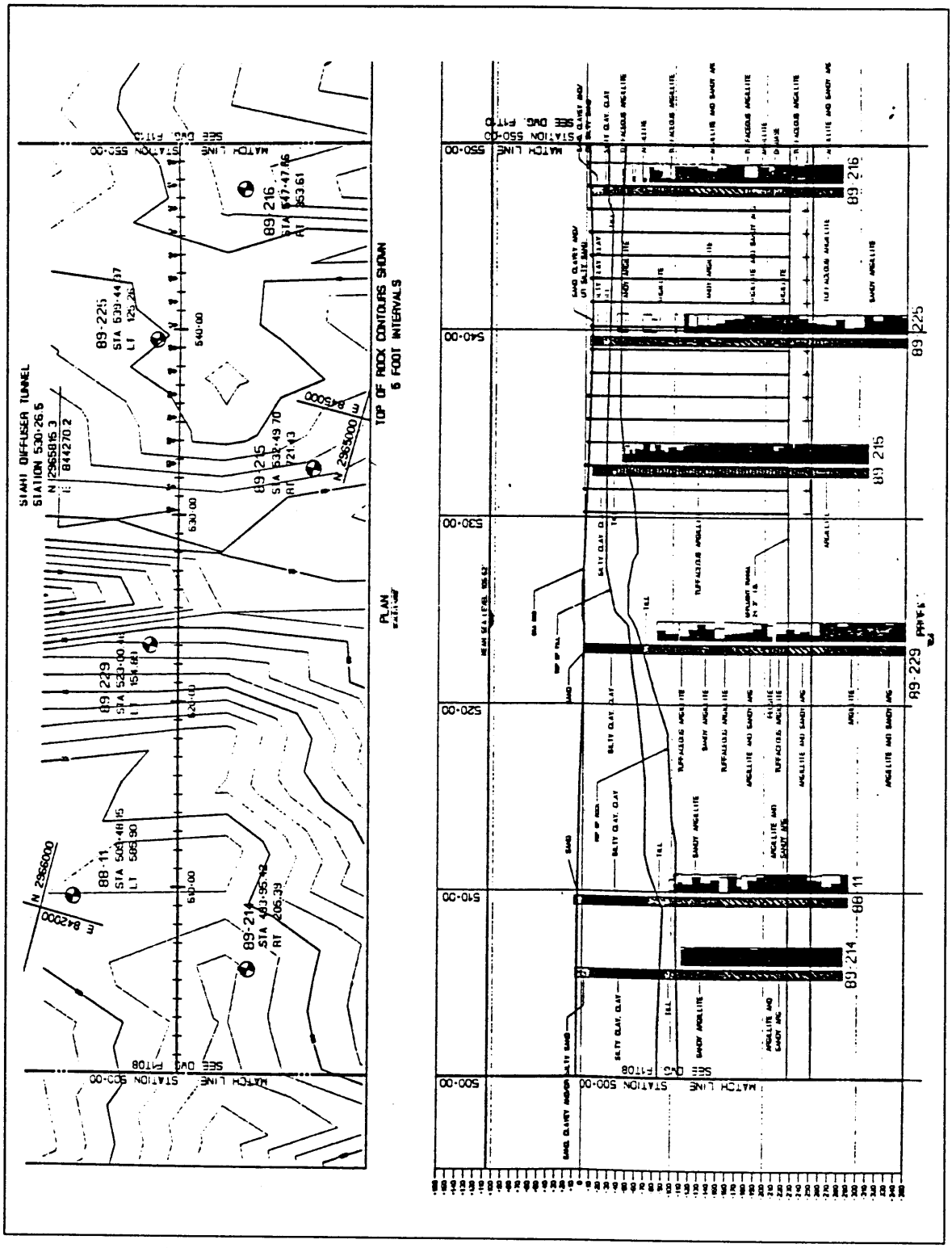

Figure 2.15: Geological Profile: Sta 500+00 to Sta 550+00

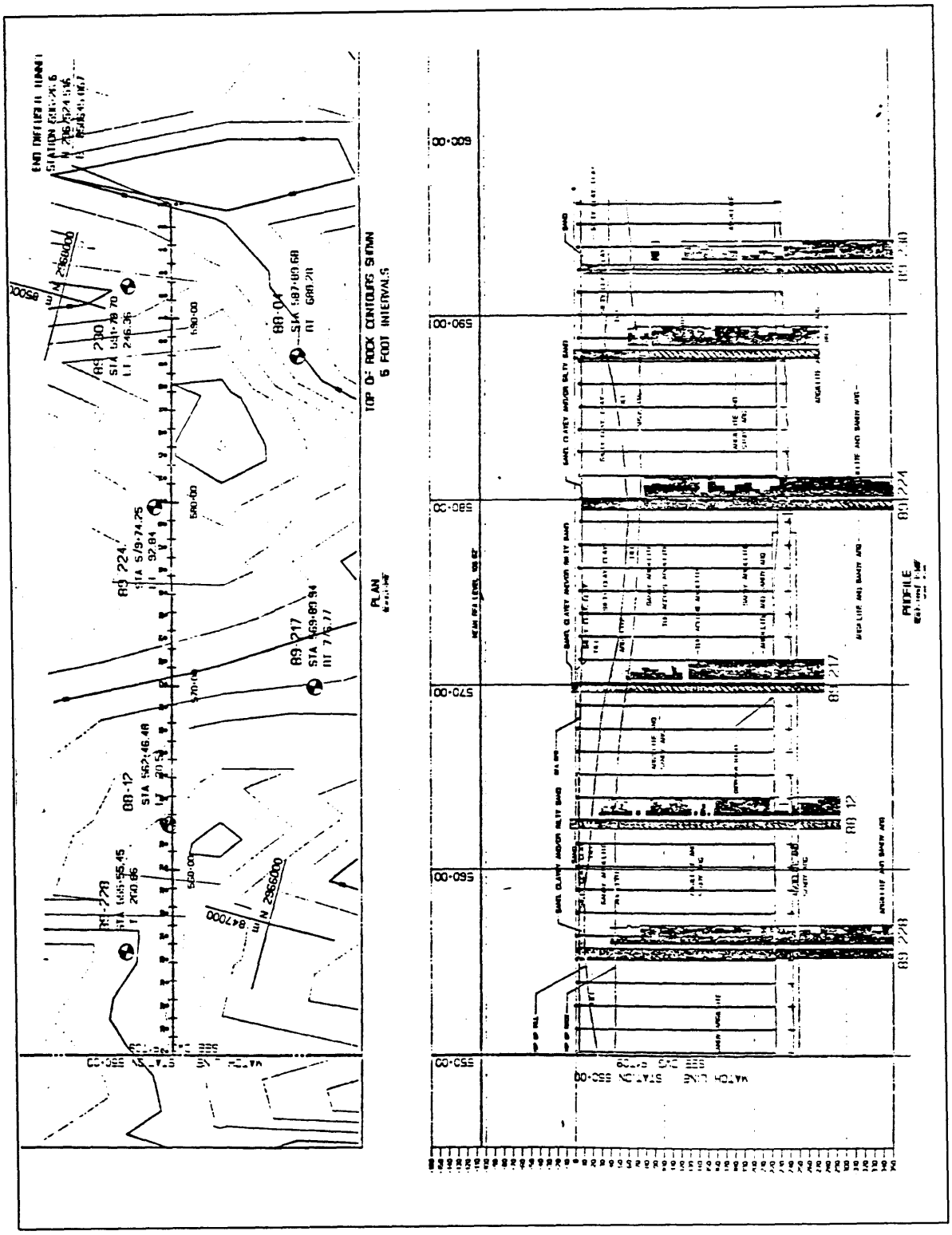

Figure 2.16: Geological Profile: Sta 550+00 to 600+00

2.5 Data Structure

2.5.1 Rock Testing Data

2.5.1.1 Pre-excavation Test Boring Program

The capability to predict the TBM performance under the particular tunnel conditions is of great importance to both the designer and the contractor. The following parameters are conventionally used to define a TBM performance:

- Penetration Rate, ft./hour = TBM advance (Length of tunnel bored in ft. per shift) / TBM Clock (Elapsed machine time recorded automatically through instrumentation in hours per shift);
- Advance Rate in ft./hour = Penetration Rate x Utilization;
- Utilization in % = TBM Clock (Elapsed machine time recorded automatically through instrumentation in hours per shift) / Shift Time (Excavation Shift time in hours per shift), where the Elapsed machine time - time automatically recorded by the TBM data acquisition system, which starts recording at the moment the TBM main cylinders are pressurized, and stops recording at the moment the pressure drops to zero.

P.J. Tarkoy introduced two index tests, to be used during exploration as well as during later testing programs to predict expected machine advance rates (Tarkoy et al, 1973).

Rebound Hardness (Hr): Rebound hardness has been used in the past to measure hardness of metals (Shore Scleroscope) and the strength of curing concrete (Schmidt Hammer). The relevance of rebound hardness in these applications is based on its ability to measure relative amounts of energy expended on plastic vs. elastic deformation. Dynamic energy reflected back into the instrument is measured.

Abrasion Hardness (Ha): The technique used to obtain abrasion hardness has been developed in the Civil Engineering Rock Mechanics Laboratory at the University of Illinois at Urbana-Champagne. A disk of rock, of NX diameter (2 1/8") and 1/4 inches thick, is secured to the revolving turntable of the abrasion machine. As the turntable revolves, the main component of travel of the rock specimen is parallel to the axis of the abrading wheel

causing it to be dragged along the surface of the rock. The abrasion hardness is defined as the reciprocal of the average weight loss.

Total hardness is calculated as $Ht = Hr \times \sqrt{Ha}$. The test sequence (Tarkoy et al, 1975) used in the outfall tunnel is shown on Figure 2.17. This procedure was implemented by Metcalf & Eddy during Outfall Tunnel pre-bid exploration program. The total hardness values obtained from the program were used in this research.

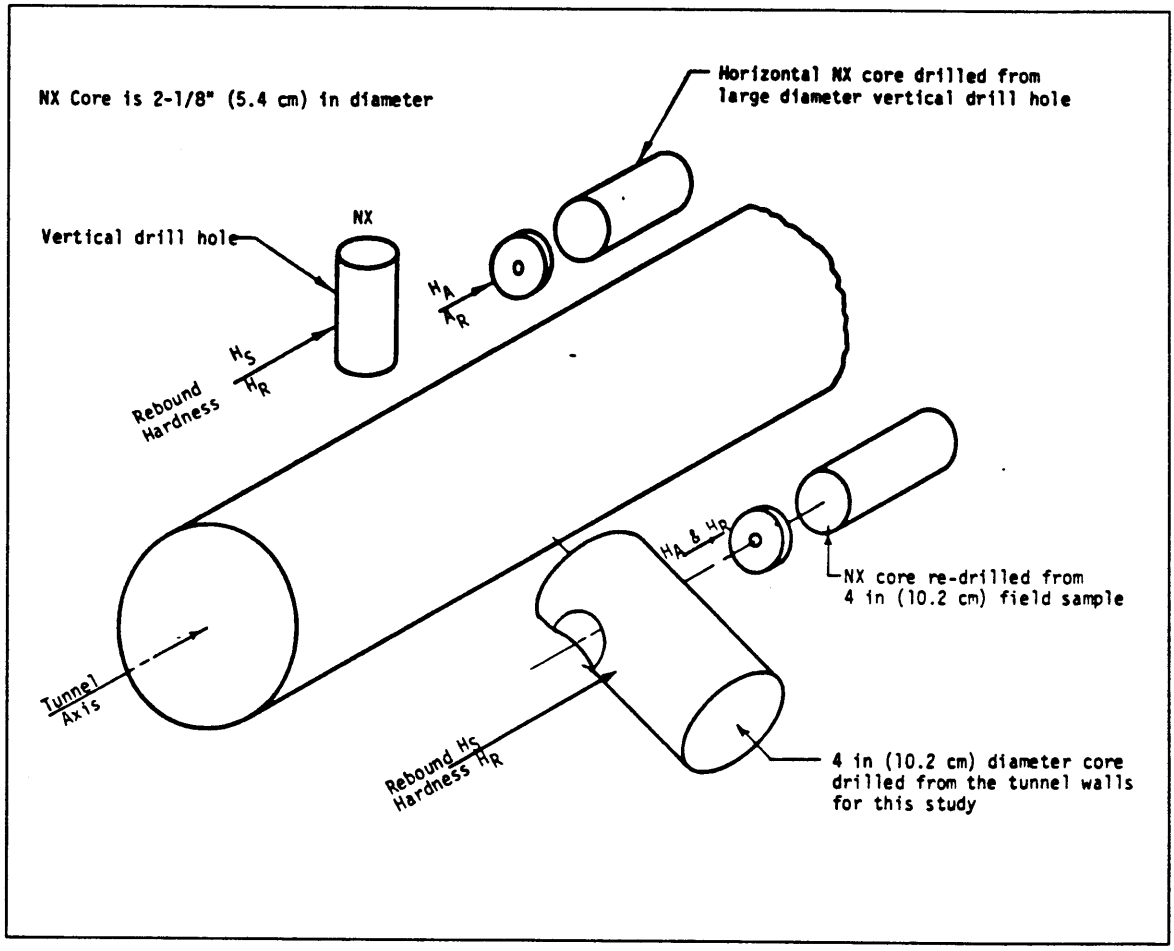

Figure 2.17: P.J. Tarkoy Testing Procedure

2.5.1.2 Construction Management Test Boring Program During Excavation.

Large diameter cylinders (d = 8 inches) were drilled out from the tunnel wall (see Figure 2.18) every 250 feet along the tunnel. From each cylinder, two standard NX-diameter samples were re-drilled in the laboratory for each test sequence: one in a direction parallel to the alignment, and the other in a direction perpendicular to the alignment. The following rock properties were obtained:

- rock type;
- water content;
- porosity;
- unit weight;
- rebound hardness;
- abrasion hardness;
- total hardness;
- uniaxial compressive strength;
- elastic modulus;
- brazilian tensile strength;
- acoustic velocities

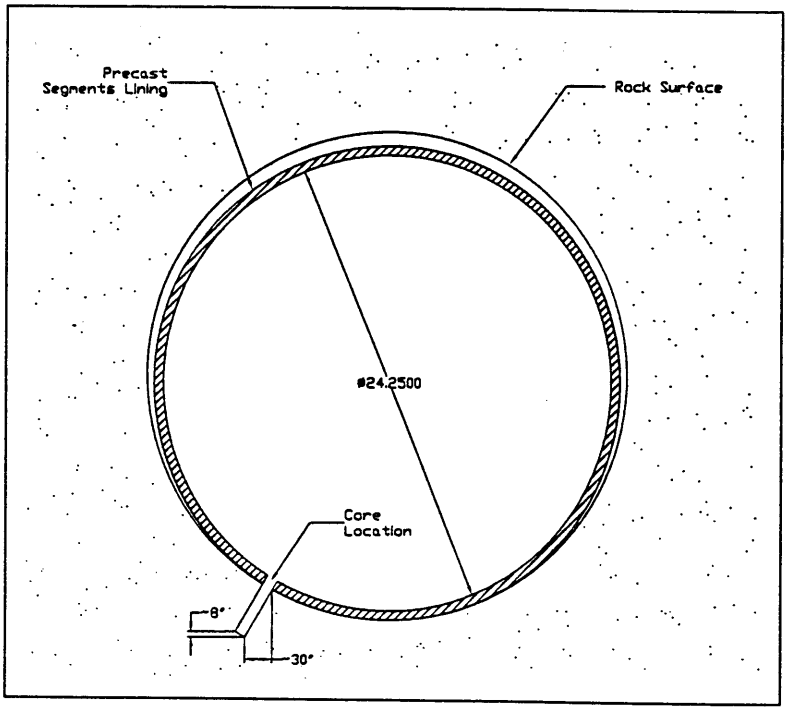

Figure 2.18: Sketch showing CM coring program

2.5.2 Downtime Data

Another dataset used for this research is the database maintained by the construction management (CM) personnel during the excavation of the tunnel. It summarizes the data collected by the CM and the Contractor Shift Engineers on a shift basis and contains the following information:

- Date (Day, month and year of the shift);
- Shift ("day", "swing", "graveyard");
- TBM Clock (Elapsed machine time recorded automatically through instrumentation);
- TBM Clock Downtime = Excavation Shift Time - TBM Clock;
- Shift End Time (Ending time in 24-hour format);
- Information on eight downtime occurrences, specifically:
  1. Date of occurrence;
  2. Shift of occurrence;
  3. Time duration;
  4. System that caused that failure;
  5. Element of the system that caused the failure;
  6. Breakdown nature (numeric code);
  7. Was the downtime scheduled or not (yes/no).

Construction Management introduced the following TBM systems and system elements downtime categories:

- TBM (T) subdividing into following elements:
  1. Cutters (CU);
  2. Drive Motors (DR);
  3. Electrical (EL);
  4. Hydraulics (HY);
  5. Lube System (LU);
  6. Maintenance (MA);
  7. Superstructure (SU).
- Lining System (L) consisting of the following elements;
  1. Erector Arm System (ER);
  2. Supply (SU);
  3. Temporary Support (TS).
- Muck Removal System (M) incorporating the following elements;
  1. Unspecified (AL);
  2. Boretec Conveyor (BO);

3. Cutterhead (CU);
4. Horizontal Conveyor (HZ);
5. Rapat/Muck Jamming (RP);
6. Stacker Conveyor (ST);
7. TBM Conveyor (TB);
8. Transfer Conveyor (TR);
9. Vertical Conveyor (VT);
10. Other unspecified (UN).

- Utilities (U) consisting of the following elements:
  1. Air (AI);
  2. Trailing Gear (BA);
  3. Dewatering (DE);
  4. Electrical (EL);
  5. Rail (RA);
  6. Shaft (SH);
  7. Ventilation (VE);
  8. Water (WA).
- Survey (S);
- Miscellaneous (C) summarizing difficult ground condition (mainly at the face):
  1. Gripper-Rock Reaction (RR);
  2. Face Grouting (GR);
  3. Grout Hole (GH);
  4. Probe Drill (PH);
  5. Inspection (IN).
- Personnel:
  1. TBM Operator (TO);
  2. Operators (OP);
  3. Miners (MI);
  4. Other (AL).

The TBM advance data are part of this database. A drawing showing the TBM profile is presented on Figure 2.19. A sample of the CM database printout is shown on Figure 2.20.

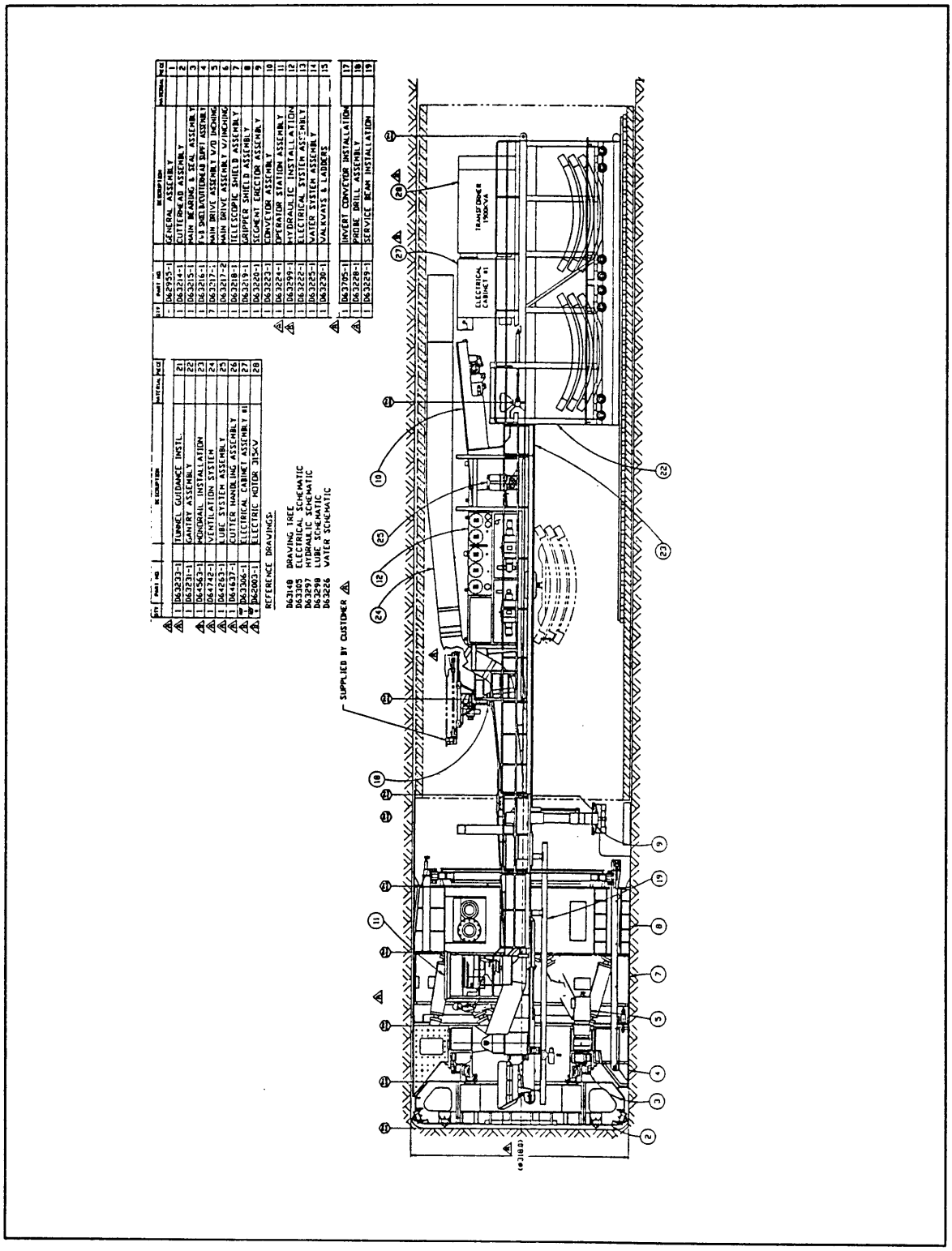

Figure 2.19: Tunnel Boring Machine Assembly Profile

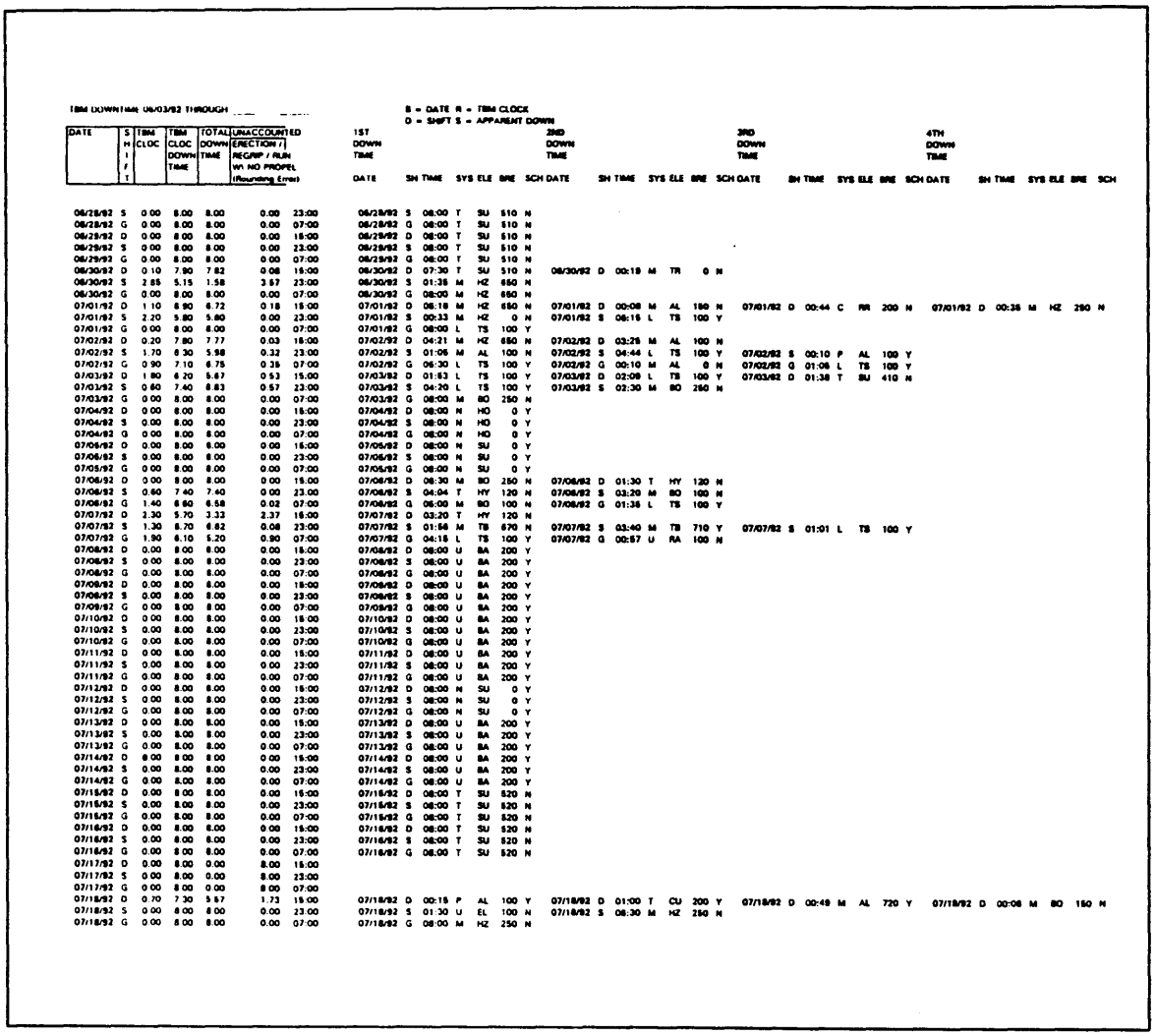

TBM DOWNTIME 06/03/92 THROUGH ____ ____

S = DATE R = TBM CLOCK
D = SHIFT S = APPARENT DOWN

DATE	S H I F T	TBM CLOC	TBM CLOC DOWN TIME	TOTAL DOWN TIME	UNACCOUNTED (ERECTOR?) REC/MP / RUN Wt NO PROPEL (Rounding Error)	1ST DOWN TIME	2ND DOWN TIME	3RD DOWN TIME	4TH DOWN TIME
						DATE SH TIME SYS ELE BRE SCH	DATE SH TIME SYS ELE BRE SCH	DATE SH TIME SYS ELE BRE SCH	DATE SH TIME SYS ELE BRE SCH
06/28/92	S	0.00	8.00	8.00	0.00 23:00	06/28/92 S 08:00 T SU 510 N			
06/28/92	G	0.00	8.00	8.00	0.00 07:00	06/28/92 G 08:00 T SU 510 N			
06/29/92	D	0.00	8.00	8.00	0.00 15:00	06/29/92 D 08:00 T SU 510 N			
06/29/92	S	0.00	8.00	8.00	0.00 23:00	06/29/92 S 08:00 T SU 510 N			
06/29/92	G	0.00	8.00	8.00	0.00 07:00	06/29/92 G 08:00 T SU 510 N			
06/30/92	D	0.10	7.90	7.82	0.08 15:00	06/30/92 D 07:30 T SU 510 N	06/30/92 D 00:15 M TR 0 N		
06/30/92	S	2.85	5.15	1.58	3.57 23:00	06/30/92 S 01:38 M HZ 650 N			
06/30/92	G	0.00	8.00	8.00	0.00 07:00	06/30/92 G 08:00 M HZ 650 N			
07/01/92	D	1.10	6.90	6.72	0.18 15:00	07/01/92 D 06:18 M HZ 650 N	07/01/92 D 00:08 M AL 150 N	07/01/92 D 00:44 C RR 200 N	07/01/92 D 00:38 M HZ 250 N
07/01/92	S	2.20	5.80	5.80	0.00 23:00	07/01/92 S 00:33 M HZ 0 N	07/01/92 S 06:15 L TS 100 Y		
07/01/92	G	0.00	8.00	8.00	0.00 07:00	07/01/92 G 08:00 L TS 100 Y			
07/02/92	D	0.20	7.80	7.77	0.03 15:00	07/02/92 D 04:21 M HZ 650 N	07/02/92 D 03:25 M AL 100 N		
07/02/92	S	1.70	6.30	5.98	0.32 23:00	07/02/92 S 01:06 M AL 100 N	07/02/92 S 04:44 L TS 100 Y	07/02/92 S 00:10 P AL 100 Y	
07/02/92	G	0.90	7.10	6.75	0.35 07:00	07/02/92 G 06:30 L TS 100 Y	07/02/92 G 00:10 M AL 0 N	07/02/92 G 01:06 L TS 100 Y	
07/03/92	D	1.80	6.20	5.67	0.53 15:00	07/03/92 D 01:53 L TS 100 Y	07/03/92 D 02:08 L TS 100 Y	07/03/92 D 01:38 T SU 410 N	
07/03/92	S	0.60	7.40	6.83	0.57 23:00	07/03/92 S 04:20 L TS 100 Y	07/03/92 S 02:30 M BO 250 N		
07/03/92	G	0.00	8.00	8.00	0.00 07:00	07/03/92 G 08:00 M BO 250 N			
07/04/92	D	0.00	8.00	8.00	0.00 15:00	07/04/92 D 08:00 N HO 0 Y			
07/04/92	S	0.00	8.00	8.00	0.00 23:00	07/04/92 S 08:00 N HO 0 Y			
07/04/92	G	0.00	8.00	8.00	0.00 07:00	07/04/92 G 08:00 N HO 0 Y			
07/05/92	D	0.00	8.00	8.00	0.00 15:00	07/05/92 D 08:00 N SU 0 Y			
07/05/92	S	0.00	8.00	8.00	0.00 23:00	07/05/92 S 08:00 N SU 0 Y			
07/05/92	G	0.00	8.00	8.00	0.00 07:00	07/05/92 G 08:00 N SU 0 Y			
07/06/92	D	0.00	8.00	8.00	0.00 15:00	07/06/92 D 08:30 M BO 250 N	07/06/92 D 01:30 T HY 120 N		
07/06/92	S	0.60	7.40	7.40	0.00 23:00	07/06/92 S 04:04 T HY 120 N	07/06/92 S 03:20 M BO 100 N		
07/06/92	G	1.40	6.60	6.58	0.02 07:00	07/06/92 G 06:00 M BO 100 N	07/06/92 G 01:36 L TS 100 Y		
07/07/92	D	2.30	5.70	3.33	2.37 16:00	07/07/92 D 03:20 T HY 120 N			
07/07/92	S	1.30	6.70	6.62	0.08 23:00	07/07/92 S 01:54 M TS 670 N	07/07/92 S 03:40 M TS 710 Y	07/07/92 S 01:01 L TS 100 Y	
07/07/92	G	1.90	6.10	5.20	0.90 07:00	07/07/92 G 04:15 L TS 100 Y	07/07/92 G 00:57 U RA 100 N		
07/08/92	D	0.00	8.00	8.00	0.00 15:00	07/08/92 D 08:00 U BA 200 Y			
07/08/92	S	0.00	8.00	8.00	0.00 23:00	07/08/92 S 08:00 U BA 200 Y			
07/08/92	G	0.00	8.00	8.00	0.00 07:00	07/08/92 G 08:00 U BA 200 Y			
07/09/92	D	0.00	8.00	8.00	0.00 15:00	07/09/92 D 08:00 U BA 200 Y			
07/09/92	S	0.00	8.00	8.00	0.00 23:00	07/09/92 S 08:00 U BA 200 Y			
07/09/92	G	0.00	8.00	8.00	0.00 07:00	07/09/92 G 08:00 U BA 200 Y			
07/10/92	D	0.00	8.00	8.00	0.00 15:00	07/10/92 D 08:00 U BA 200 Y			
07/10/92	S	0.00	8.00	8.00	0.00 23:00	07/10/92 S 08:00 U BA 200 Y			
07/10/92	G	0.00	8.00	8.00	0.00 07:00	07/10/92 G 08:00 U BA 200 Y			
07/11/92	D	0.00	8.00	8.00	0.00 15:00	07/11/92 D 08:00 U BA 200 Y			
07/11/92	S	0.00	8.00	8.00	0.00 23:00	07/11/92 S 08:00 U BA 200 Y			
07/11/92	G	0.00	8.00	8.00	0.00 07:00	07/11/92 G 08:00 U BA 200 Y			
07/12/92	D	0.00	8.00	8.00	0.00 15:00	07/12/92 D 08:00 N SU 0 Y			
07/12/92	S	0.00	8.00	8.00	0.00 23:00	07/12/92 S 08:00 N SU 0 Y			
07/12/92	G	0.00	8.00	8.00	0.00 07:00	07/12/92 G 08:00 N SU 0 Y			
07/13/92	D	0.00	8.00	8.00	0.00 15:00	07/13/92 D 08:00 U BA 200 Y			
07/13/92	S	0.00	8.00	8.00	0.00 23:00	07/13/92 S 08:00 U BA 200 Y			
07/13/92	G	0.00	8.00	8.00	0.00 07:00	07/13/92 G 08:00 U BA 200 Y			
07/14/92	D	0.00	8.00	8.00	0.00 15:00	07/14/92 D 08:00 U BA 200 Y			
07/14/92	S	0.00	8.00	8.00	0.00 23:00	07/14/92 S 08:00 U BA 200 Y			
07/14/92	G	0.00	8.00	8.00	0.00 07:00	07/14/92 G 08:00 U BA 200 Y			
07/15/92	D	0.00	8.00	8.00	0.00 15:00	07/15/92 D 08:00 T SU 520 N			
07/15/92	S	0.00	8.00	8.00	0.00 23:00	07/15/92 S 08:00 T SU 520 N			
07/15/92	G	0.00	8.00	8.00	0.00 07:00	07/15/92 G 08:00 T SU 520 N			
07/16/92	D	0.00	8.00	8.00	0.00 15:00	07/16/92 D 08:00 T SU 520 N			
07/16/92	S	0.00	8.00	8.00	0.00 23:00	07/16/92 S 08:00 T SU 520 N			
07/16/92	G	0.00	8.00	8.00	0.00 07:00	07/16/92 G 08:00 T SU 520 N			
07/17/92	D	0.00	8.00	0.00	8.00 15:00				
07/17/92	S	0.00	8.00	0.00	8.00 23:00				
07/17/92	G	0.00	8.00	0.00	8.00 07:00				
07/18/92	D	0.70	7.30	5.57	1.73 15:00	07/18/92 D 00:15 P AL 100 Y	07/18/92 D 01:00 T CU 200 Y	07/18/92 D 00:49 M AL 720 Y	07/18/92 D 00:08 M BO 150 N
07/18/92	S	0.00	8.00	8.00	0.00 23:00	07/18/92 S 01:30 U EL 100 N	07/18/92 S 06:30 M HZ 250 N		
07/18/92	G	0.00	8.00	8.00	0.00 07:00	07/18/92 G 08:00 M HZ 250 N			

Figure 2.20: Sample of CM database used for this thesis

Chapter 3

Statistical Methods Used For The Analysis

3.1 Datasets Organization

All calculations were performed using the SAS programming language and statistical procedures. There were several steps leading to creation of the dataset which became the basis for all types of analysis. A code was written to implement the algorithm shown in Figure 3.1 (for unscheduled downtime only). As a result of code execution, the following data were obtained:

- Start Station - distance from the shaft in hundred feet at the beginning of the shift;
- End Station - distance from the shaft in hundred feet at the end of the shift;
- Start Date - beginning of shift date;
- End Date - end of shift date;
- Start Time - beginning of shift time;
- End Time - end of shift time;
- TBM Clock - elapsed machine time;
- TBM Downtime - time during which TBM was not cutting rock;
- Shift Time;
- T-system Number of Failures (see Chapter 2);
- T-system Failure Duration;
- T-system, CU-element Number of Failures;
- T-system, CU-element Failure Duration;
- M-system Number of Failures (see Chapter 2);
- M-system Failure Duration;
- M-system, HZ-element Number of Failures;
- M-system, HZ-element Failure Duration;
- L-system Number of Failures;
- L-system Failure Duration;
- U-system Number of Failures;
- U-system Failure Duration;
- O-system Number of Failures;
- O-system Failure Duration.

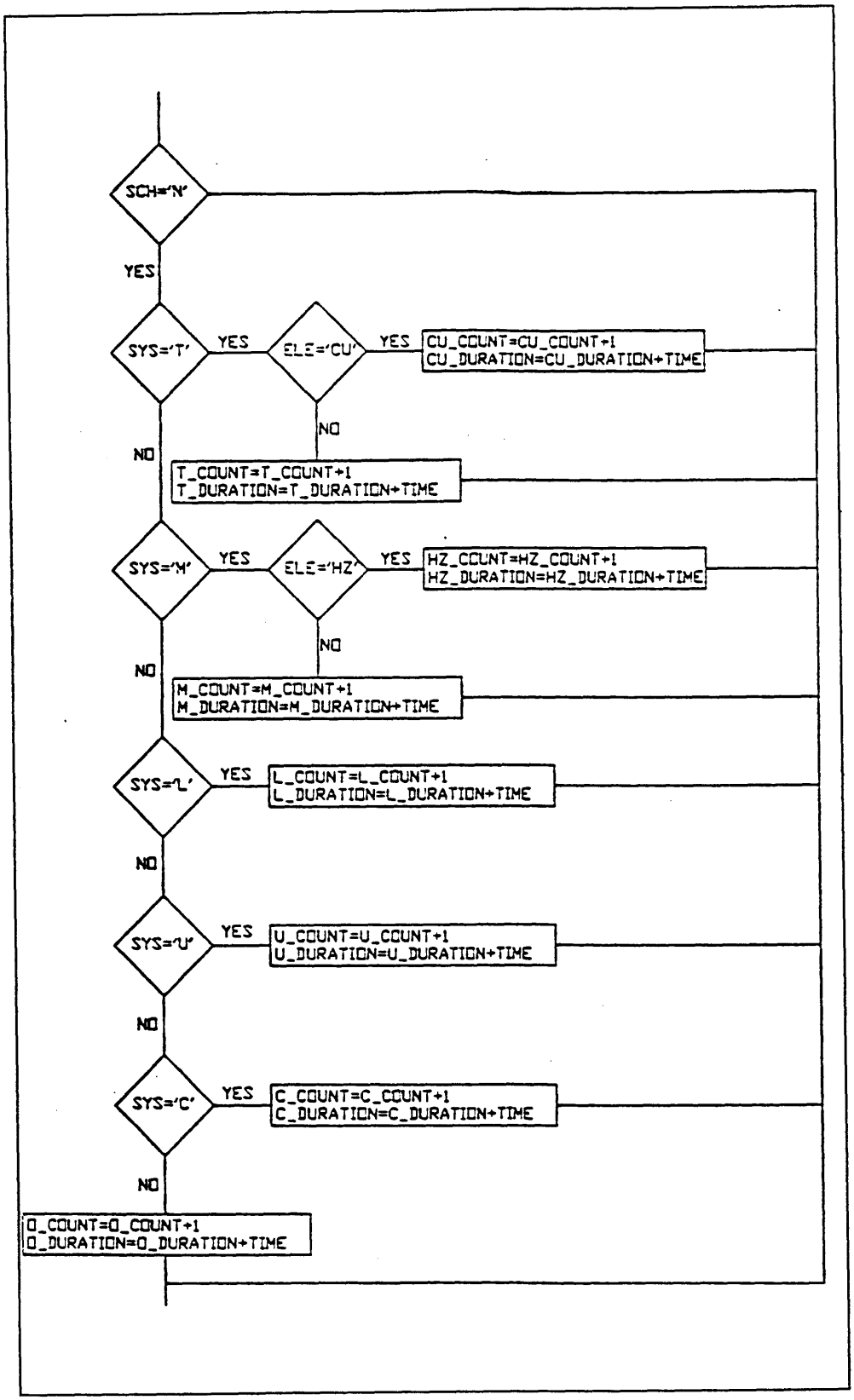

Figure 3.1: Algorithm of Preliminary Analysis

Based on the field experience, the following downtime categories were selected as the variables most likely to show some correlation with the total hardness:

- TBM mechanical system (T-system);
- Cutters (T-system, CU-element) - a component of the TBM mechanical system (T-system), assumed to show behavior different from the T-system failure data;
- Muck removal system (M-system);
- Horizontal conveyor (M-system, HZ-element) - a component of the muck removal system (M-system) assumed to show the behavior different from the M-system failure data;
- Support installation system (L-system).

The statistical analysis tools allow the researcher not only to test the assumptions made at the beginning of a research, but to obtain qualitative characteristics serving as an evidence in favor or against the hypothesis. These will be presented in Chapters 4 and 5. The second important task was to create a dataset that would contain the rock testing data. The coring locations were spaced 250 feet along the tunnel, which makes the total hardness data discrete. Therefore, to convert the discrete data into continuous information the total hardness value was assumed to be constant within the midpoints of the adjacent locations. The borders of the interval were defined as follows:

if there are three consecutive ID-points (coring locations) ID(i-1), ID(i) and ID(i+1), then

$$\text{Left Border}(i) = \text{ID}(i-1) + [\text{ID}(i) - \text{ID}(i-1)]/2$$

$$\text{Right Border}(i) = \text{ID}(i) + [\text{ID}(i+1) - \text{ID}(i)]/2.$$

Thus follows the total hardness data set format (see Figure 3.2):

- ID Station - point along the tunnel at which the rock sample was cored;
- Left Border - station corresponding to the closest to the shaft point along the tunnel defining the window within which total hardness is assumed to be constant;
- Right Border - station corresponding to the closest to the face point along the tunnel defining the window within which total hardness is assumed to be constant.

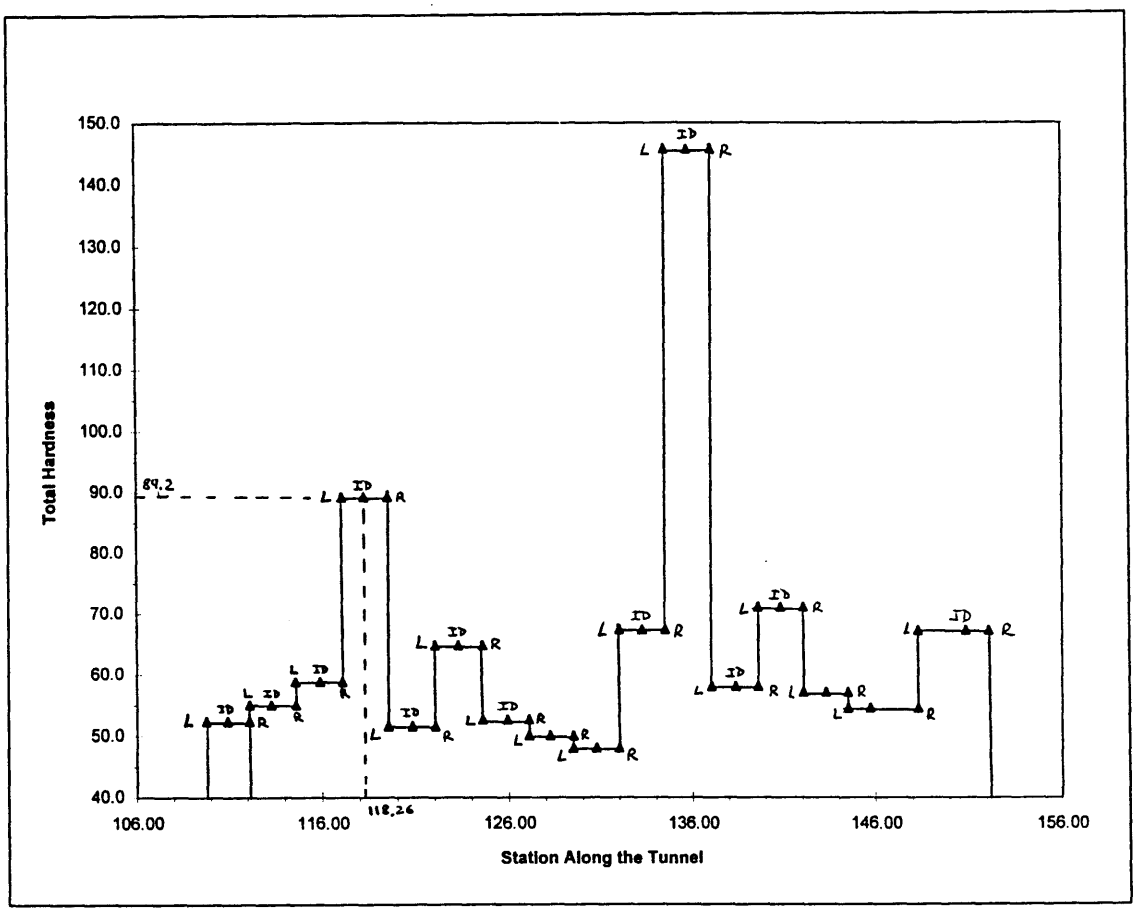

Figure 3.2: Rock Total Hardness Model

3.2 Data Analysis

Since purpose of this research is to find possible correlations between failure categories and total hardness, the window, within which total hardness is assumed to be constant, became the interval of interest for the analysis. The parameter that connects two datasets used for the analysis is the location along the tunnel, namely the tunnel station. For the downtime data set that is the start station and the end station. For the rock total hardness data set these are the left and right borders of the interval. Each total hardness interval includes several shift-based records, as shown on Figure 3.3:

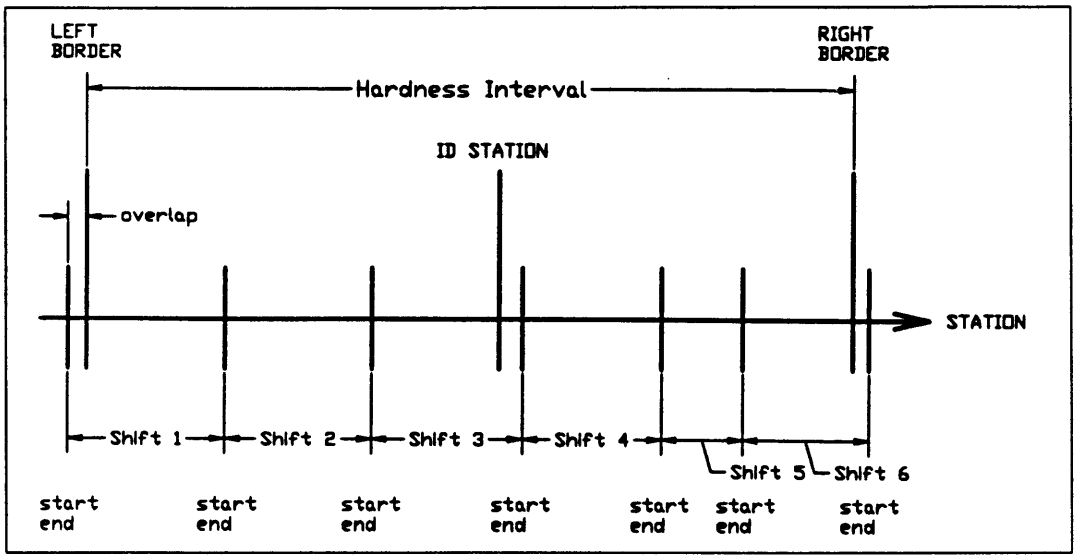

Figure 3.3: Graphic Illustration of the Combining the Hardness and Downtime Data Sets

To account for the non-uniform interval length, the total number of failures was normalized by the interval length. This parameter was defined as Local Failure Rate (LFR) = Number of Failures / Length of the Interval. Thus, the created data sets contain as many records as the total hardness data set. Each record contains the ID station, the hardness interval borders, the total hardness value, and the total number of failures for each failure category. In searching for possible correlation between the categorized downtime and the rock total hardness, total hardness values were divided into the following intervals:

1. 0 <= total hardness < 20;
2. 20 <= total hardness < 40;
3. 40 <= total hardness < 60;
4. 60 <= total hardness < 80;
5. 80 <= total hardness < 100;
6. 100 <= total hardness < 120;
7. 120 <= total hardness < 140;
8. 140 <= total hardness < 160.

For each of the above described interval the average failure rate was computed as follows:

$$FailureRate = \frac{\sum_{i=1}^{N} NF(i)}{\sum_{i=1}^{N} L(i)},$$

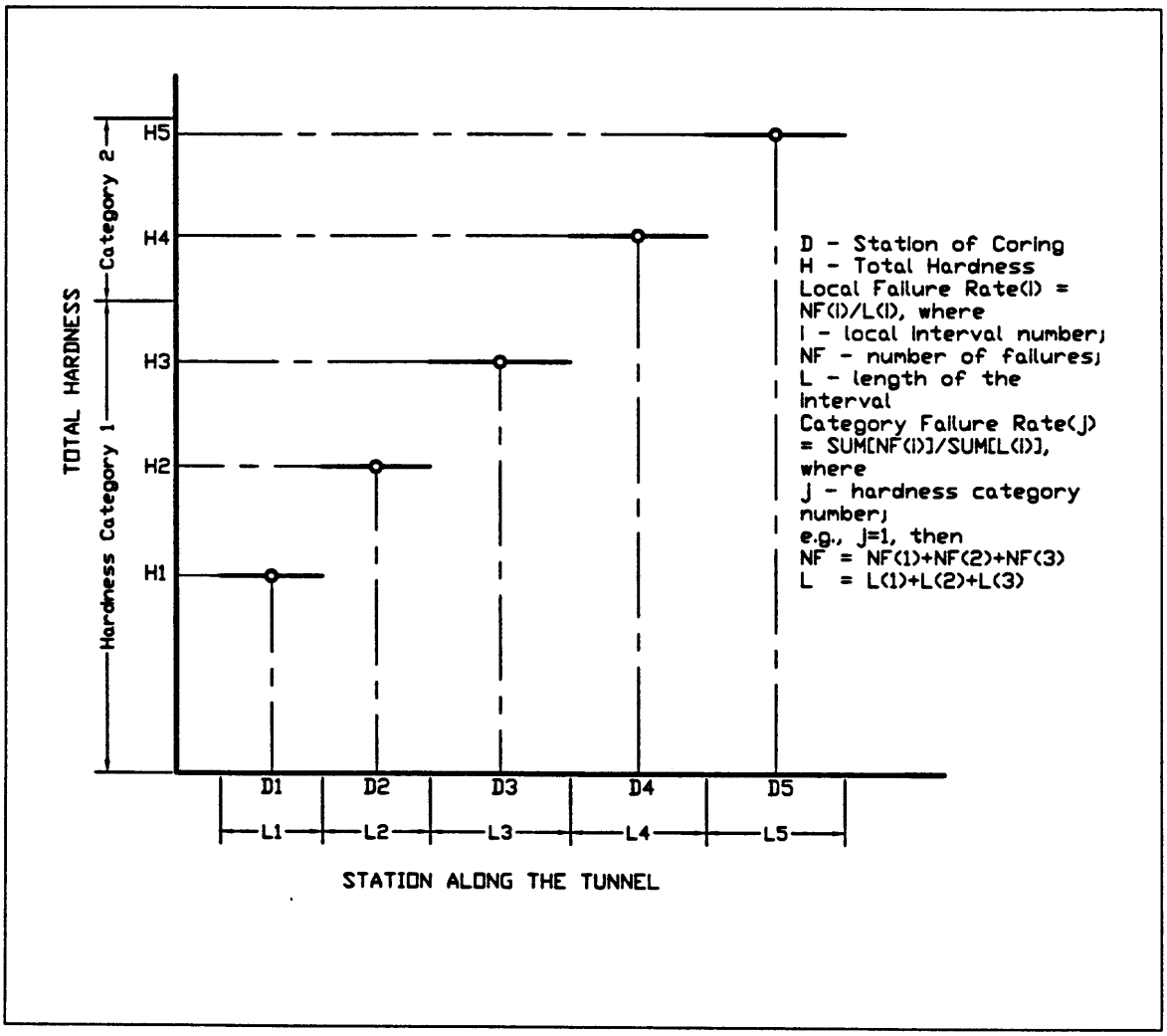

Figure 3.4: Graphic Illustration of Local and Generalized Failure Rates

where NF - number of failures, calculated over the local total hardness interval, defined above; L - length of the local interval; N - number of local intervals (see Figure 3.4). This parameter will be referred to as generalized failure rate (GFR). By plotting the

generalized failure rate against the total hardness interval number (category number), one can visually assess the correlation, and get an idea about the nature of a function that could describe this correlation. Another use of the GFR rate is to calculate the residuals of local failure rates as follows: $R = LFR - GFR$, and use them for detection of outliers.

After determining which downtime categories correlate with total hardness, regression analysis was performed, and quantitative regression parameters were obtained (see Appendix 2 for background information). The analysis of the occurrence probability of a particular failure type was performed using the logistic regression procedure of the SAS System.

The general sequence of data investigation described in this chapter was repeated several times to compare different types of rock hardness data available:

- CM (Construction Management) test boring program
  1. L-core data (samples drilled in a direction perpendicular to the tunnel alignment) including Diabase samples;
  2. L-core data for Argillite only;
  3. E-core data (samples drilled in a direction parallel to the alignment) for all rock types;
  4. E-core data for Argillite only;
- Pre-bid exploration program data.

The results of the analysis along with the discussion of the outcomes are presented in Chapters 4, 5, and 6

Chapter 4

Results. Discussion of the outcomes

4.1 Introduction

The main problem addressed in this chapter is distinguishing those failure categories that are impacted by the total hardness. One would also be interested in modeling a relation with a function with the known mathematical properties. The following graphical representations were produced using the technique described in Chapter 3:

- generalized failure rate (GFR) vs. rock hardness category - illustrates the failure rate change for the total hardness value groups, as opposed to the individual total hardness data points (see Chapter 3 for the total hardness group definition);
- residuals of LFR vs. rock total hardness - shows the dispersion of the individual data points from the average (GFR in this case);
- local failure rate (LFR) vs. rock total hardness - actual failure data points distribution.

Based on the visual inspection of these plots, the failure categories showing the signs of a correlation were subjected to a regression analysis. The set of plots described above was produced for L-core data set (total hardness values obtained as a result of the index tests performed on the samples drilled in a direction perpendicular to the direction of mining) as well as E-core data set (total hardness values obtained as a result of the index tests performed on the samples drilled in a direction parallel to the direction of mining). In addition, to investigate the impact of the Diabase intrusions into mostly homogeneous (Argillite) rock mass, two subsets were created out of each dataset: one containing all the data points, and the other that contained only Argillite samples.

4.2 L-core Data Set Analysis Results

As was described in Chapter 3, the entire range of the rock total hardness values was divided into eight categories. The following histograms (Figures 4.1 and 4.2) show the total hardness distribution along the tunnel in terms of the length.

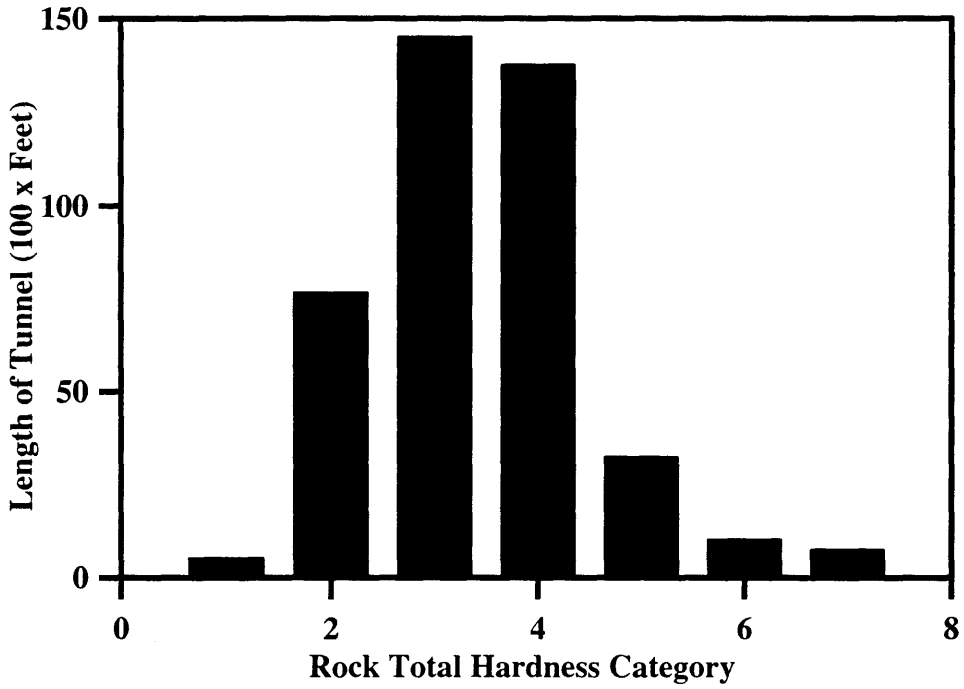

Figure 4.1: Rock Total Hardness Distribution Along the Tunnel (All Data)

These figures (Figures 4.1 and 4.2) can be interpreted as follows:

Data Set	Total Length	Percent	Length of 20<=Ht<120	Percent	Length of 0<Ht<20 Ht>120	Percent
All Data	41161 ft.	100	39894 ft.	97%	1267 ft.	3%
Argillite	38580 ft.	100	37816 ft.	98%	764 ft.	2%

Table 4.1: Total Hardness Distribution Along the Tunnel

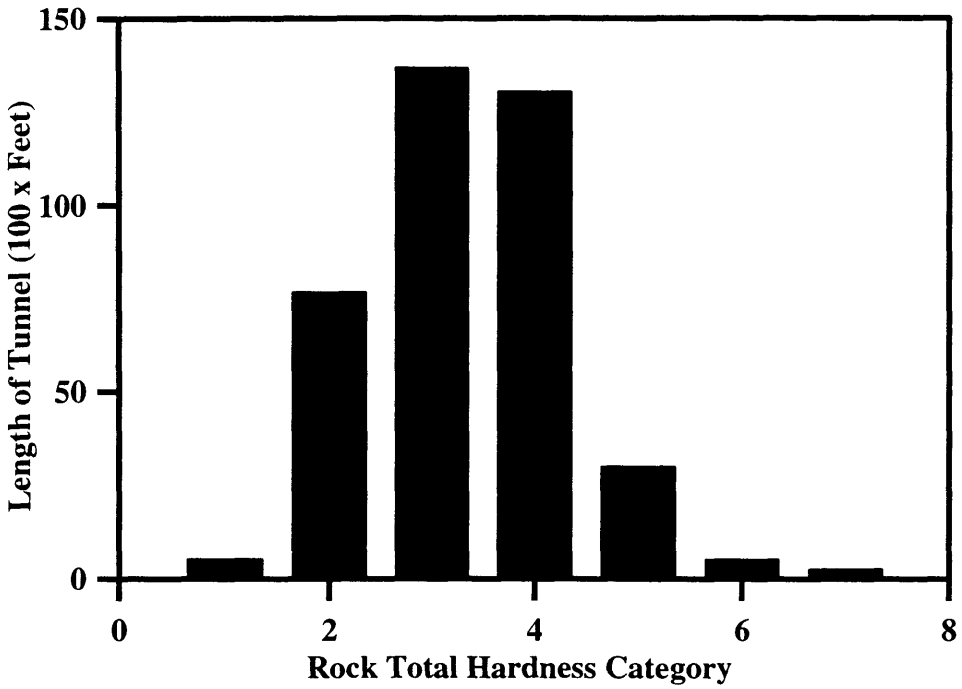

Figure 4.2: Rock Total Hardness Distribution Along the Tunnel (Argillite Data)

The results are as follows:

1. T-system (TBM drive motors, electrical, hydraulic systems only) related failures

The GFR plots (see Figures 4.3 and 4.4) show that T-system failure rate tends to decrease with increasing total hardness. The points representing the categories 1 (0<=hardness<20) and 7 (120<=hardness<140) do not seem to belong to the same population as the other ones. These categories can be ignored or assumed to be outliers, since they represent between 2% and 3% of the general population. Therefore, the model function would be monotonically decreasing and non-linear. Another observation is that the Diabase data points behave in the same way as the Argillite data points of the same total hardness.

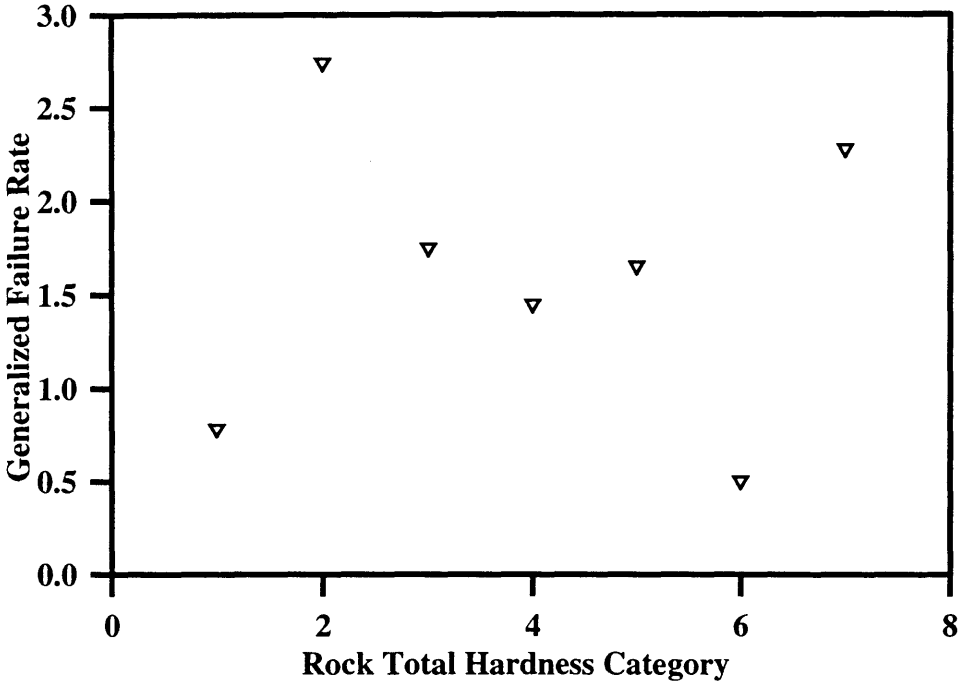

Figure 4.3: Generalized Failure Rates for T-system Failures (All Data)

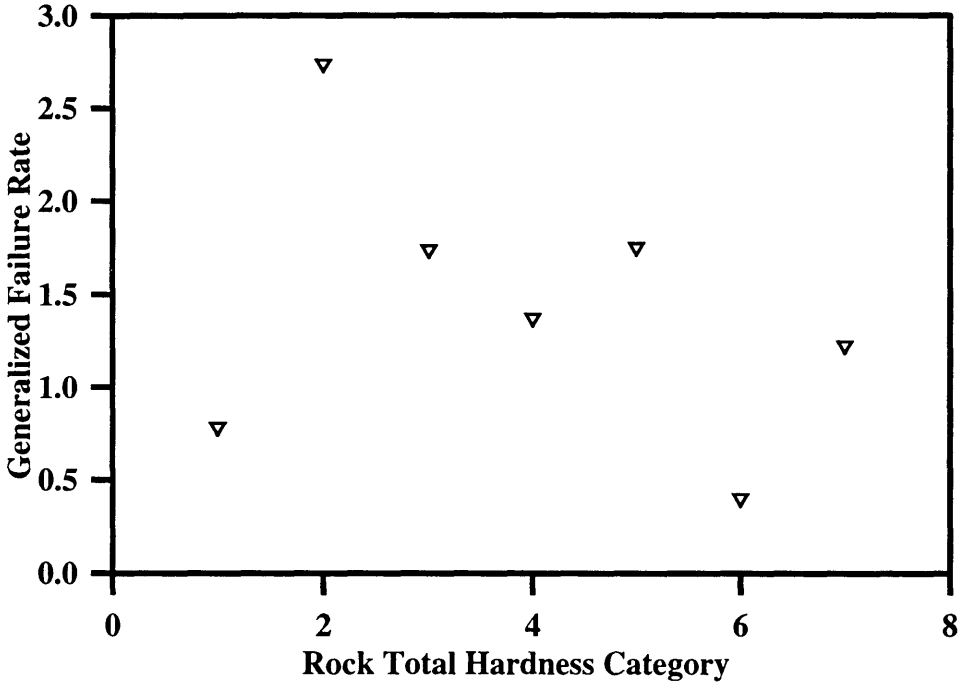

Figure 4.4: Generalized Failure Rates for T-system failures (Argillite Data)

The residuals of the individual local failure rate (see Figures 4.5 and 4.6) points show that except for two unusually high value data points the data are consistent and GFR repre-

sent the data well.

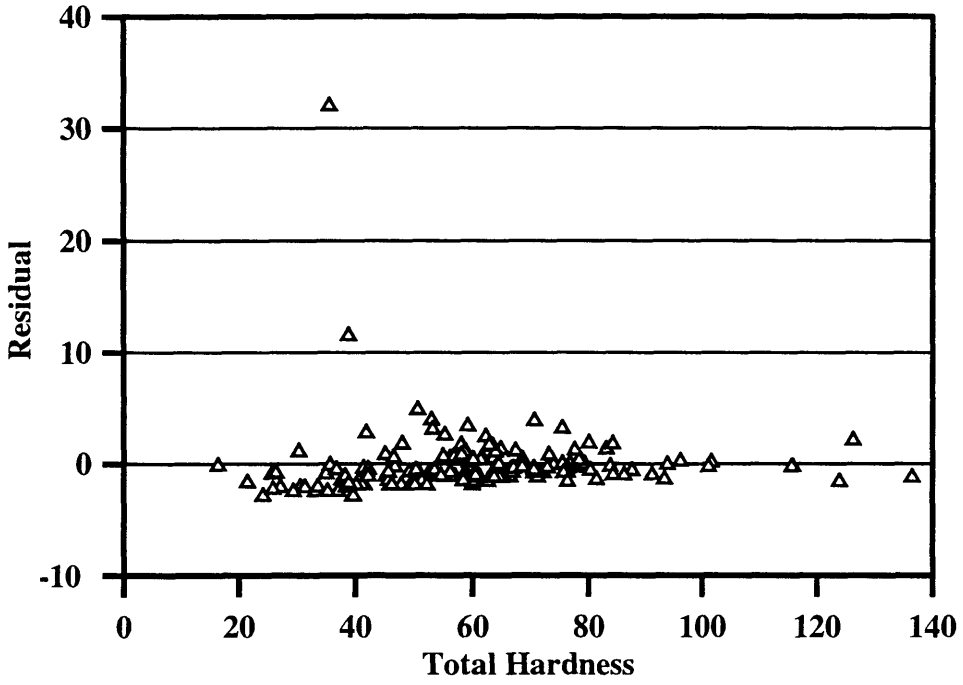

Figure 4.5: T-system LFR residuals (All Data)

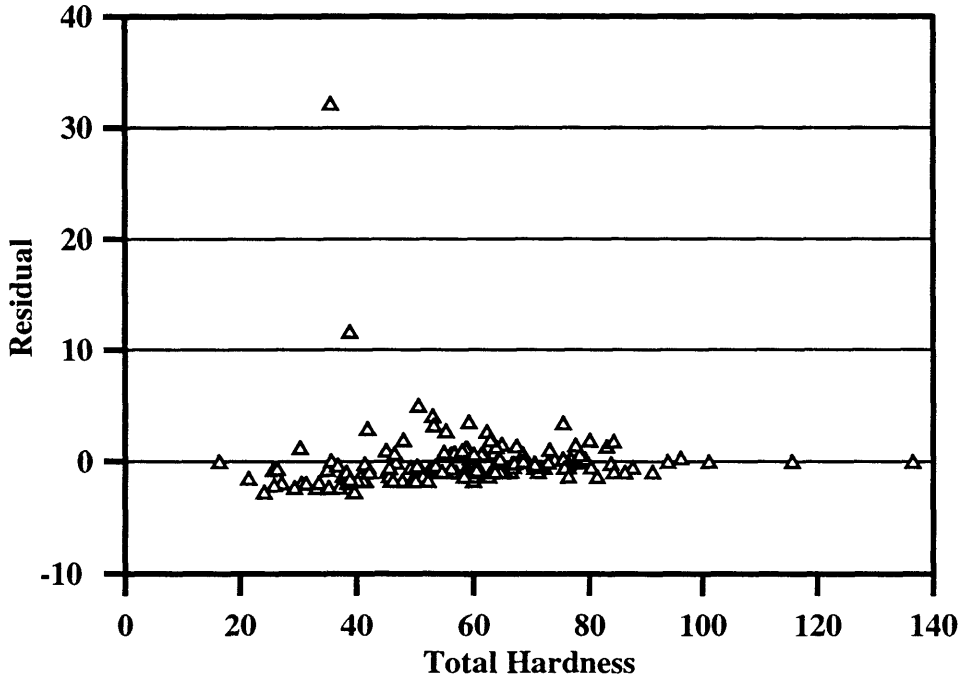

Figure 4.6: T-system LFR residuals (Argillite Data)

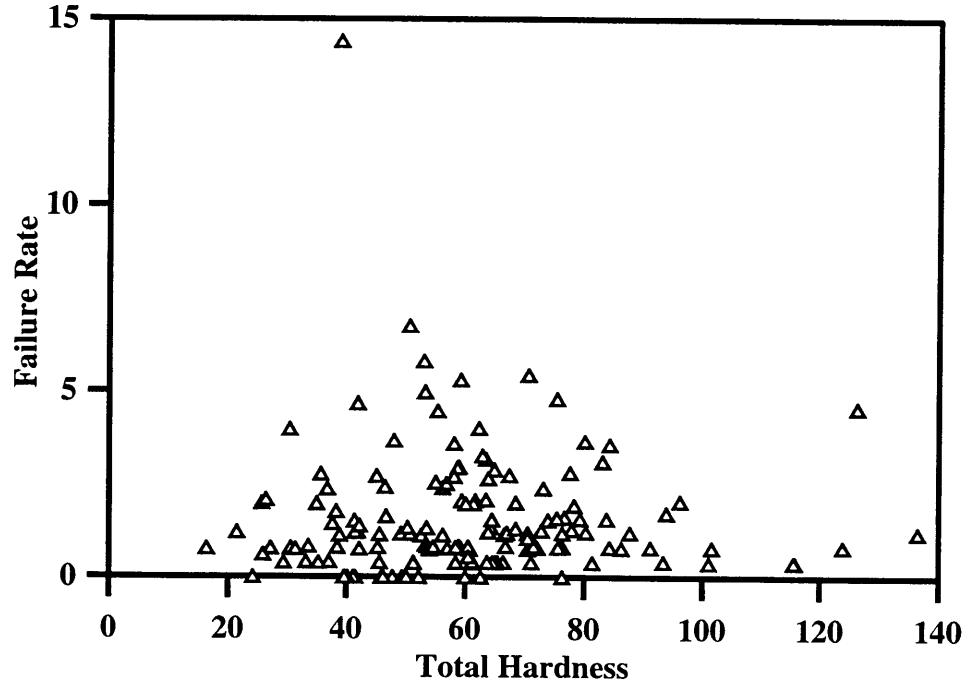

Figure 4.7: T-system Local Failure Rates (All Data)

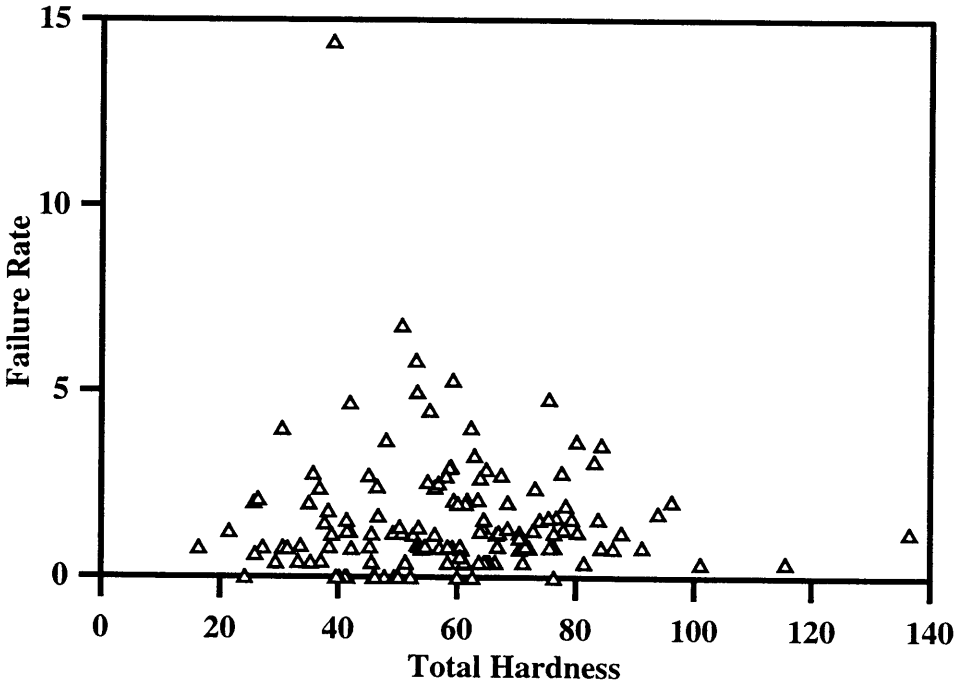

Figure 4.8: T-system Local Failure Rates (Argillite Data)

The LFR plots (see Figures 4.9 and 4.10) show that there is a failure rate decrease as the total hardness increases, which becomes more clearly expressed starting at Ht = 40. Another observation is that the highest failure rate (after the elimination of the outlier) belongs to the Argillite sample, since it appears on both figures.

2. CU-element (cutters only) related failures

The GFR plots (Figures 4.9 and 4.10) for cutter related failures lead to the conclusion that downtimes caused by cutters increase with increasing total hardness, except for the last data point which as in case of T-system failures, falls out of the general population. The residuals plots (Figures 4.11 and 4.12) indicate that the variance or dispersion increases with increasing total hardness, which supports the fact that as far as the cutters are concerned, the harder the rock, the more uncertain the reliability of the cutters. Comparing the Figures 4.11 and 4.12 one would conclude that although Diabase samples have generally greater total hardness values, the behavior of the Argillite and the Diabase samples of the same total hardness is very similar. Figures 4.13 and 4.14 present the LFR plots. It can be concluded from the examining of those figures that the increasing total hardness not only causes higher failure rate but also greater data dispersion thus increasing the uncertainty.

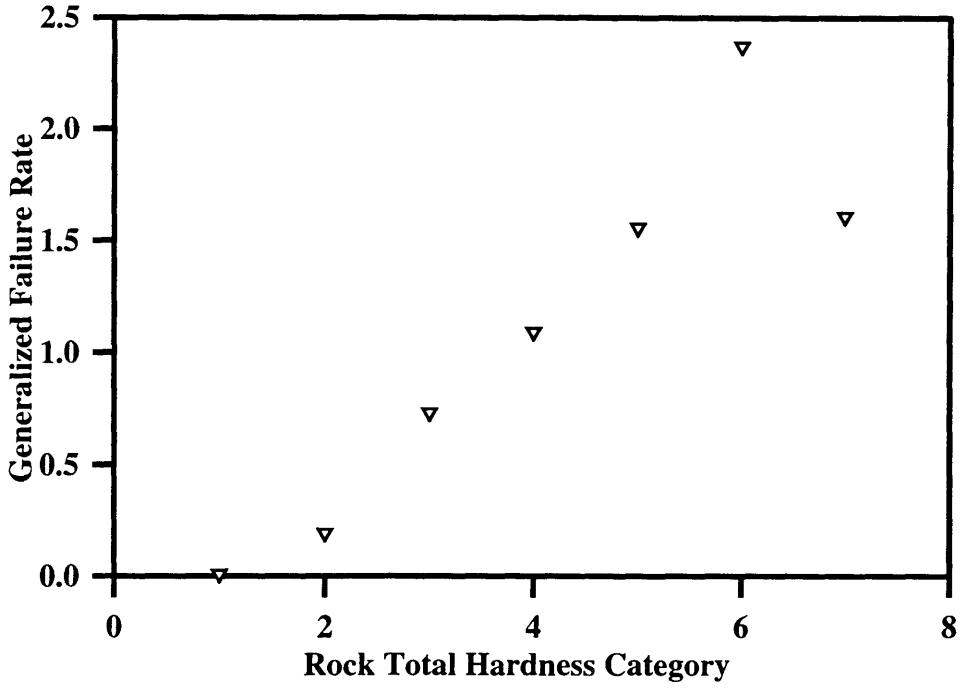

Figure 4.9: Generalized Failure Rates for T-system, CU-element (All Data)

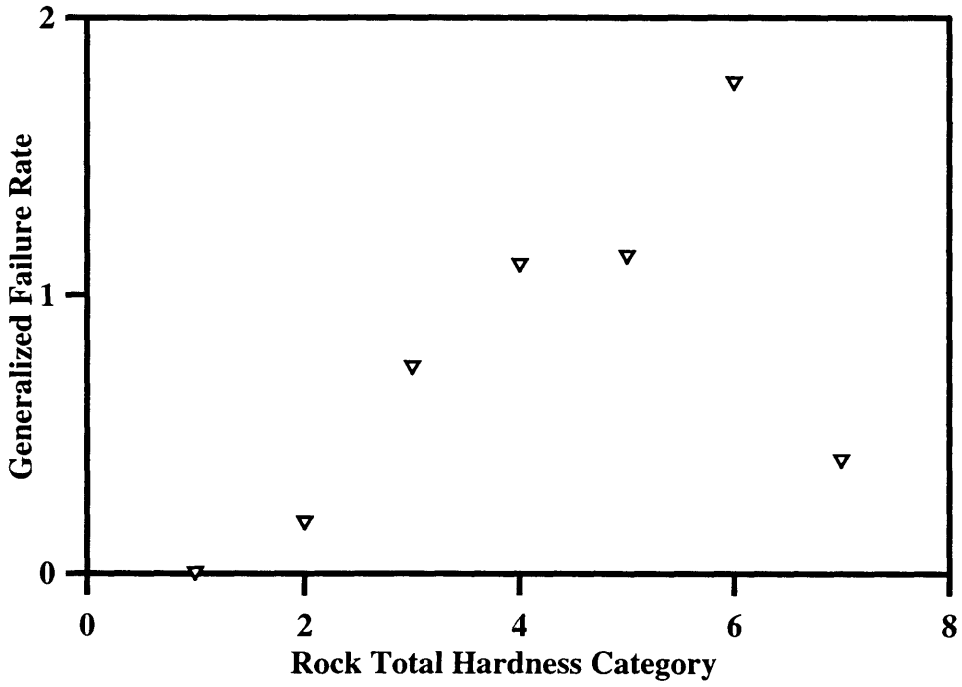

Figure 4.10: Generalized Failure Rates for T-system, CU-element (Argillite Data)

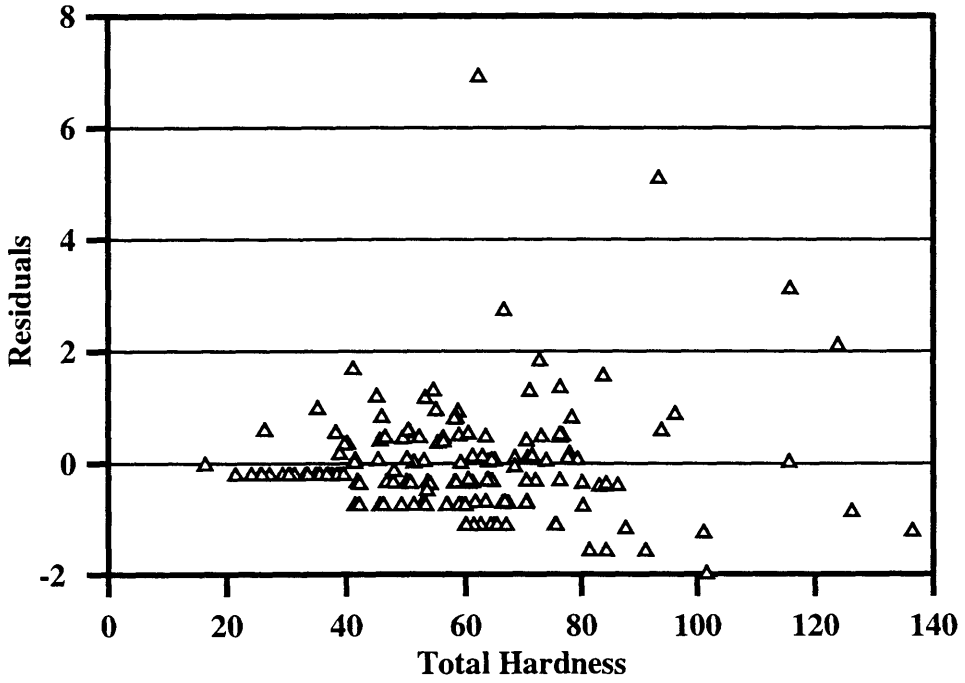

Figure 4.11: T-system, CU-element LFR Residuals (All Data)

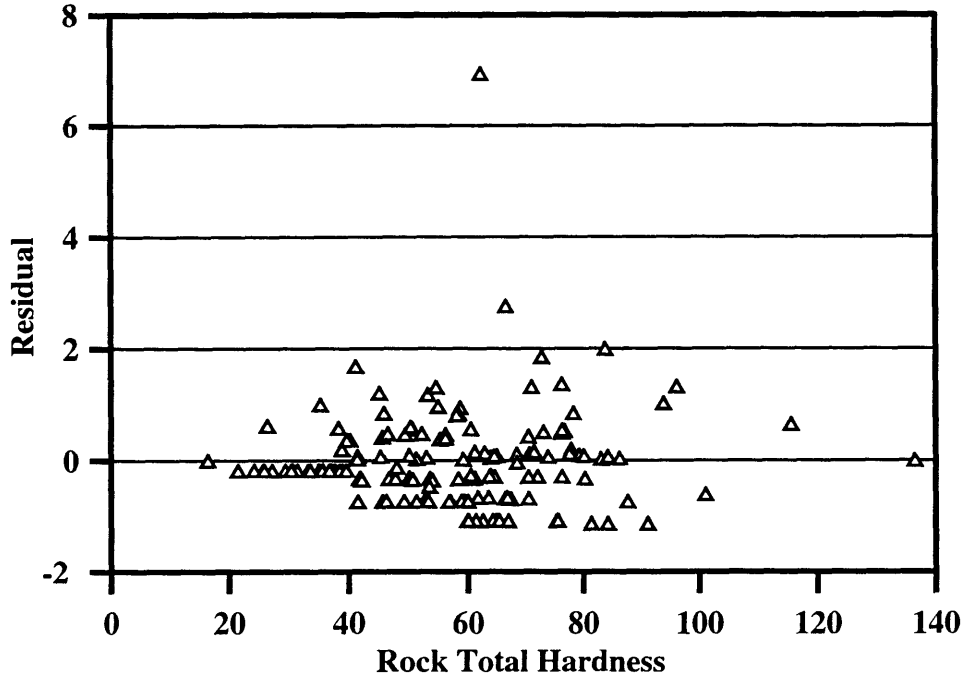

Figure 4.12: T-system, CU-element LFR Residuals (Argillite Data)

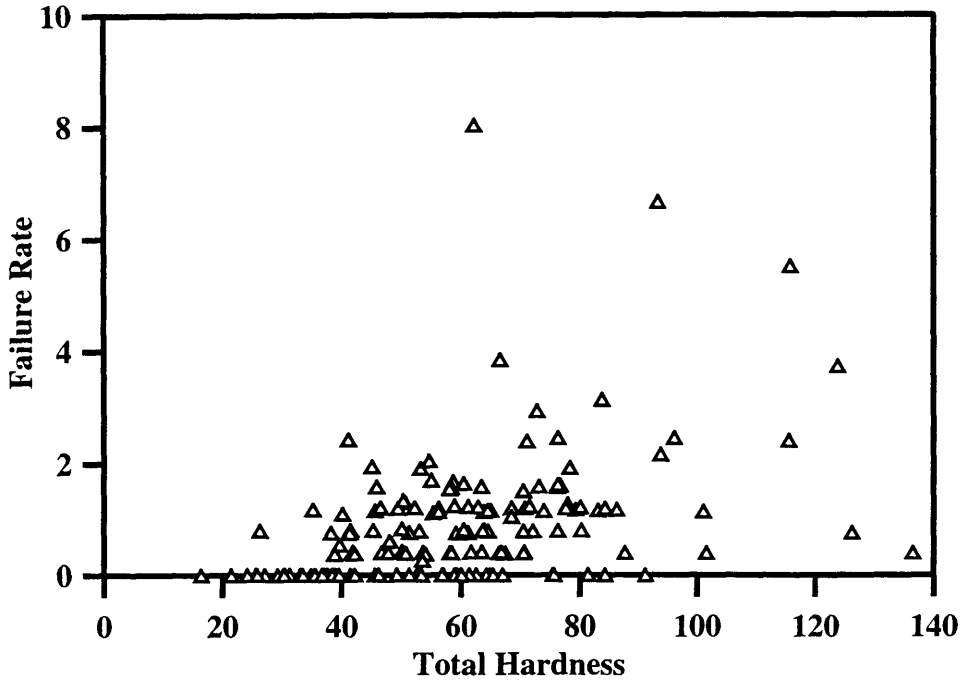

Figure 4.13: T-system, CU-element Local Failure Rate (All Data)

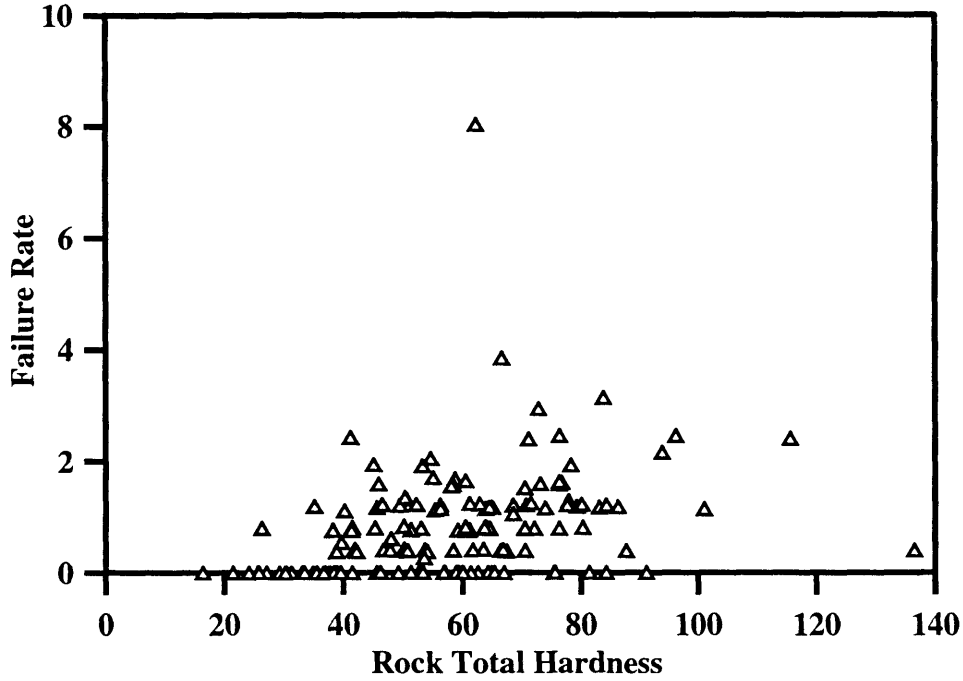

Figure 4.14: T-system, CU-element Local Failure Rate (Argillite Data)

3. M-system (muck removal system, excluding horizontal conveyor) failures.

The GFR plots (see Figures 4.15 and 4.16) show that failure rate decreases as rock total hardness increases, except for the category 7 (Ht>120), which as in previous cases, does not appear to belong to the same population as the rest of the total hardness data points. They also suggest the non-linearity of the modeling function. This downtime category as well as the T-system failures were subject to the so called Poisson regression analysis (see Appendix A). The residual plots (see Figures 4.17 and 4.18) show that the data are consistent and have no obvious outliers, although the dispersion is significant. The variance does not seem to change much as the hardness changes, which indicates that the average failure rates (GFR) can, in fact, substitute the individual data points (LFR). Finally, LFR plots show the actual data distribution (see Figures 4.19 and 4.20).

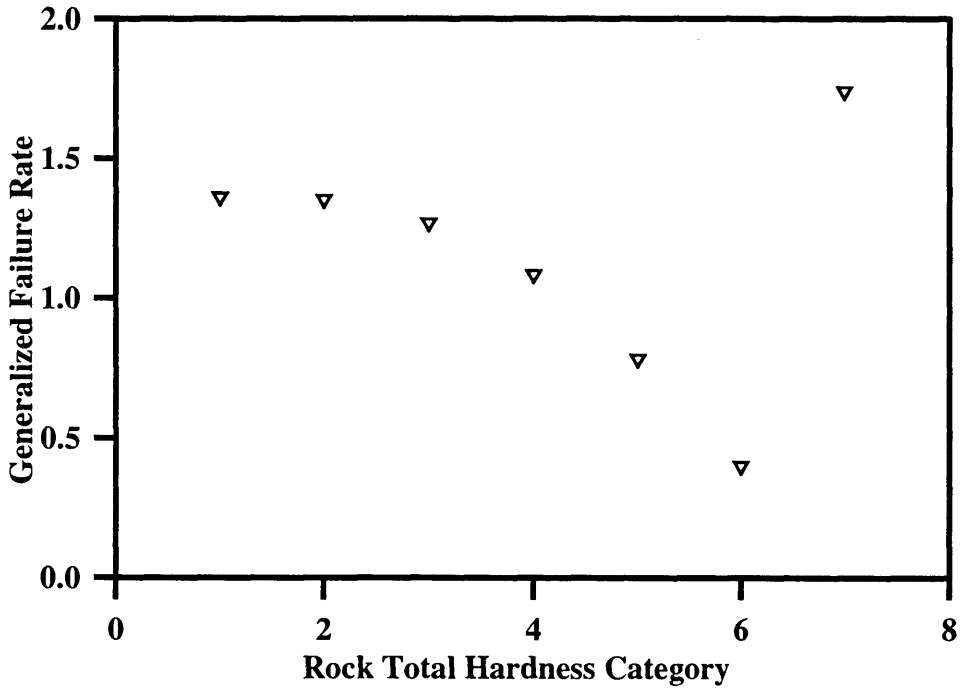

Figure 4.15: M-system Generalized Failure Rates (All Data)

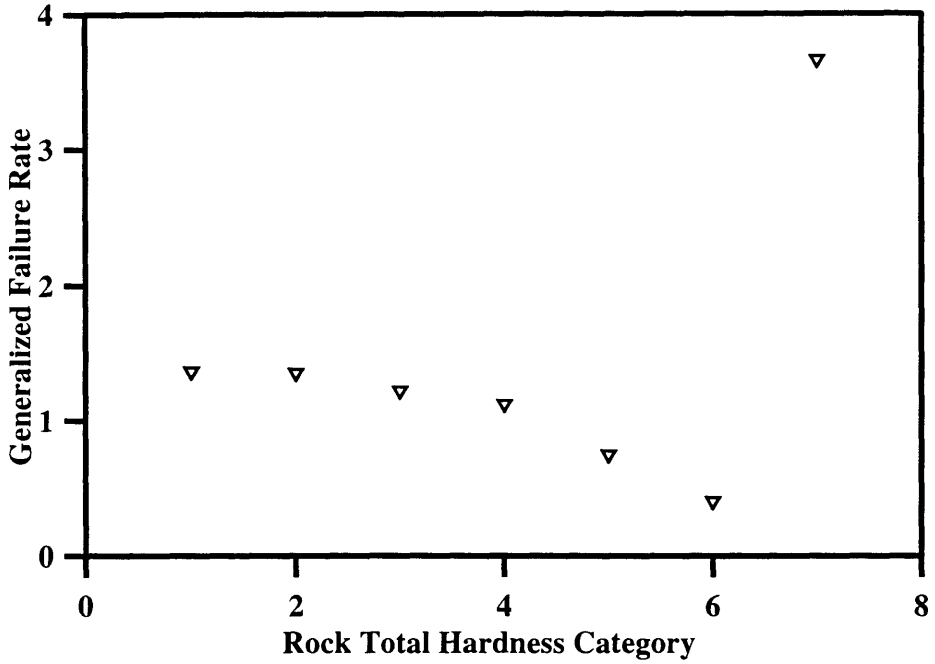

Figure 4.16: M-system Generalized Failure Rates (Argillite Only)

Examining the Figures 4.16 and 4.17 leads to the following conclusions:

- total hardness values greater than 120 are unusually high as far as this analysis is concerned, since they contradict with the general trend;
- Argillite sample data behavior is no different from that of the Diabase sample data points.

Figure 4.19 shows that the point for category 7 on Figure 4.15 was computed as an average of the three points having total hardness values greater than 120; two points were Diabase and one - Argillite. Figure 4.20 clearly shows just one point having the total hardness value greater than 120, and it is this point that produced the unusually high failure rate value at point 7 (Figure 4.16). One would assume that the Diabase, being a generally harder rock than Argillite, should cause more failures, but we do not see this here. Residual plots (see Figures 4.17 and 4.18) show that the error introduced as a result of the substituting the failure rates with their averages (GFR), is within plus/minus 2.

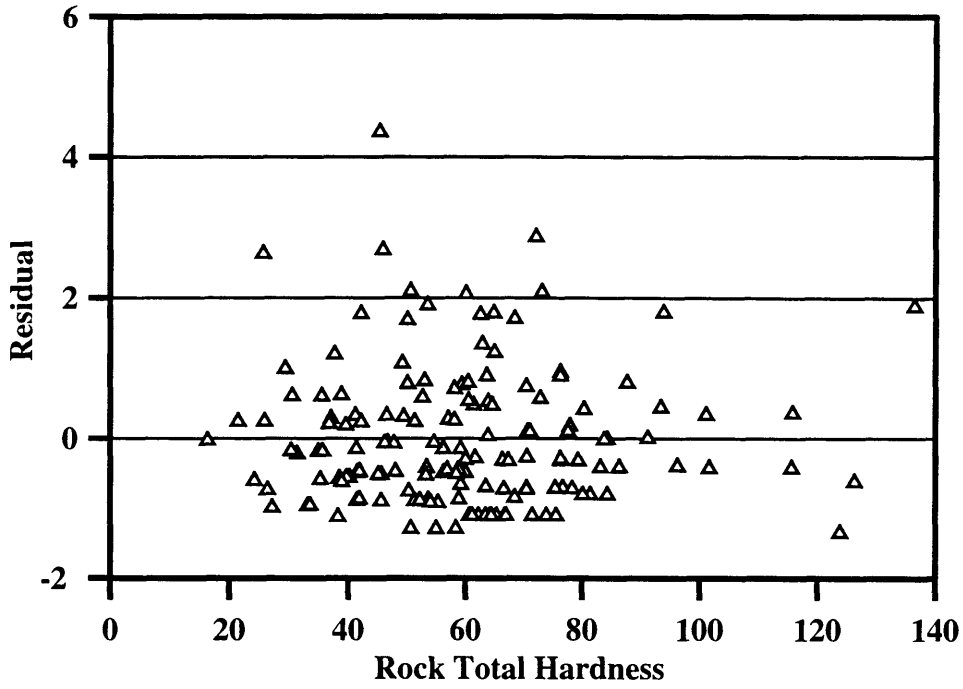

Figure 4.17: M-system LFR Residuals (All Data)

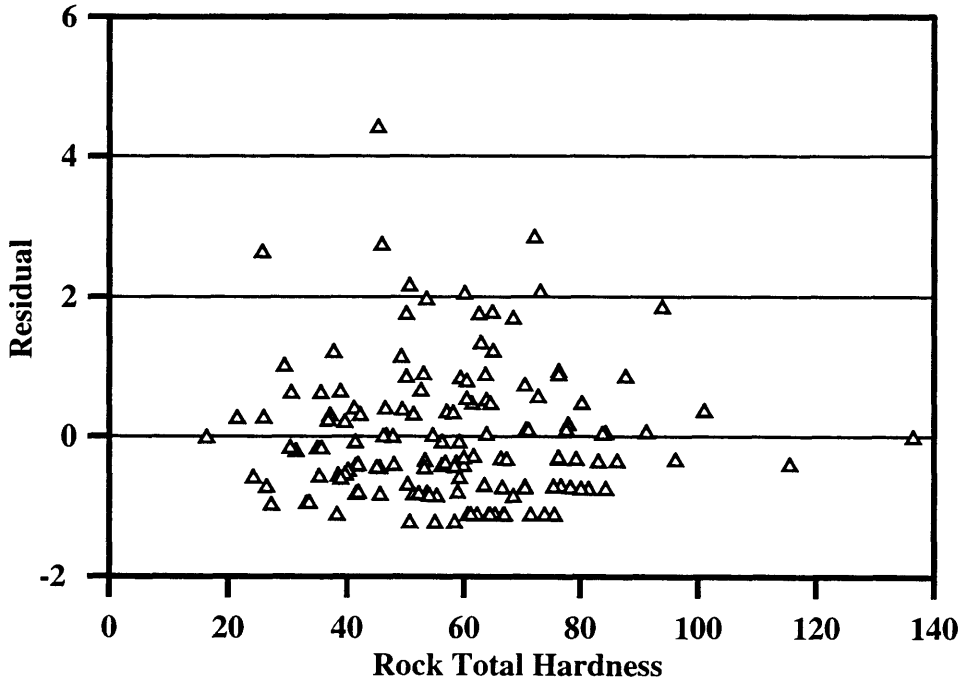

Figure 4.18: M-system LFR Residuals (Argillite Data)

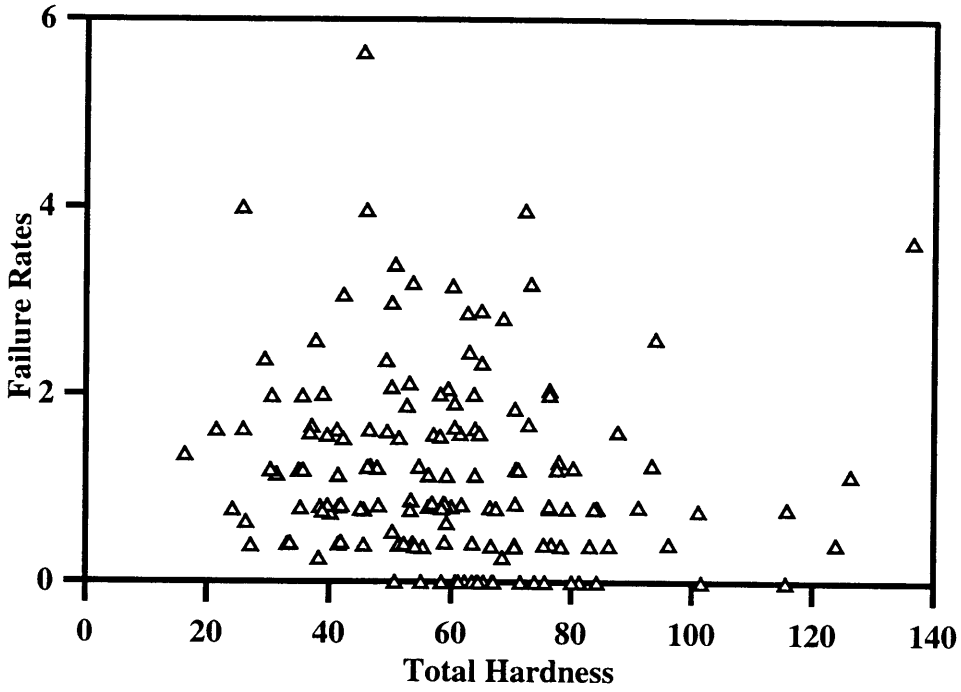

Figure 4.19: M-system Failure Rates (All Data)

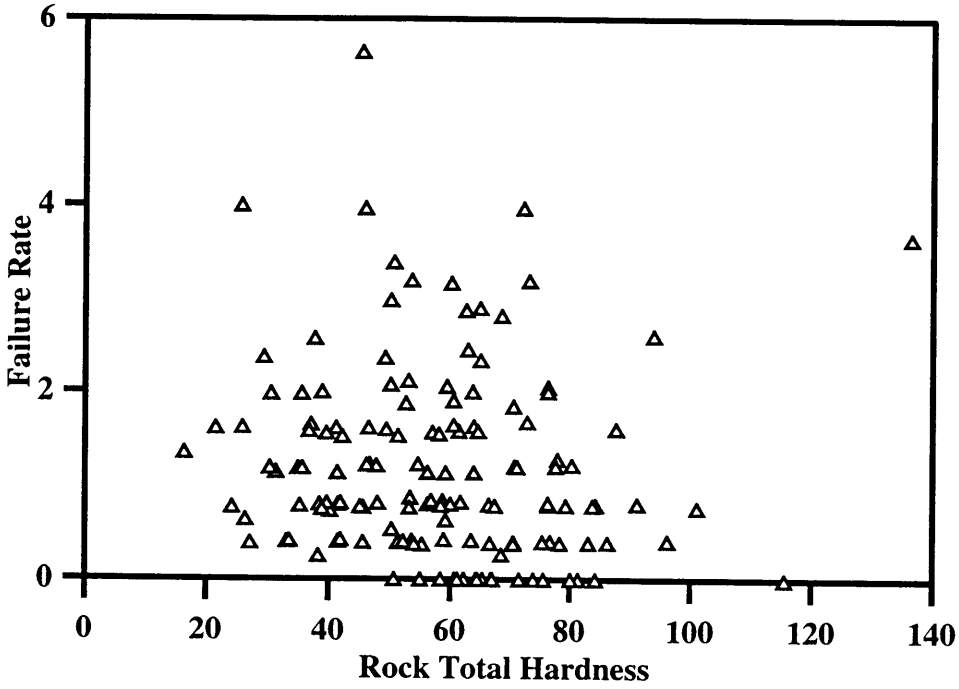

Figure 4.20: M-system Failure Rates (Argillite Only)

4. M-system, HZ-element (horizontal conveyor only) failures.

GFR plots for this failure category (see Figures 4.21 and 4.22) show that except for those already mentioned unusually high and unusually low data points corresponding to the hardness categories 1 and 7, HZ-element failure rate is constant. Individual data points are scattered around the value of 1. The muck removal system includes several conveyor types (horizontal, vertical, transfer etc.,) but only horizontal conveyor data having been separated from the population, showed constant failure rate, while the rest of the subsystems showed a non-linear decrease (see Figures 4.15 and 4.16). The horizontal conveyor transports the muck from the TBM to the tunnel shaft. It is an important part of the muck removal system, but it evidently shows a behavior different from the rest of the system. The reason is that the horizontal conveyor is engaged in the muck removal operation after the TBM conveyors. Therefore, blocky angular pieces of muck causing the TBM conveyors failure, would likely be removed before they reach the horizontal conveyor. Also, the space constraints are much more serious for the TBM conveyors than for the horizontal conveyor (see Figure 2.19). Thus, one could conclude that system components are fairly independent and can be looked at separately. They also may behave quite differently from each other. Having said that, the author would like to stress the point that as far as the reliability of the complex system is concerned, and a tunnel boring machine is indeed an example of one, it can be well represented as the sum of the individual subsystem reliabilities. Thus far, the data not only support that conclusion, but also illustrate it.

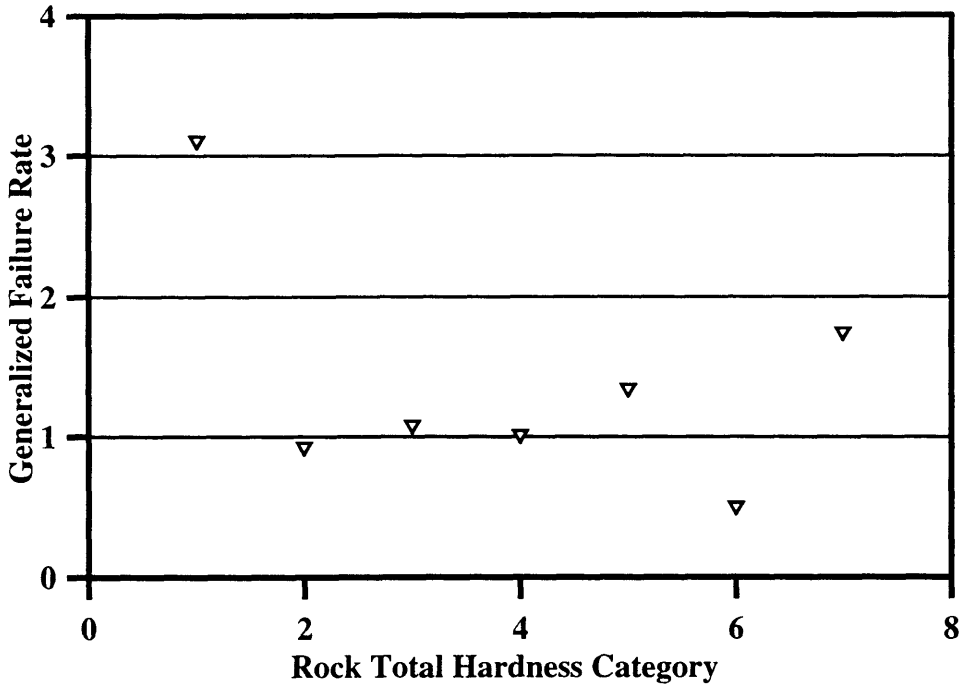

Figure 4.21: M-system, HZ-element Generalized Failure Rates (All Data)

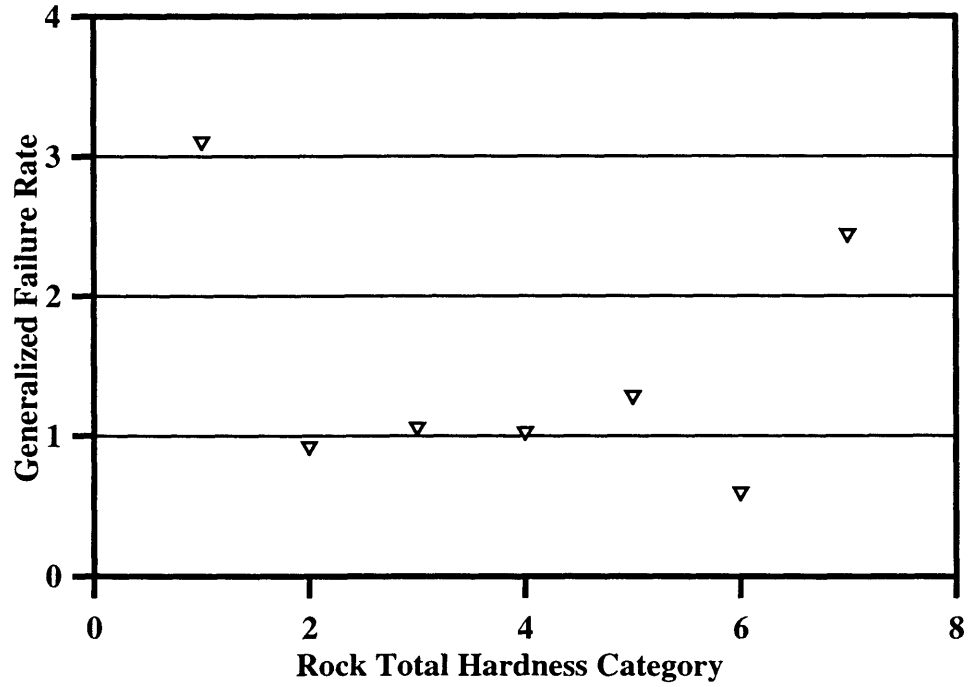

Figure 4.22: M-system, HZ-element Generalized Failure Rates (Argillite Data)

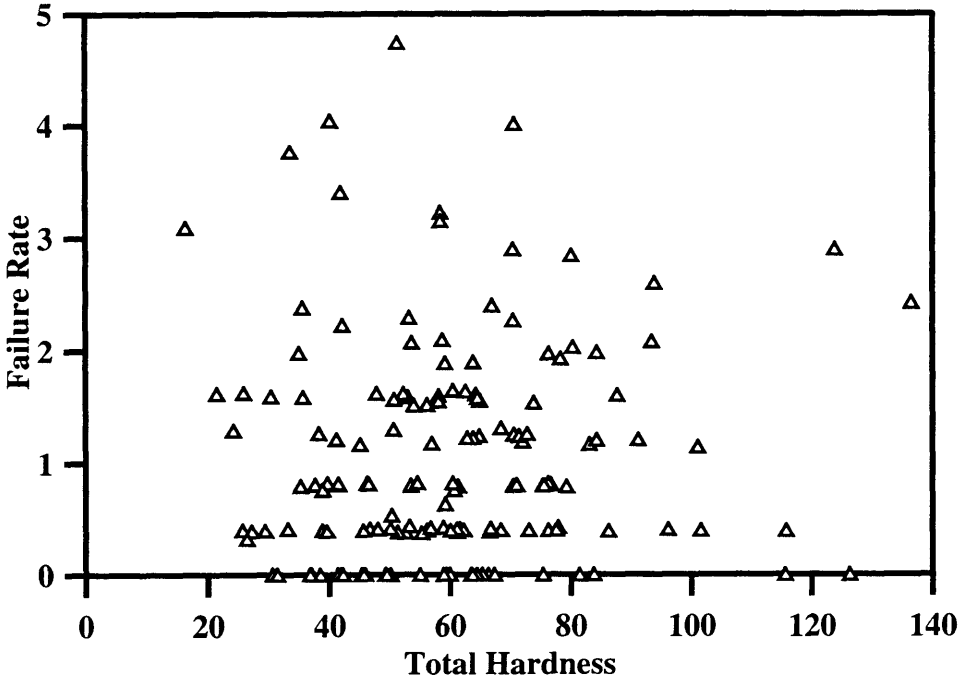

Figure 4.23: M-system, HZ-element Local Failure Rates (All Data)

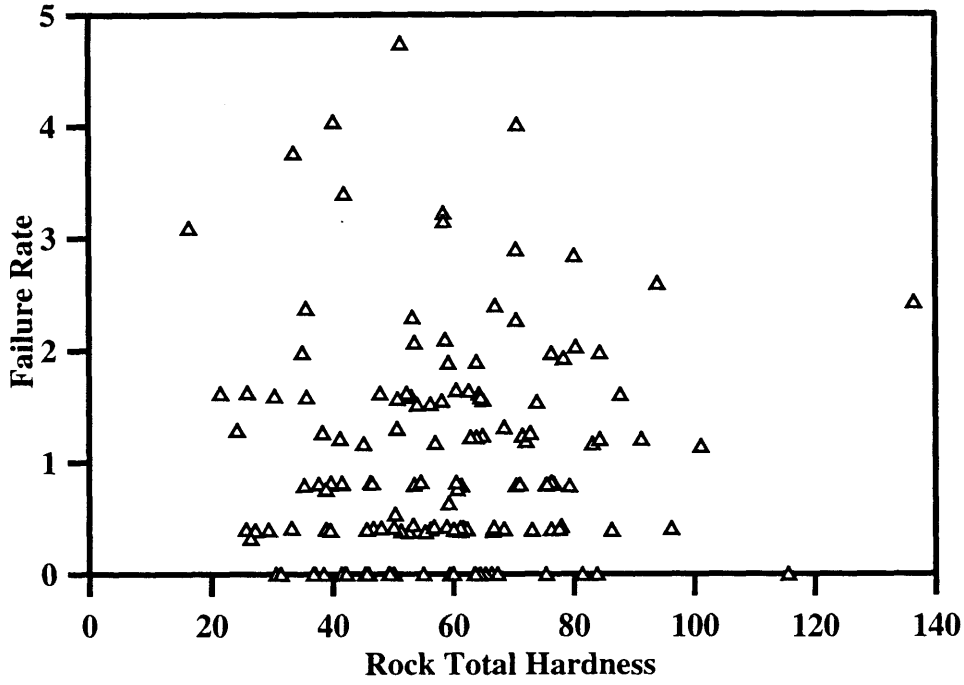

Figure 4.24: M-system, HZ-element Local Failure Rates (Argillite Data)

5. L-system (support installation systems) failures.

The GFR plots (see Figures 4.25 and 4.26) show no impact of the total hardness on the L-system failure rate. However, failure rate decreases substantially as tunnel excavation progresses (increasing station value). Figures 4.27 and 4.28 illustrate this phenomenon called "learning curve". The same crew performing the same operation, and encountering the same kind of problems, "learns" from the experience and does not repeat the same mistakes. This downtime category was subjected to the "Poisson Regression" analysis.

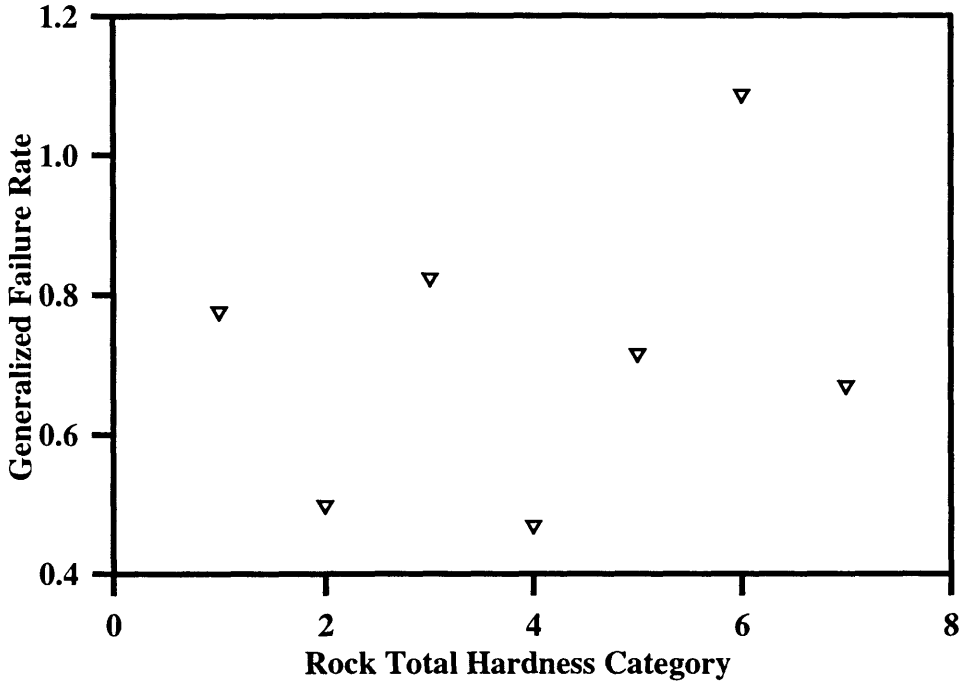

Figure 4.25: L-system Generalized Failure Rates (All Data)

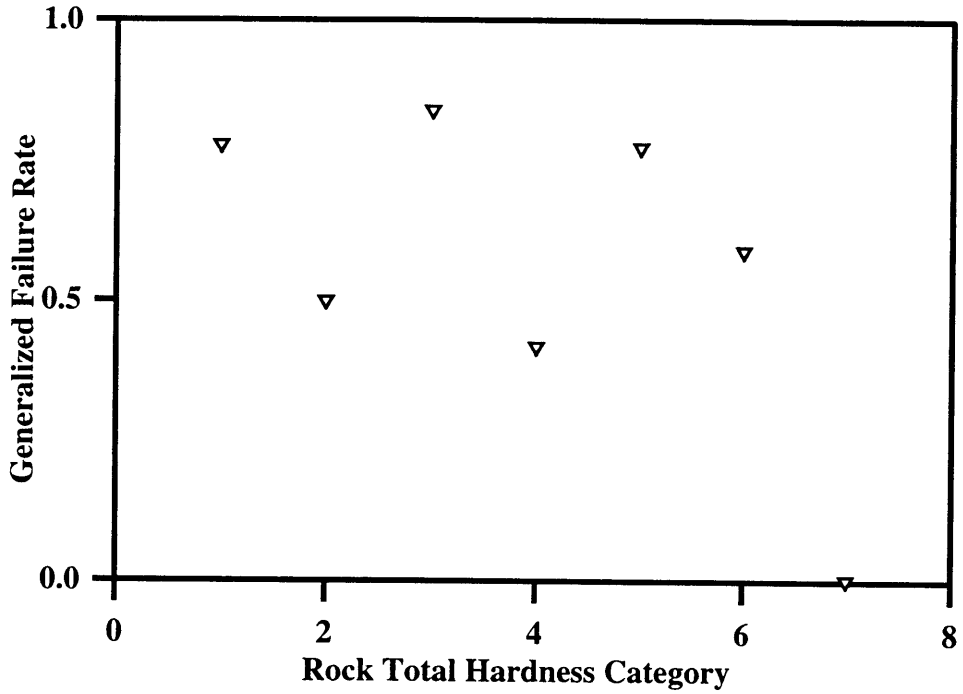

Figure 4.26: L-system Generalized Failure Rates (Argillite Data)

The following figures present the failure rate change with the tunnel progress i.e, TBM advance. The qualitative parameter defining the progress is station.

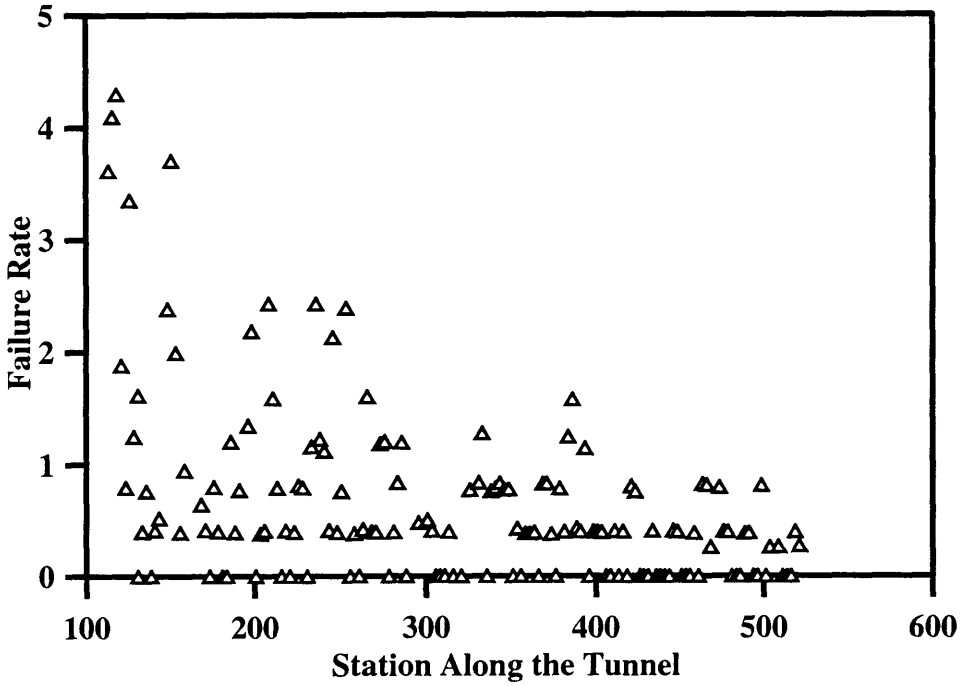

Figure 4.27: L-system Local Failure Rates (All Data)

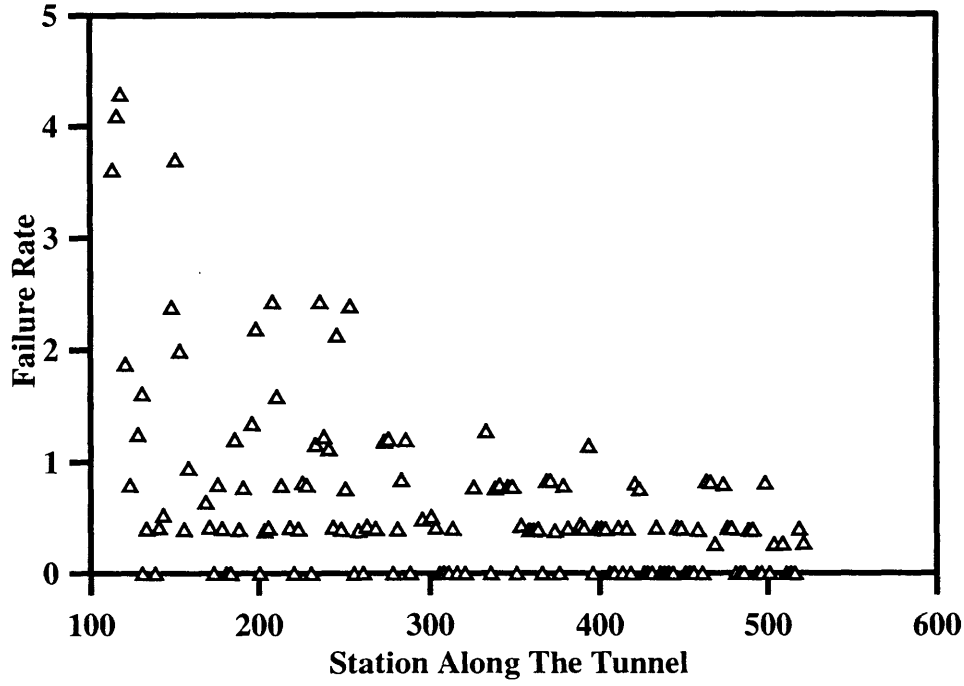

Figure 4.28: L-system Local Failure Rates (Argillite Data)

Based on the above, one can conclude:

- Tunnel Boring Machine failures have to be categorized by their cause in order to establish correlations to the rock properties;
- a Tunnel Boring Machine can be viewed as a mechanical system consisting of three major subsystems, namely the TBM mechanical system, the TBM muck removal system, and the TBM support installation system;
- when the algorithm for the analysis was constructed, the following assumptions were made: 1) cutters (CU-element), a subsystem of the TBM mechanical system (T-system), show behavior different from the rest of the T-system population; 2) horizontal conveyor (HZ-element), a subsystem of the TBM muck removal system (M-system) behaves differently compared to the M-system population;
- these assumptions have been proven to be true;
- data points for categories 1 and 7 in the GFR plots i.e., $0 < Ht <= 20$ and $120 < Ht <= 140$, do not follow the general trend, therefore the results obtained from the analysis are true for any value of the total hardness between 20 and 120;
- failure rates obtained from the data points representing the Diabase samples show the same behavior as the ones representing the Argillite samples with the same total hardness for all downtime categories;

4.3 E-core Data Set Analysis Results

The discussion that follows is arranged in the order established for L-core results.

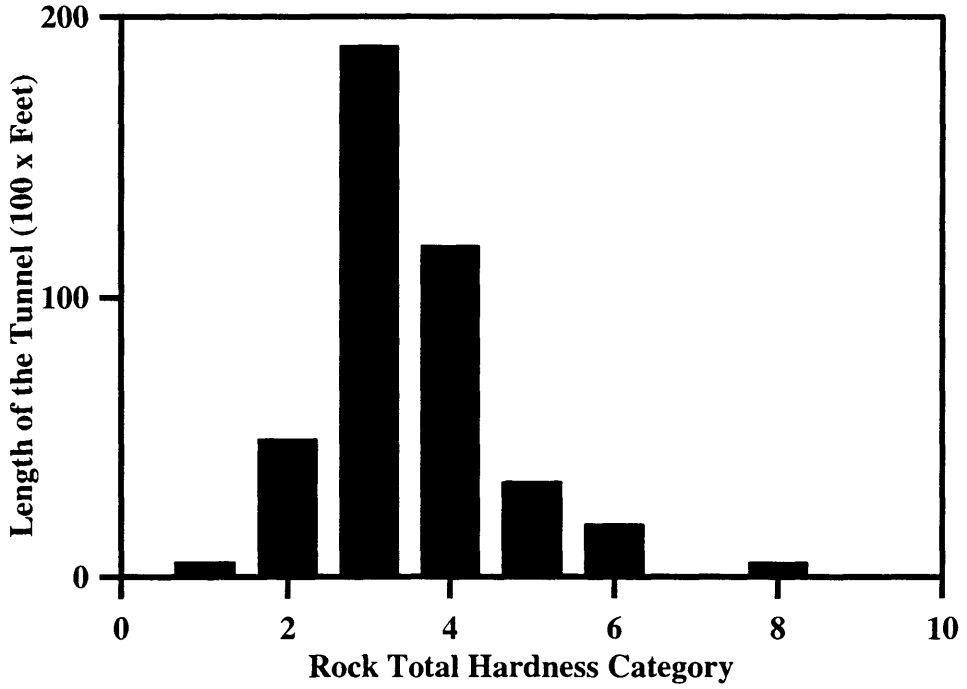

Figure 4.29: Rock Total Hardness Distribution Along the Tunnel (All Data)

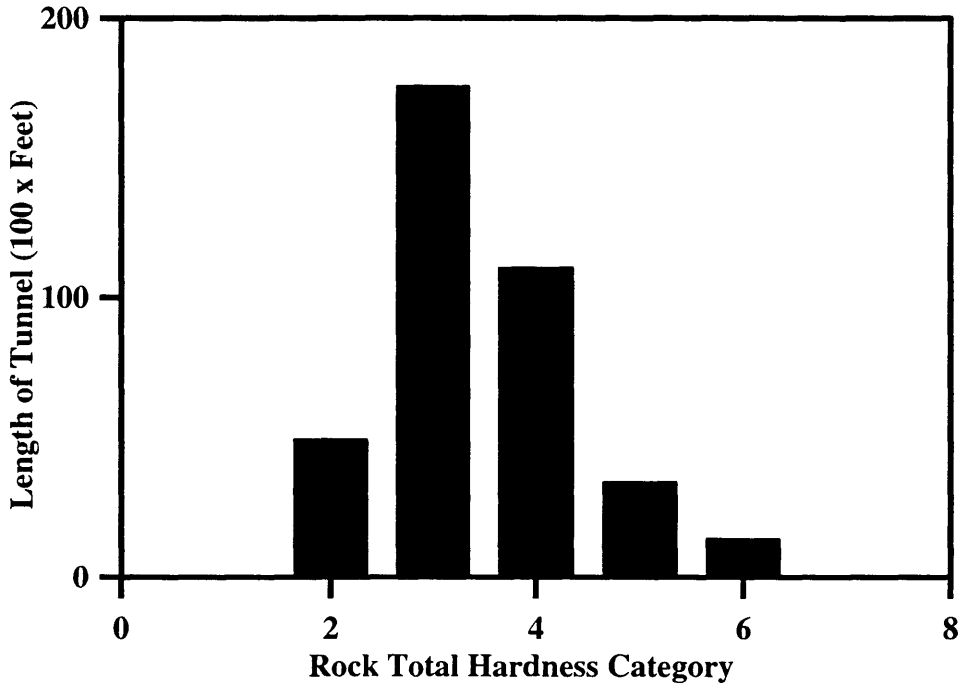

Figure 4.30: Rock Total Hardness Distribution Along the Tunnel (Argillite Data)

The interpretation of the Figures 4.30 and 4.31 is presented in the Table 4.2:

Data Set	Total Length	Percent	Length of 20<=Ht<120	Percent	Length of 0<Ht<20 Ht>120	Percent
All Data	41878 ft.	100	40875 ft.	97.6%	1003 ft.	2.4%
Argillite	38249 ft.	100	38249 ft.	100%	0 ft.	0%

Table 4.2: Total Hardness Distribution Along the Tunnel (E-core)

The E-core drilling direction was parallel to the direction of the TBM advance, which makes the results obtained from these data particularly interesting. There are only three data points that are beyond the total hardness range between 20 and 120. That, plus the fact that all correlations established for the L-core data, were observed within the same total hardness range (20 <= Ht <= 120), lead us to believe that this range is indeed the limit for the conclusions already made and yet to be made.

1. T-system (TBM drive motors, electrical and hydraulic systems) related failure

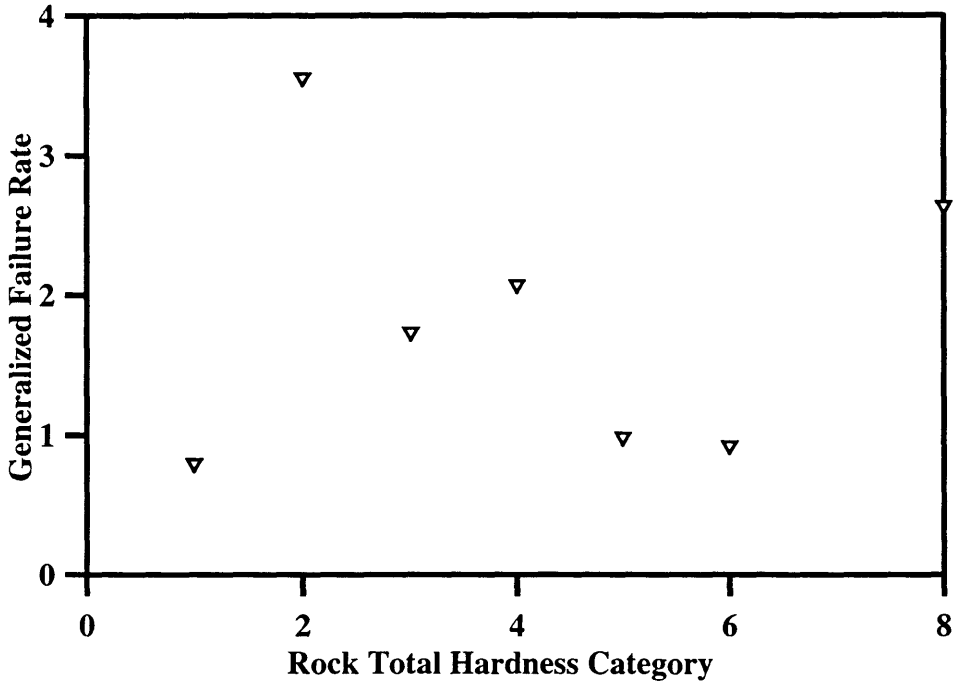

Figure 4.31: Generalized Failure Rates for T-system (All Data)

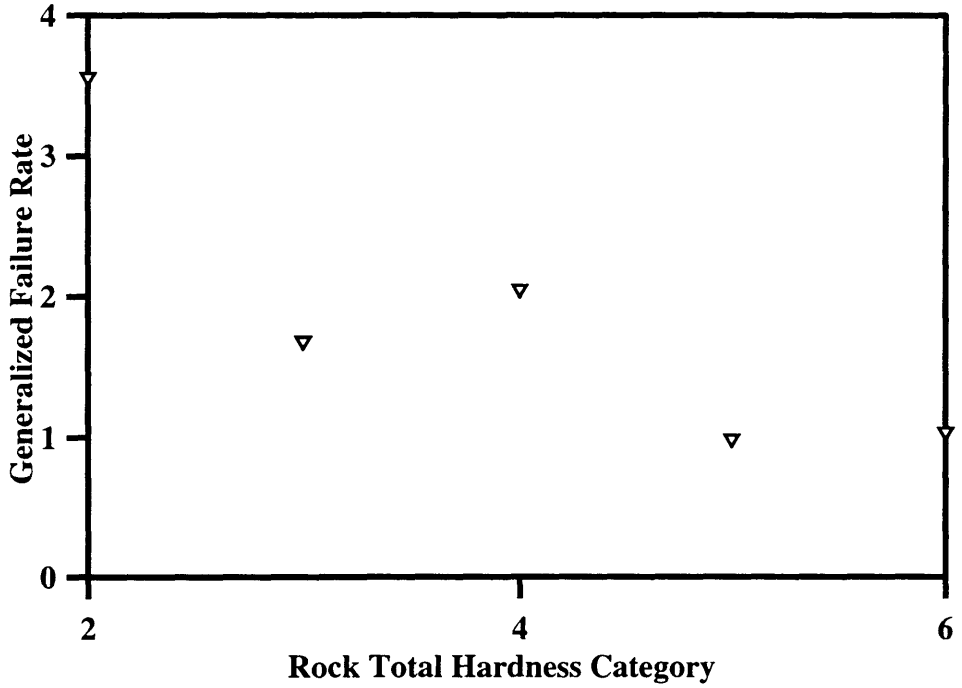

Figure 4.32: Generalized Failure Rates for T-system (Argillite Data)

The GFR plots (see Figures 4.32 and 4.33) show that failure rate decreases as the total hardness increases, which corresponds to the result obtained from the L-core data set. Total hardness values that are between 20 and 120 seem to define the population, which is also analogous to the L-core analysis. The residual plots (see Figures 4.34 and 4.35) show that the data are generally consistent, except for the couple of the data points representing the events of anomalous nature, which were also captured in the L-core analysis. The LFR plots (see Figures 4.36 and 4.37) show the same triangular shape distribution as the L-core data.

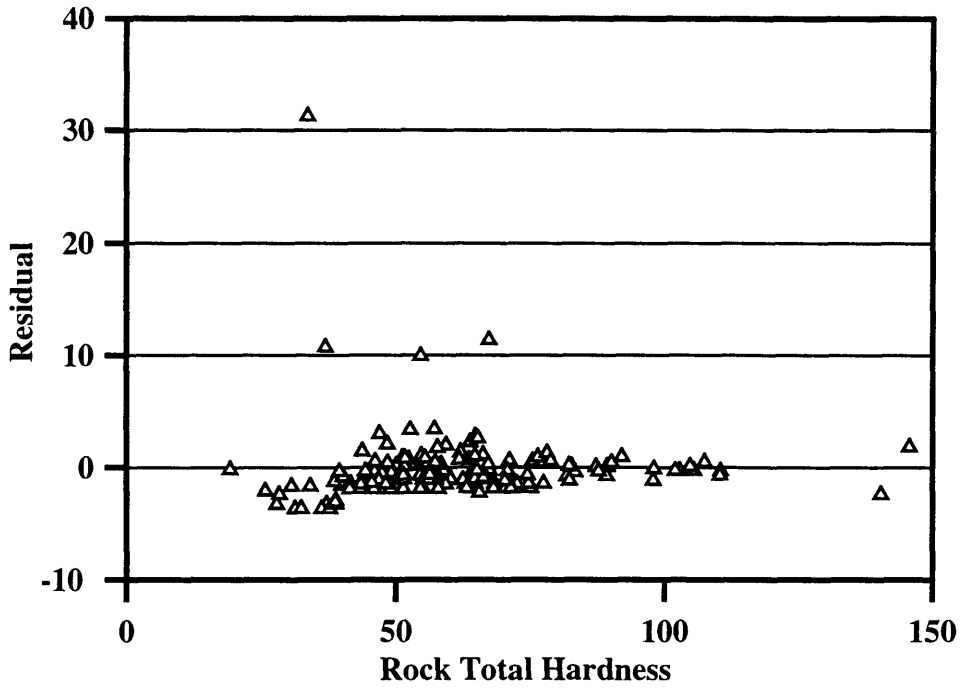

Figure 4.33: Residuals for T-system Related Failures (All Data)

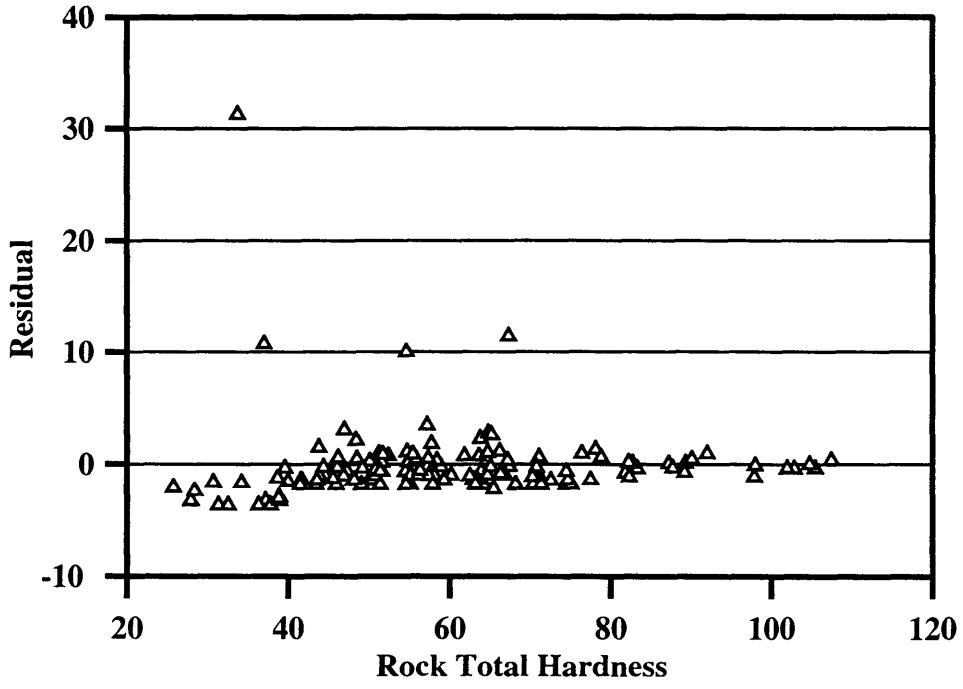

Figure 4.34: Residuals for T-system Related Failures (Argillite Data)

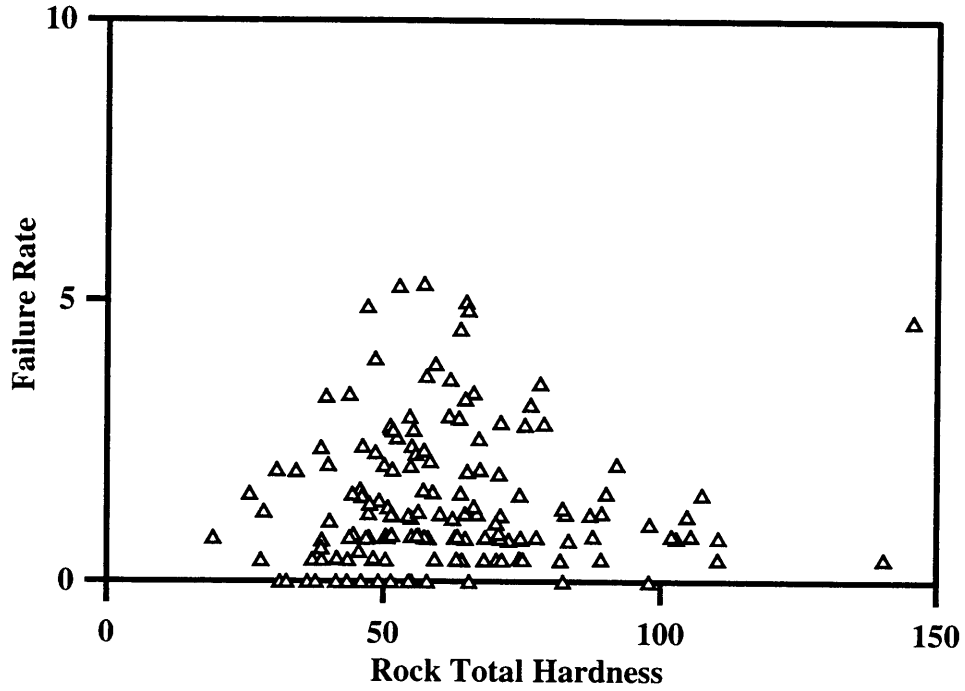

Figure 4.35: T-system Failure Rates for All Data

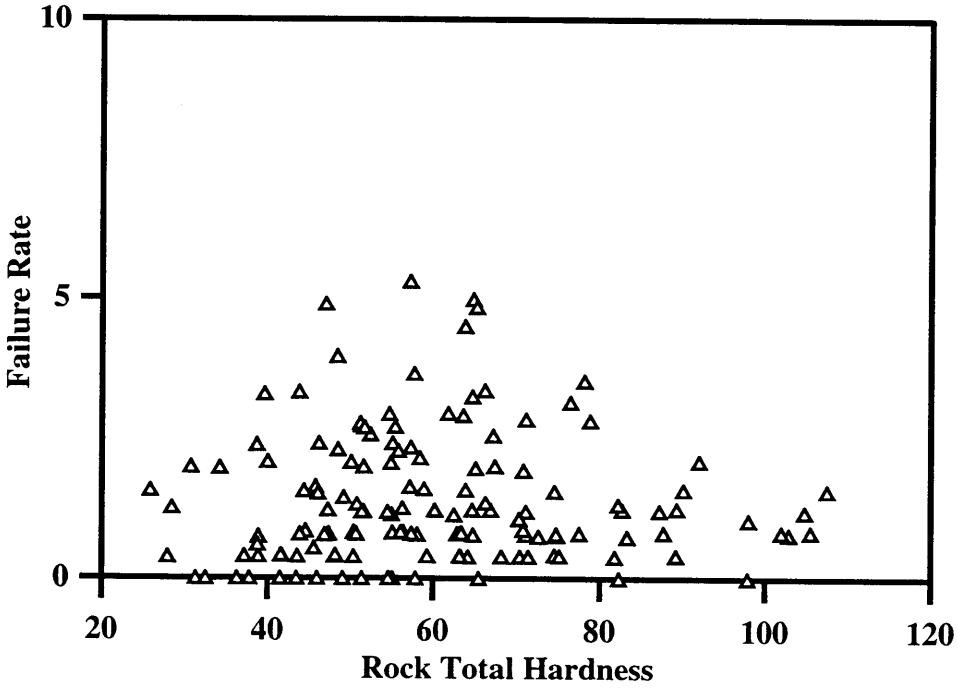

Figure 4.36: T-system Failure Rate for Argillite Data

2. CU-element (cutters) related failures

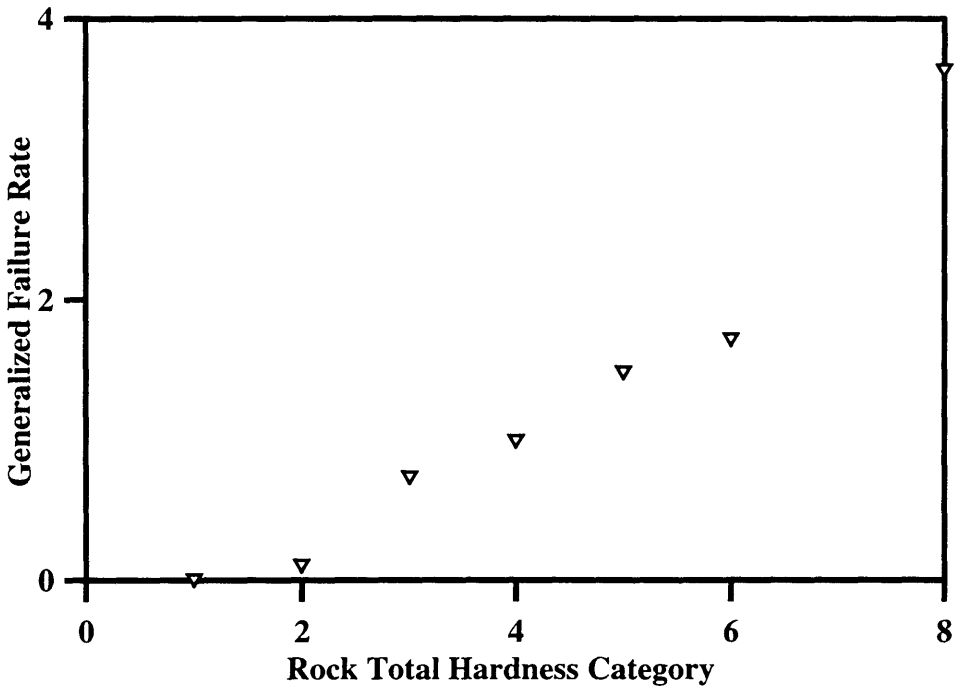

Figure 4.37: Generalized Failure Rates for CU-element (All Data)

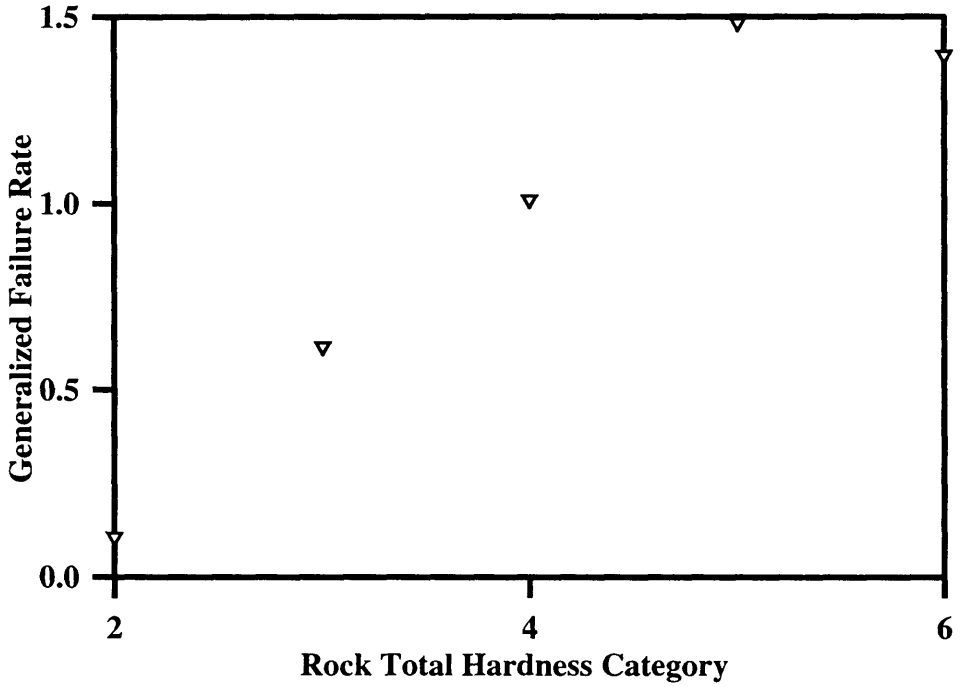

Figure 4.38: Generalized Failure Rates for CU-element (Argillite Data)

The GFR plots (see Figures 4.38 and 4.39) clearly show a fairly strong correlation between cutter related failure rate and the total hardness. The correlation appears to be stronger than the one observed in L-core analysis. This fact does support an assumption that the index tests on anisotropic rock should be conducted in a direction parallel to the direction of mining. The residual plots (see Figures 4.40 and 4.41) show the same phenomenon of increasing data variance as observed in L-core analysis. The harder the rock becomes the more uncertainty is introduced to the cutter behavior. The individual LFR values shown on Figures 4.42 and 4.43 show, as in case of the L-core data, the increasing failure rate with the increasing total hardness. The same conclusion can be made regarding the data dispersion.

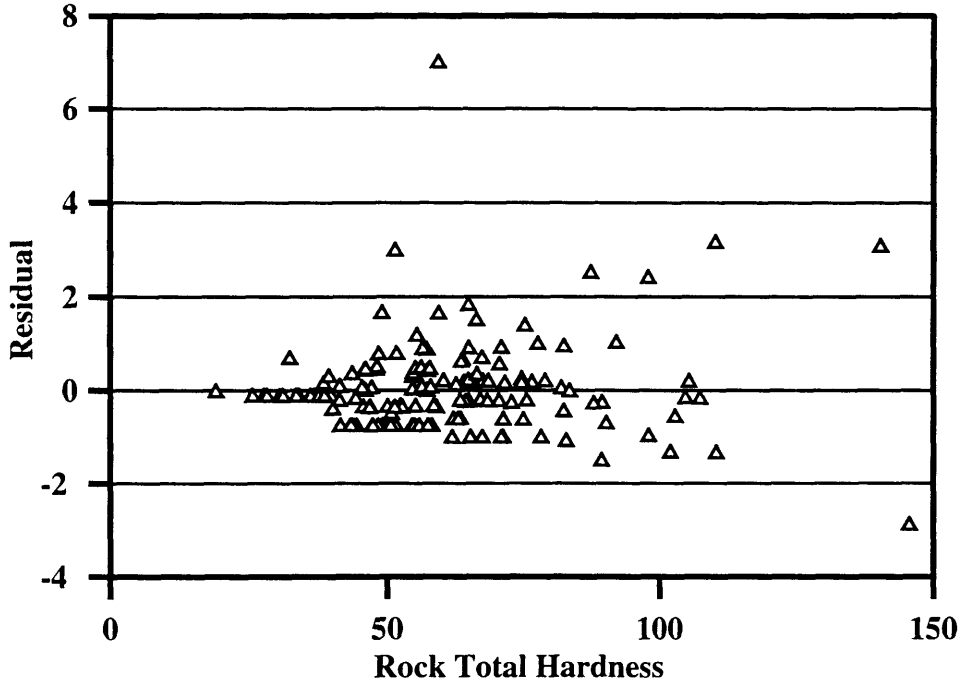

Figure 4.39: T-system, CU-element LFR Residuals (All Data)

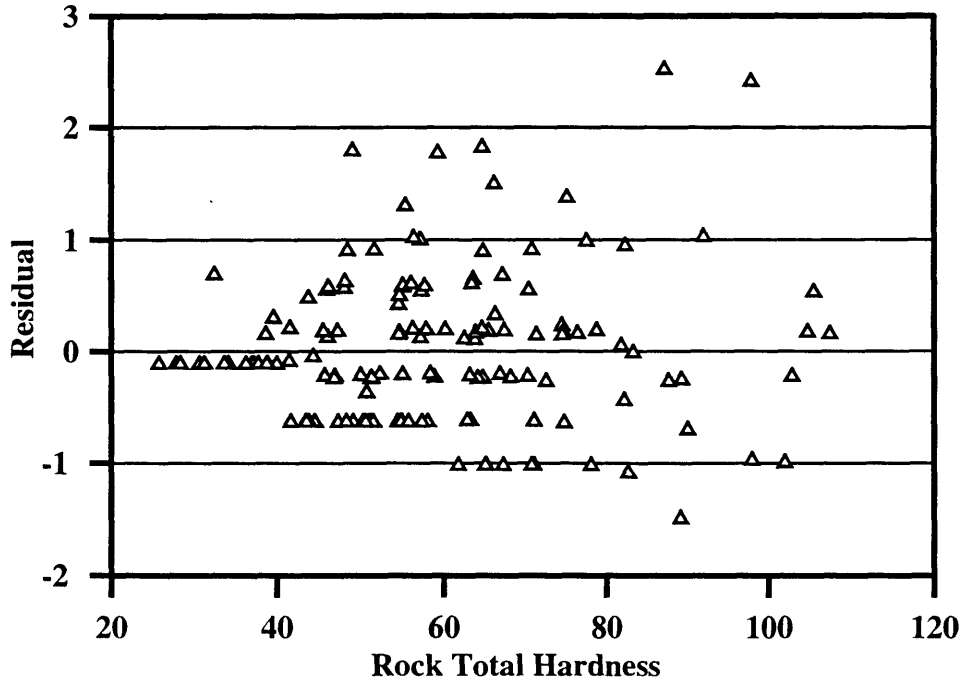

Figure 4.40: T-system, CU-element LFR Residuals (Argillite Data)

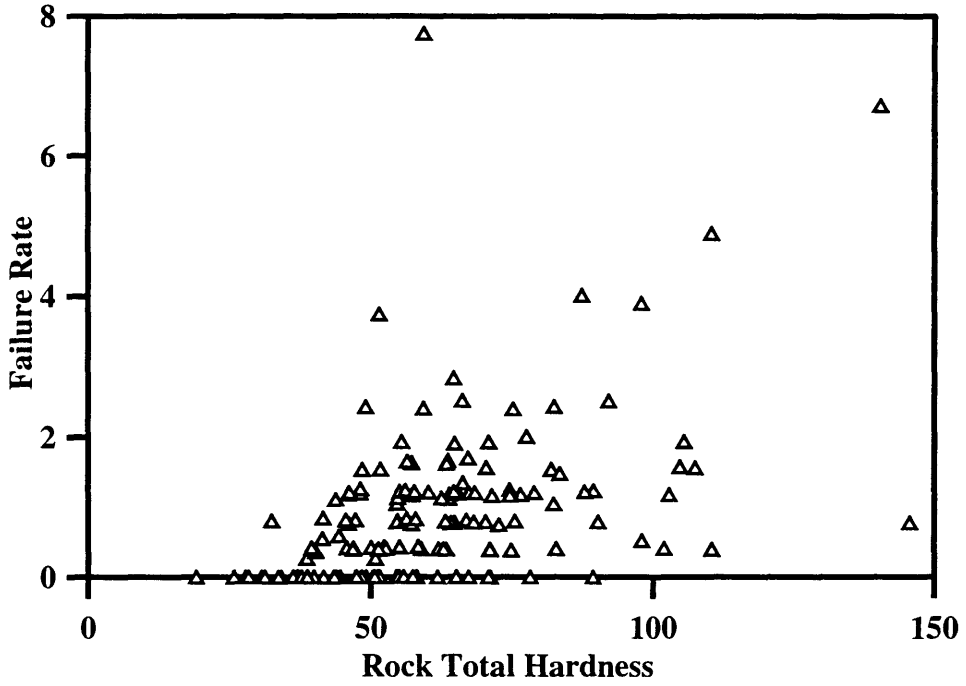

Figure 4.41: T-system, CU-element Local Failure Rate (All Data)

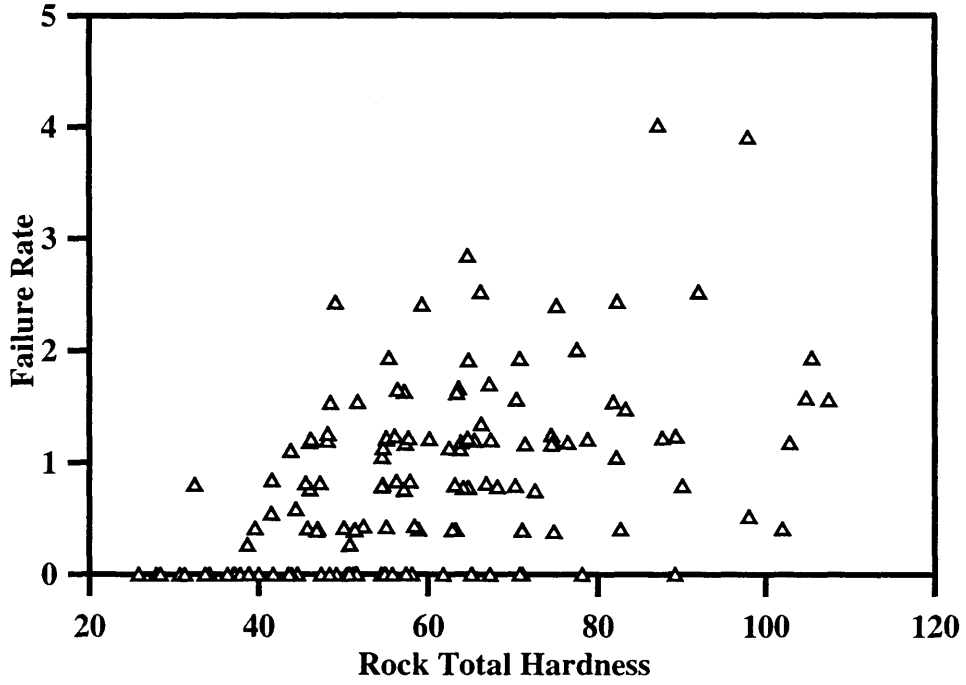

Figure 4.42: T-system, CU-element Local Failure Rate (Argillite Data)

3. M-system (muck removal system, excluding horizontal conveyor) failures.

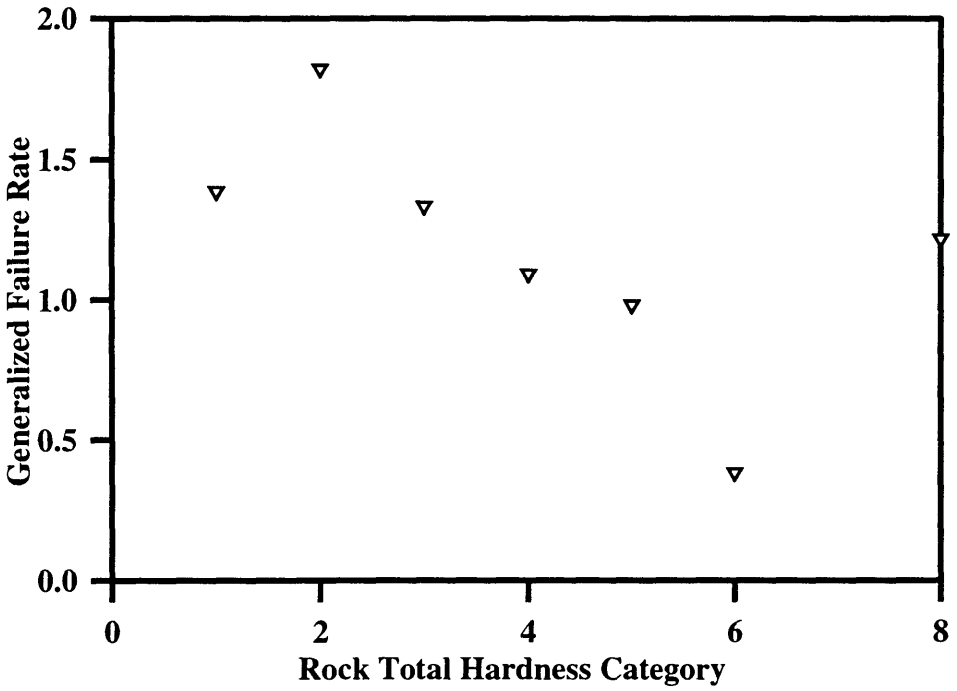

Figure 4.43: M-system Generalized Failure Rates (All Data)

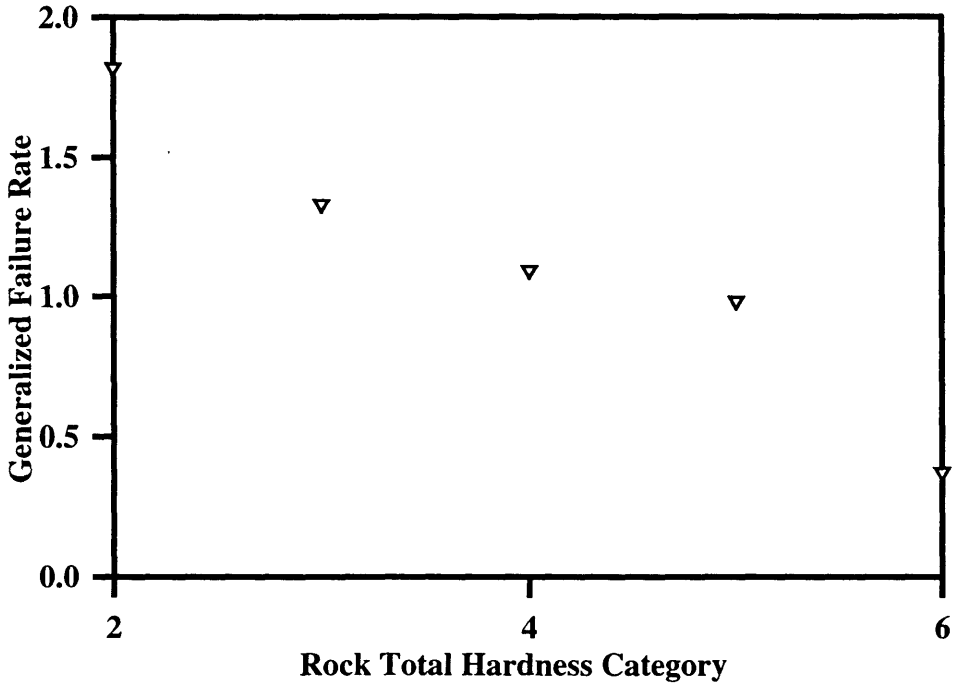

Figure 4.44: M-system Generalized Failure Rates (Argillite Data)

Figures 4.44 and 4.45 present GFR plots for M-system failures. For the total hardness range between 20 and 120, it can be concluded that M-system failure rate monotonically decreases as the total hardness increases. This result checks with the result obtained from L-core analysis, but the trend is more linear. Residual plots (see Figures 4.46 and 4.47) show that the dispersion seems to decrease as the total hardness increases. Therefore, it can be concluded that the softer rock presents more uncertainties for the muck removal system performance (excluding the horizontal conveyor), which can be explained by the fact that "soft" or fractured rock produces blocky, angular, non-uniform pieces of muck. Soft rock is also less stable, which along with the blocky muck can directly or indirectly cause the system failure. The muck removal system includes the cutterhead, whose revolving motion in the cutting process can be affected by the less stable "face". Thus, one could make a conclusion of the muck removal system being more reliable in harder rock. Another interesting observation is that the Diabase intrusions do not cause more failures (see Figures 4.48 and 4.49).

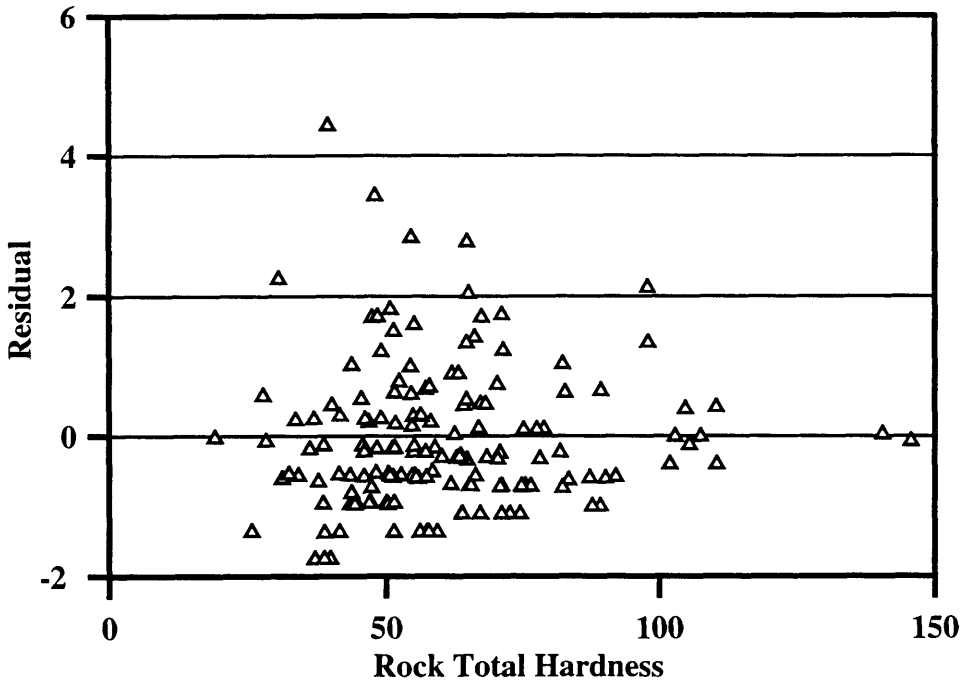

Figure 4.45: M-system LFR Residuals (All Data)

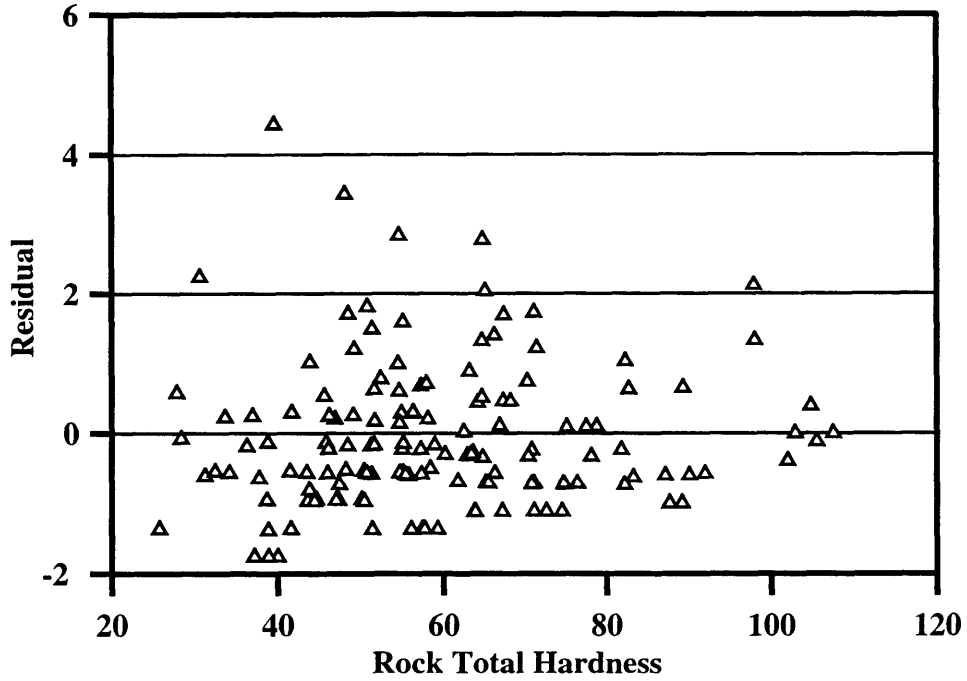

Figure 4.46: M-system LFR Residuals (Argillite Data)

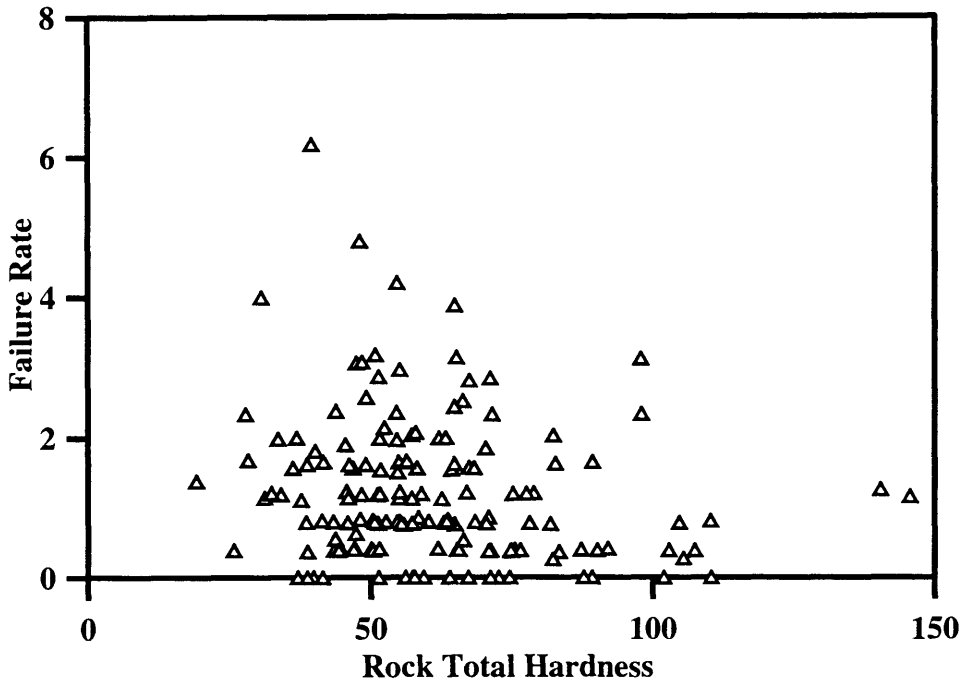

Figure 4.47: M-system Failure Rates (All Data)

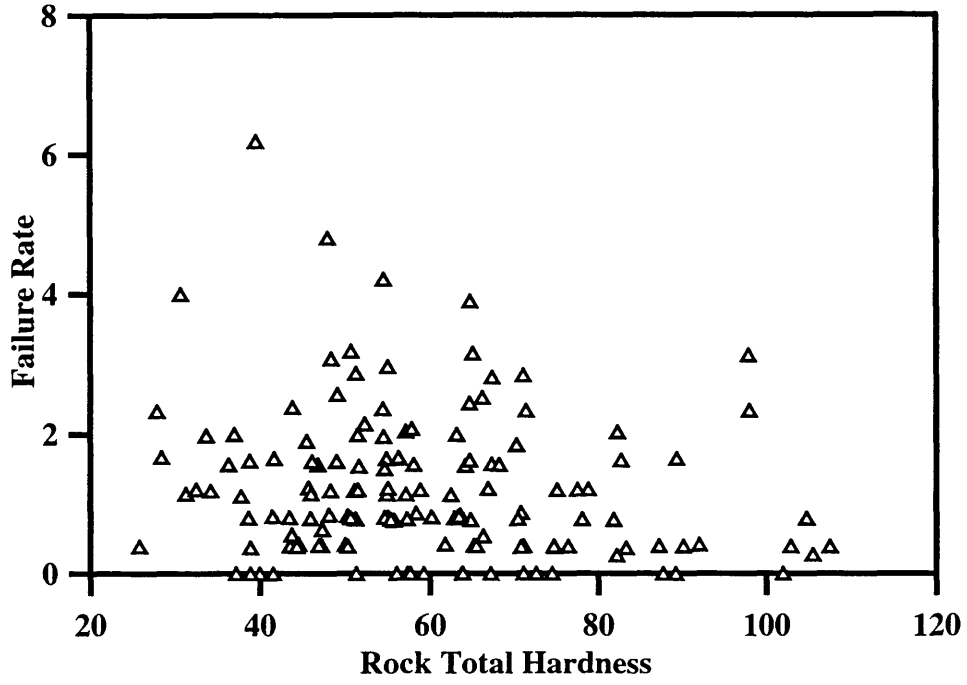

Figure 4.48: M-system Failure Rates (Argillite Data)

4. M-system, HZ-element (horizontal conveyor only) failures.

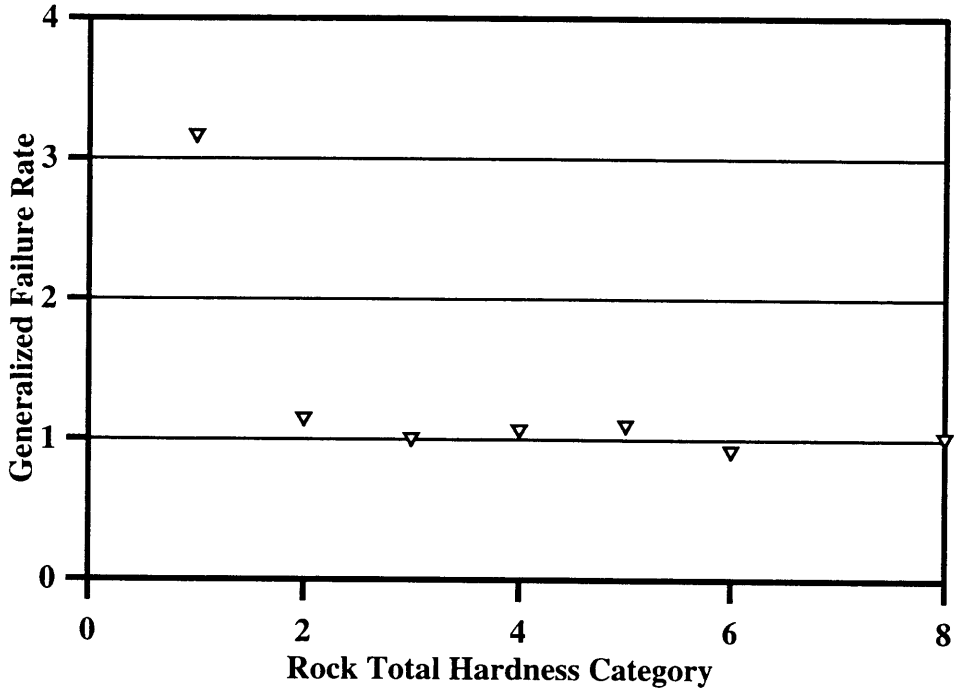

Figure 4.49: Generalized Failure Rates for HZ-element (All Data)

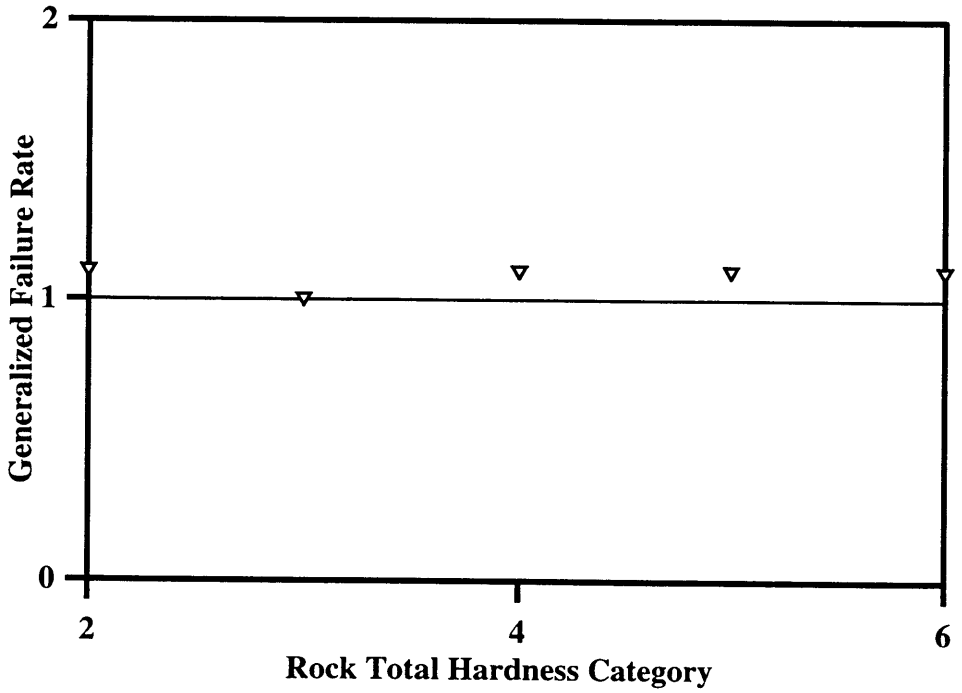

Figure 4.50: Generalized Failure Rates for HZ-element (Argillite Data)

The results are completely analogous to the L-core data analyses. GFR plots (see Figures 4.50 and 4.51) show that the horizontal conveyor data behavior is entirely different from the rest of the M-system population failures. Specifically, Figure 4.51 shows that the failure rate is constant and equal 1.

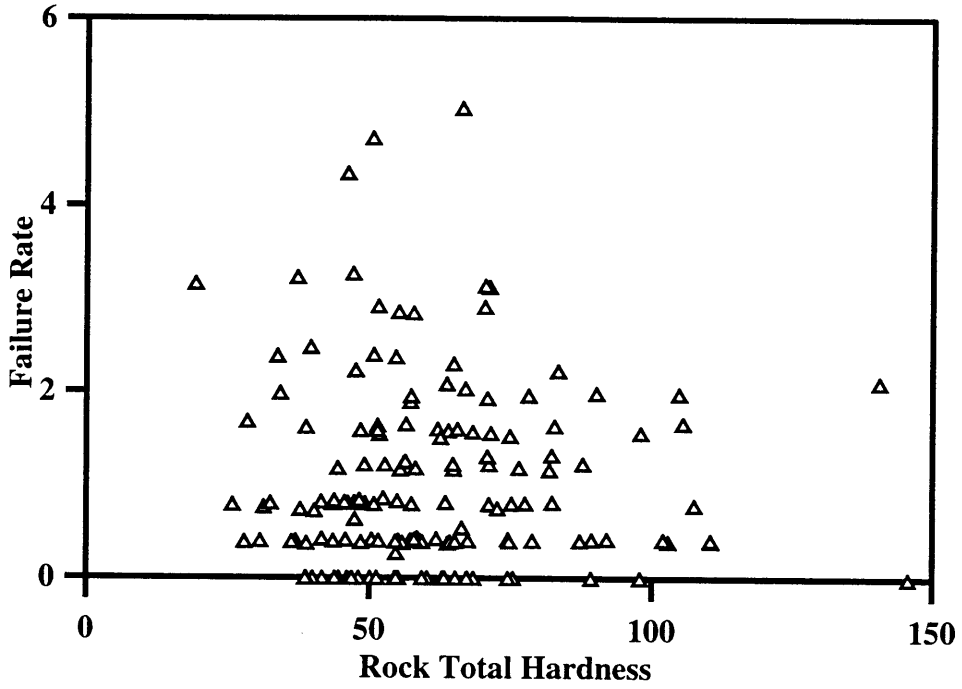

Figure 4.51: M-system, HZ-element Failure Rates (All Data)

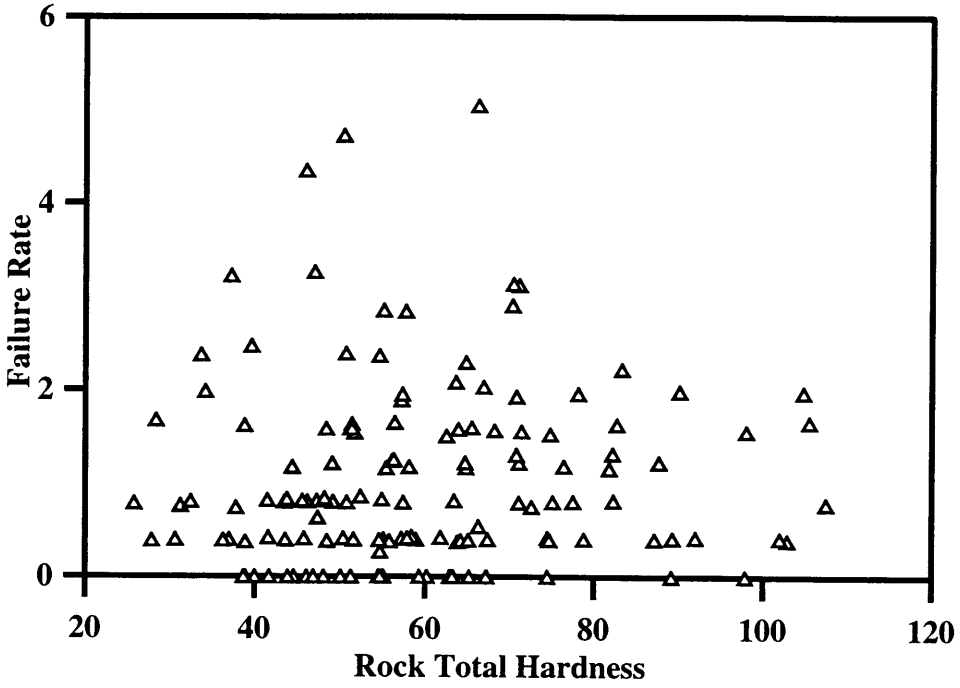

Figure 4.52: M-system, HZ-element Failure Rates (Argillite Data)

5. L-system (support installation systems) failures.

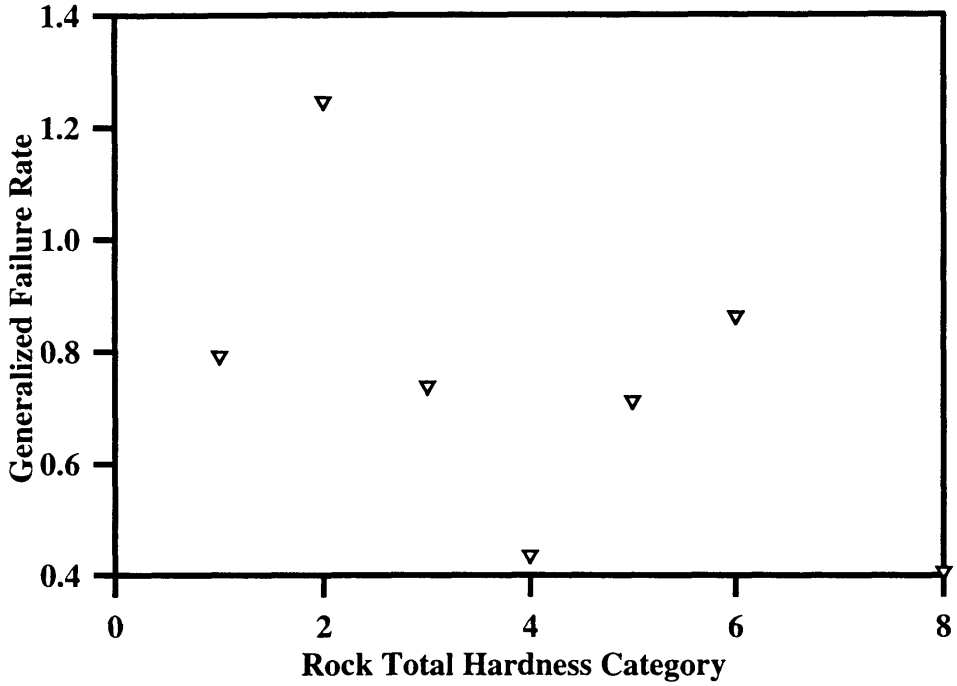

Figure 4.53: Generalized Failure Rates for L-system (All Data)

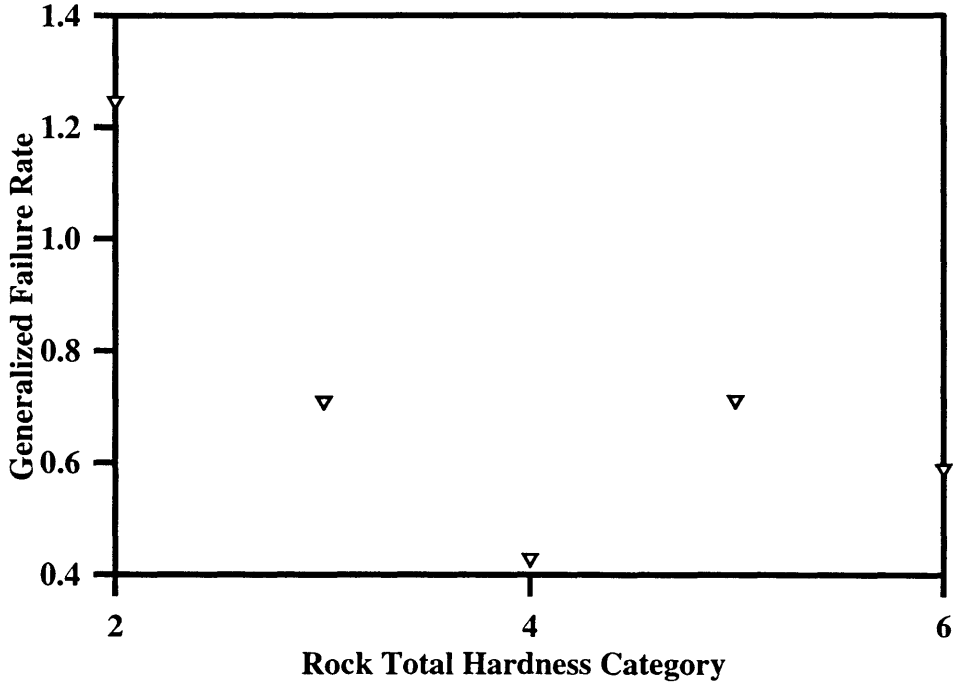

Figure 4.54: Generalized Failure Rates for L-system (Argillite Data)

GFR plots (see Figures 4.54 and 4.55) show no correlation between the L-system failure rate and the total hardness. Analogous to the L-core analysis, a fairly strong correlation between the failure rates and location (station) can be observed. Figures 4.56 and 4.57 illustrate this observation. The assumption of the exponentially decreasing function was tested by the means of the SAS System Poisson Regression procedure (see the following sections).

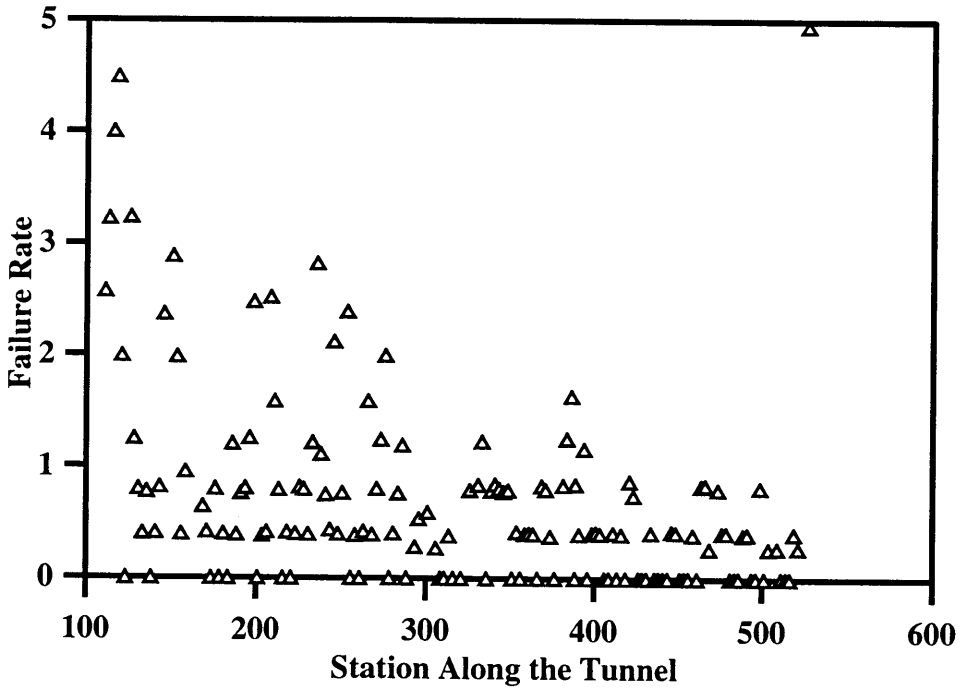

Figure 4.55: Failure Rates for L-system (All Data)

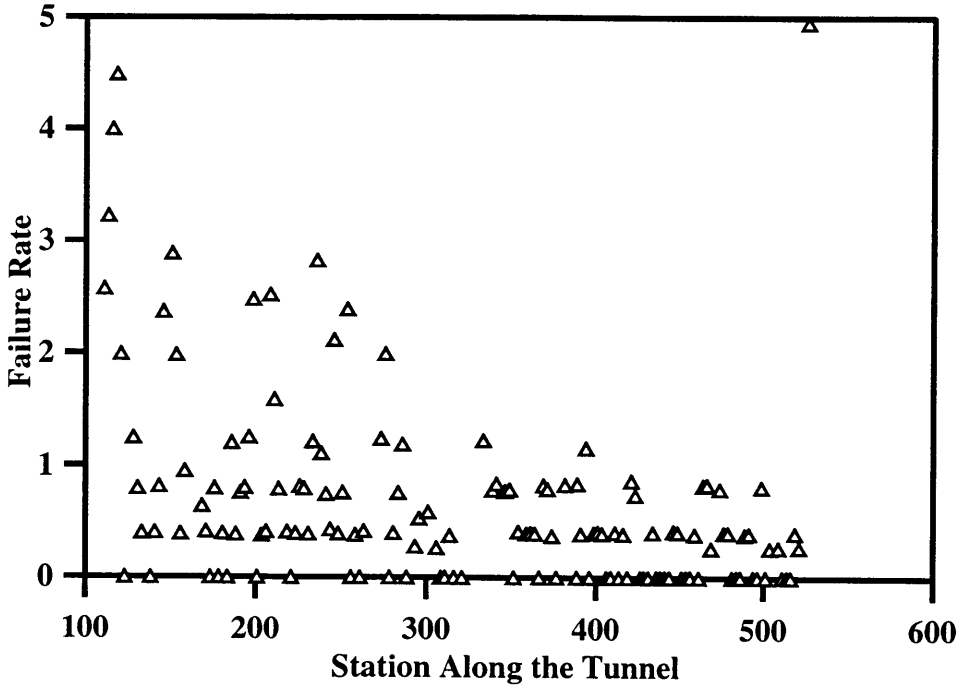

Figure 4.56: Failure Rates for L-system (Argillite Data)

The following can be concluded based on the examining the above presented figures:

- the analysis of the E-core total hardness based data set produced results similar to the ones obtained from the analysis of the L-core data;
- a smaller data dispersion was observed, which suggests that the test results obtained from the samples drilled parallel to the direction of the TBM advance, are more consistent.

4.4 Regression Analysis

Thus far, we have identified the relationships between the downtime categories and total hardness. Regression analyses were used to study these relationships more closely i.e., to obtain a set of mathematical parameters that characterize the strength of such relationships. The Poisson Regression requires integer numbers as an input i.e., the failure counts as opposed to the failure rates. The data set was created for that reason using constant interval length of 200 feet. Basis for the analysis was the E-core data set. The linear regression procedure of the SAS System was used to model CU-system number of failures. The SAS System GLIM (generalized linear models) procedure (see Appendix A), implementing the Poisson regression was used to model M-system and L-system number of failures. At this point the author feels necessary to include a brief overview of the qualitative parameters produced by the SAS system procedures to assess the significance level of the derived models:

- the **null hypothesis** (H_0) is a statement about the values of one or more parameters (usually zero parameter value);
- the **alternative hypothesis** (H_a) is a statement that contradicts the null hypothesis (non-zero parameter value);
- a **type I error** occurs when we incorrectly reject H_0;
- a **type II error** occurs when we incorrectly fail to reject H_0;
- the **significance level** of a hypothesis test is the maximum acceptable probability of rejecting a true null hypothesis;
- the **p value** is the probability of committing a type I error;
- the **regression model** in general form is $y=\beta_0+\beta_1 x+\varepsilon$, where β_0 - intercept, β_1 - coefficient, and ε - error;
- the **null hypothesis** is $\beta_0=0$ and $\beta_1=0$;
- the **value of R^2** [R^2=SSR/TSS, where SSR - sum of squares due to the regression, and TSS - total sum of squares (see Appendix A)] is known as the coefficient of determination, and is measure of the relative strength of the corresponding regression;
- the **F-statistic** [F=MSR/MSE, where MSR - mean sum of squares due to the regression, and MSE - the residual mean sum of squares (see Appendix A)] will tend to have values larger than those associated with F-distribution when H_0 is true;
- the **p value** in this case is the probability of the F-statistic value being larger than F-distribution value;
- the Chi-square-statistic will tend to have values larger than those associated with Chi-

square-distribution when H_0 is true.

- the **p value** in this case is the probability of the Chi-square-statistic value being larger than Chi-square-distribution value (Freund et al, 1996).

The results are presented below:

1. CU-system Number of Failures:

Number of Failures = -0.6657 + 0.0383*(Total Hardness)

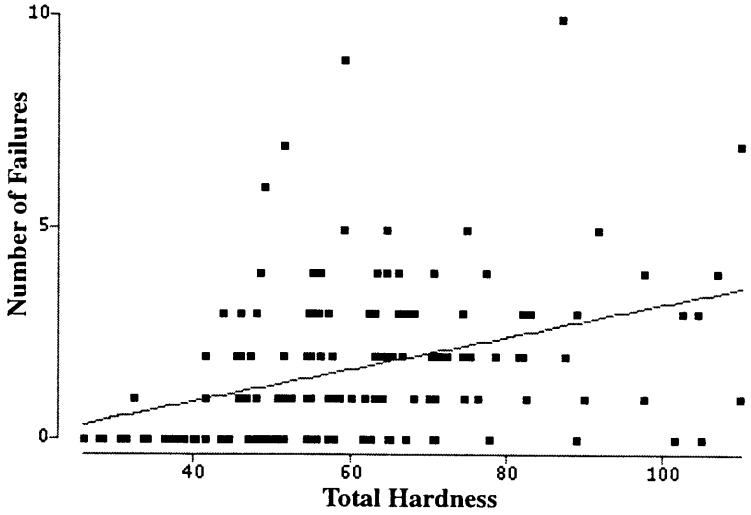

Figure 4.57: Results of the Regression Analysis of CU-element Failures (All Data)

The solid line on Figure 4.57 presents the number of cutter related failures as predicted by the regression. Figure 4.58 shows the result of the excluding the outliers from the regression. Coefficients of determination were R^2=0.1424 for the unmodified dataset and R^2=0.1948 for the modified one. The coefficient of determination gives the proportion of variability in a response variable explained by regression.

Number of Failures = -0.7233 + 0.0364(Total Hardness)*

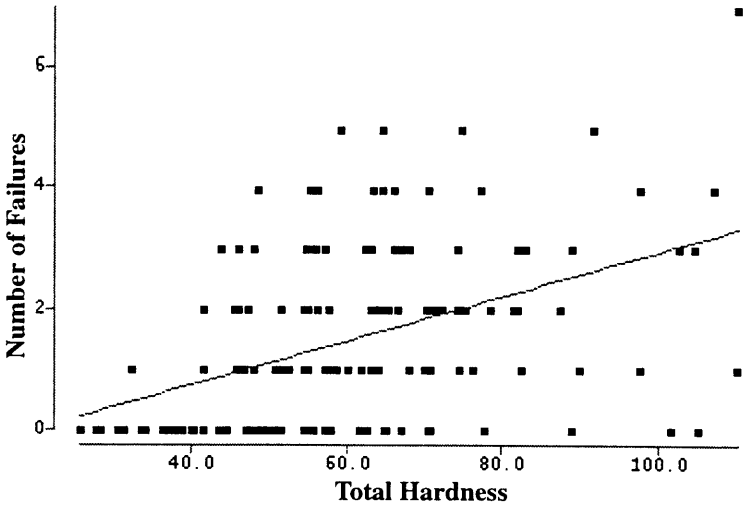

Figure 4.58: Results of the Regression Analysis of CU-element Failures (Truncated Data)

Goodness of fit was tested using the F-statistic. The P-value is the conditional probability of observing a value of the computed statistic larger than the observed value. A small P provides evidence against the Null Hypothesis.

Model:	Degrees of Freedom:	F-statistic:	P > F:
Unmodified	149	24.7369	0.0001
Modified	145	35.0714	0.0001

Table 4.3: Results of Goodness-of-Fit Test for Cutter Failures Linear Models

Table 4.3 presents an evidence of the established correlation between the cutter related number of failures and the total hardness.

2. T-system Number of Failures:

The Poisson Regression (see Appendix B) performed on the data set containing T-system (excluding CU-element) related failures yielded the following results:

Number of Failures = exp(1.576 - 0.0066*(Total Hardness)

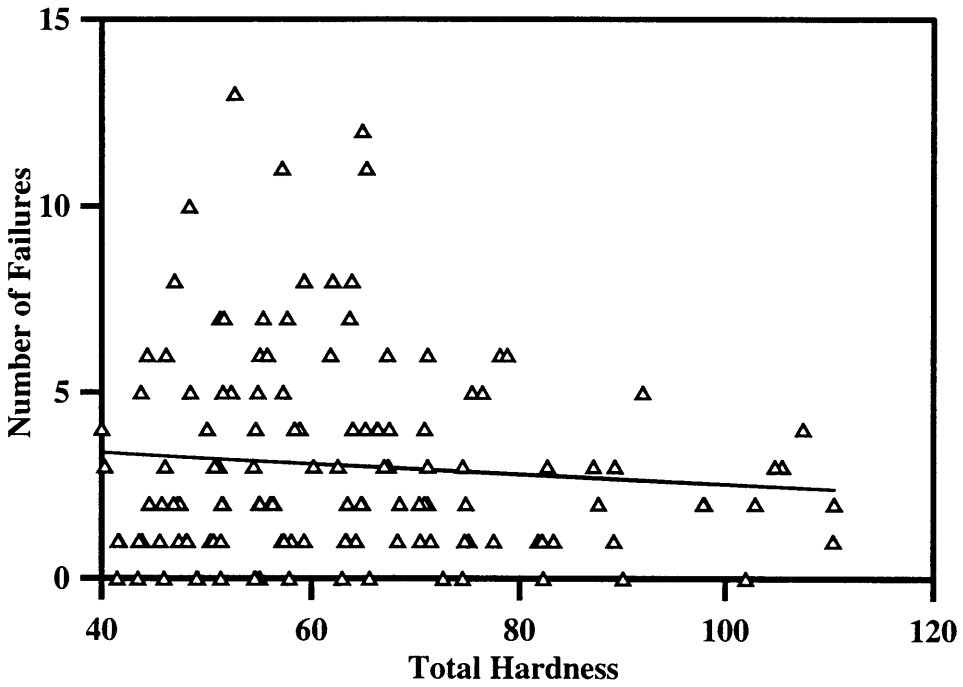

Figure 4.59: Actual and Estimated Values for T-system Number of Failures

The model was tested using F-statistic:

MSR (mean sum of squares due to regression)	MSE (residual/ error mean sum of squares)	F-statistic	F-distribution for p=0.005
202.5	2.371	85.41	5.30

Table 4.4: Results of Goodness-of-Fit Test for T-system Failure Non-linear Model

F-statistic is much larger than the table value of F-distribution for p=0.005, therefore the true p value is actually much less than 0.005. Another way to assess the significance of

the regression coefficients is to calculate the 95% confidence interval lower and upper limits:Regression Sum of Squares (RSS) - 432.999;

Parameter	Estimate	95% confidence lower limit	95% confidence upper limit
intercept	1.412	1.014	1.81
hardness coefficient	-0.049	-0.011	0.0013

Table 4.5: 95% Confidence Limits for T-system Failure Non-linear Model

The different signs of the lower and upper limit values suggest that the true value of the hardness coefficient can in fact be zero, therefore the impact of the total hardness on the T-system number of failures is very small. Although the correlation is weak, the model presents an evidence in favor of the conclusion made earlier in the chapter about a better performance of the TBM mechanical system in harder rock.

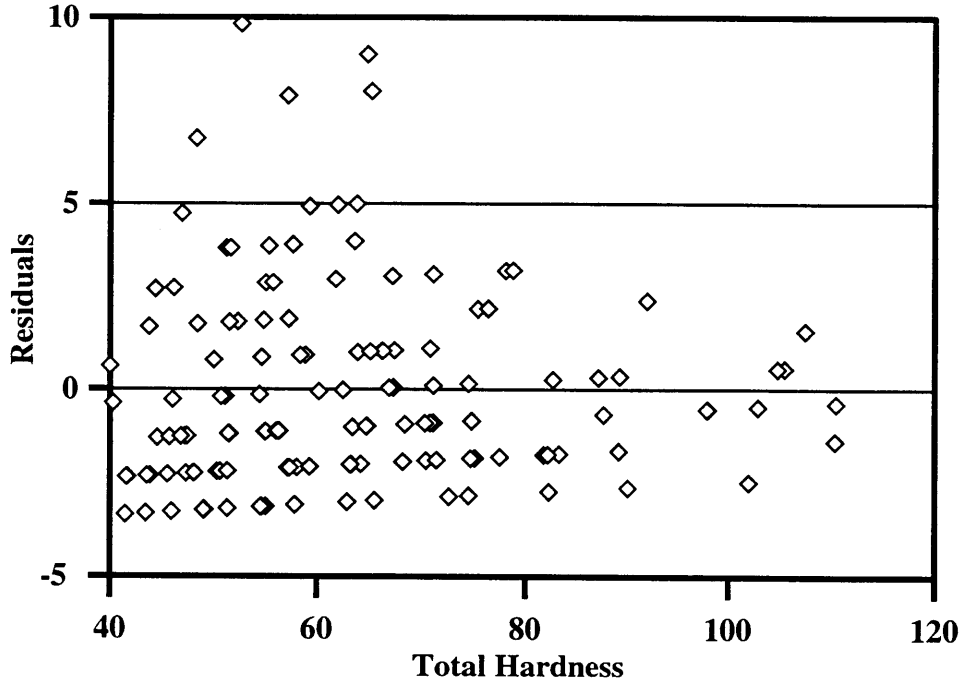

Figure 4.60: Residuals of T-system Predicted Number of Failures

The Figure 4.62 presents the residuals of the estimated values. The variance decreases significantly as the total hardness increases, which supports the point that there is less uncertainty introduced to the TBM mechanical system in harder rock.

3. M-system Number of Failures:

The results of the execution of the Poisson Regression procedure are presented below:

The model was tested using F-statistic:

MSR (mean sum of squares due to regression)	MSE (residual/ error mean sum of squares)	F-statistic	F-distribution for p=0.005
182.5	2.189	83.39	5.30

Table 4.6: Results of Goodness-of-Fit Test for M-system Failure Non-linear Model

F-statistic is much larger than the table value of F-distribution for p=0.005, therefore the true p value is actually much less than 0.005. Another way to assess the significance of the regression coefficients is to calculate the 95% confidence interval lower and upper limits:

Parameter	Estimate	95% confidence lower limit	95% confidence upper limit
intercept	1.412	1.046	1.778
hardness coefficient	-0.009	-0.015	-0.0029

Table 4.7: 95% Confidence Limits for M-system Failure Non-linear Model

Figure 4.61 shows the number of failures estimated by the model, and Figure 4.62 shows the residuals. Despite the significant dispersion the regression model presents evidence in favor of the conclusion made earlier: harder rock is a better environment for the muck removal system of the TBM.

*Number of Failures = exp(1.412 - 0.009*Total Hardness)*

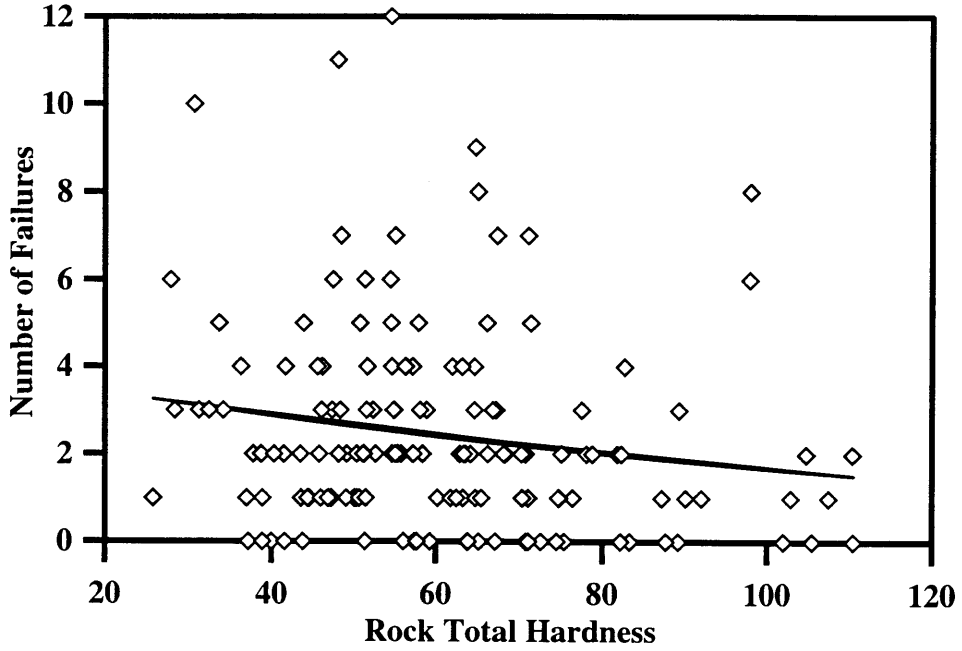

Figure 4.61: Actual and Estimated Values of M-system Number of Failures

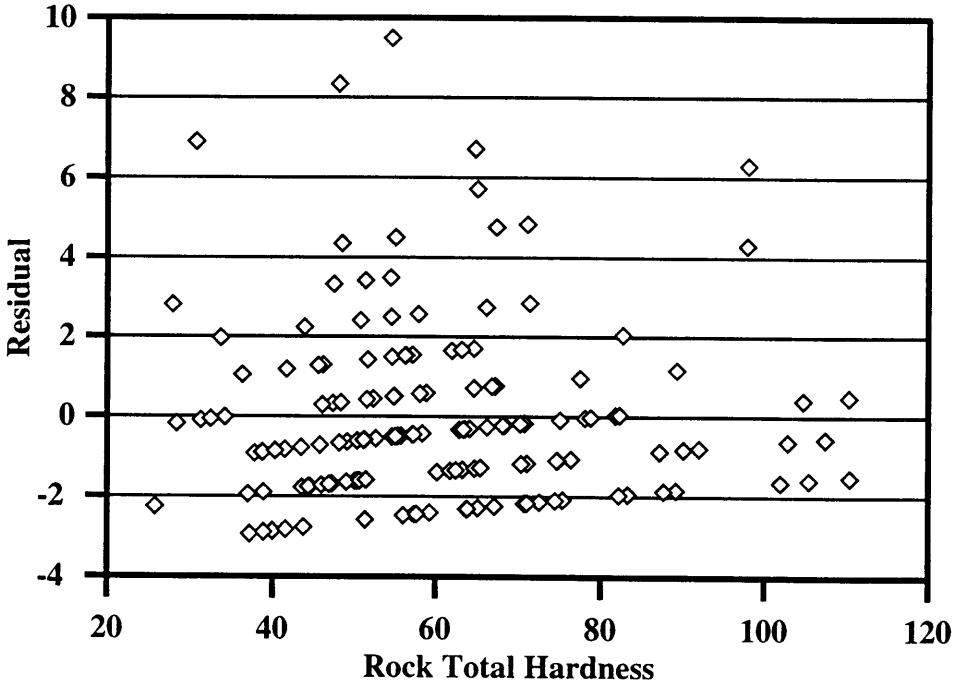

Figure 4.62: Residuals of the Estimated M-system Number of Failures

4. L-system Number of Failures ("Learning Curve"):

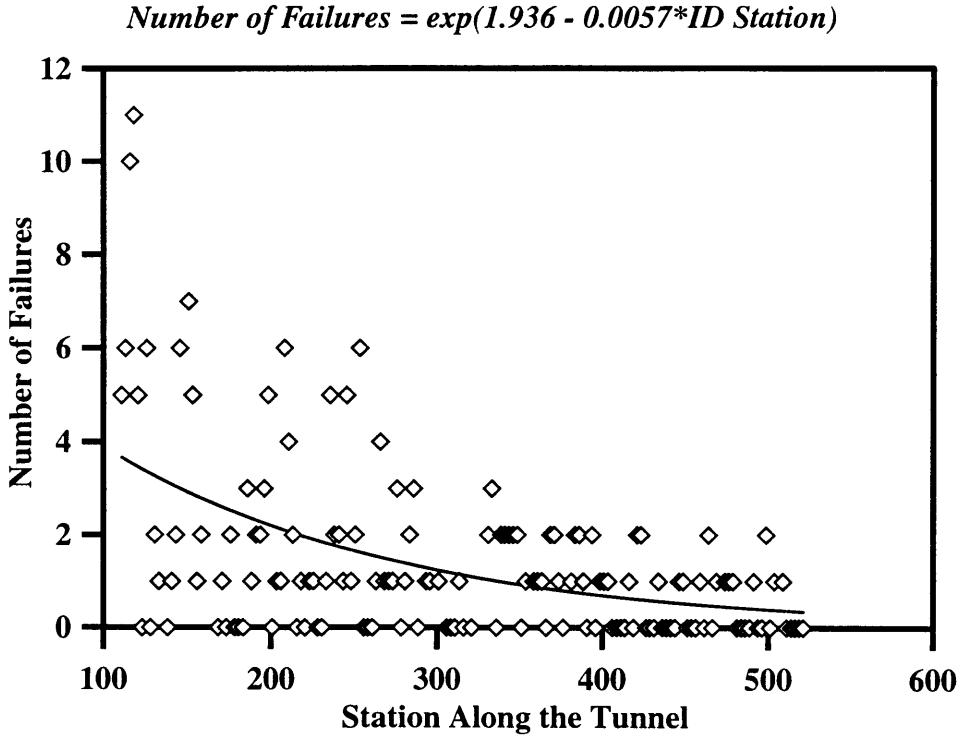

Figure 4.63: Actual and Estimated Values of the L-system Number of Failures

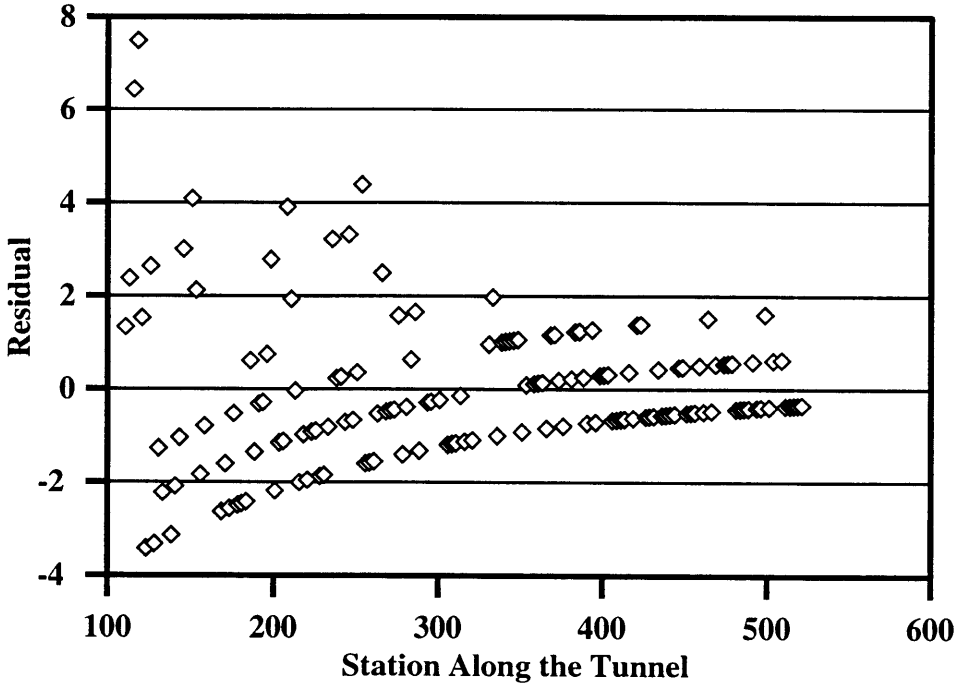

Figure 4.64: Residuals of the Estimated L-system Number of Failures

Figures 4.63 and 4.64 present the estimated values of the L-system number of failures and its residuals respectively. The regression parameters are as follows:

MSR (mean sum of squares due to regression)	MSE (residual/ error mean sum of squares)	F-statistic	F-distribution for p=0.005
105.5	1.414	74.61	5.30

Table 4.8: Results of Goodness-of-Fit Test for L-system Failure Non-linear Model

F-statistic is much larger than the table value of F-distribution for p=0.005, therefore the true p value is actually much less than 0.005. Another way to assess the significance of the regression coefficients is to calculate the 95% confidence interval lower and upper limits:

Parameter	Estimate	95% confidence lower limit	95% confidence upper limit
intercept	1.936	1.595	2.278
ID stat. coefficient	-0.00575	-0.00704	-0.00446

Table 4.9: 95% Confidence Limits for L-system Failure Non-linear Model

The lower and upper limit values are very close to the estimated value, thus presenting an evidence of a very strong location influence on the L-system number of failures.

4.5 Failure Occurrence Probability Investigation.

The question was raised how would one assess the probability of occurrence of a particular failure category e.g., cutter failures as opposed to muck removal system failures. A code was written that implemented a simple task of assigning 1 to a dummy variable every time there was a record (shift), where at least one failure of a particular category occurred, assigning 0 otherwise. The SAS System Logistic Regression (see Appendix B) procedure was executed twice for each failure category: first to investigate the total hardness impact on the probability of failure; and second to investigate the location (station) impact on probability of failure. Only production shifts were included in the analysis. The logistic regression produces a probability function as follows: $p = \frac{e^{A+A1\times X}}{1+e^{A+A1\times X}}$, where p - probability; A - intercept; A1 - coefficient; X - independent variable.

The results are presented below:

1. T-system failures

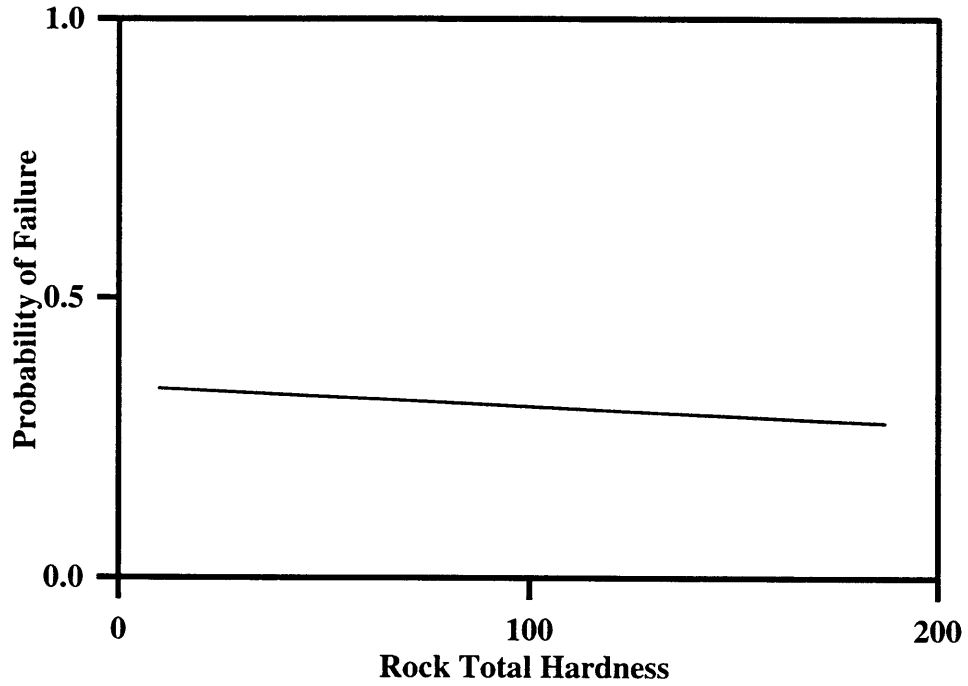

Figure 4.65: Probability of T-system Failure Occurrence vs. Total Hardness

The probability of T-system occurrence (see Figures 4.65) stays essentially constant. The p-value for the A1 coefficient was 0.57, so one could with 57% confidence assume the coefficient to be equal to zero.

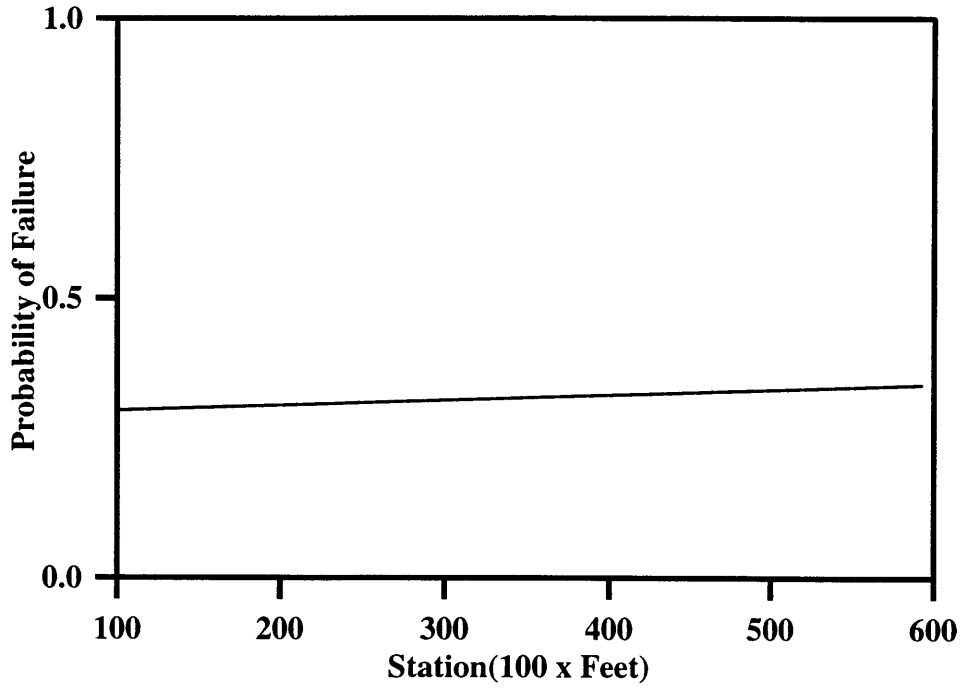

Figure 4.66: Probability of T-system Failure Occurrence vs. Station

Figure 4.66 shows virtually no impact of the location on the T-system failure occurrence. The p-value was 0.3647.

2. CU-element failures

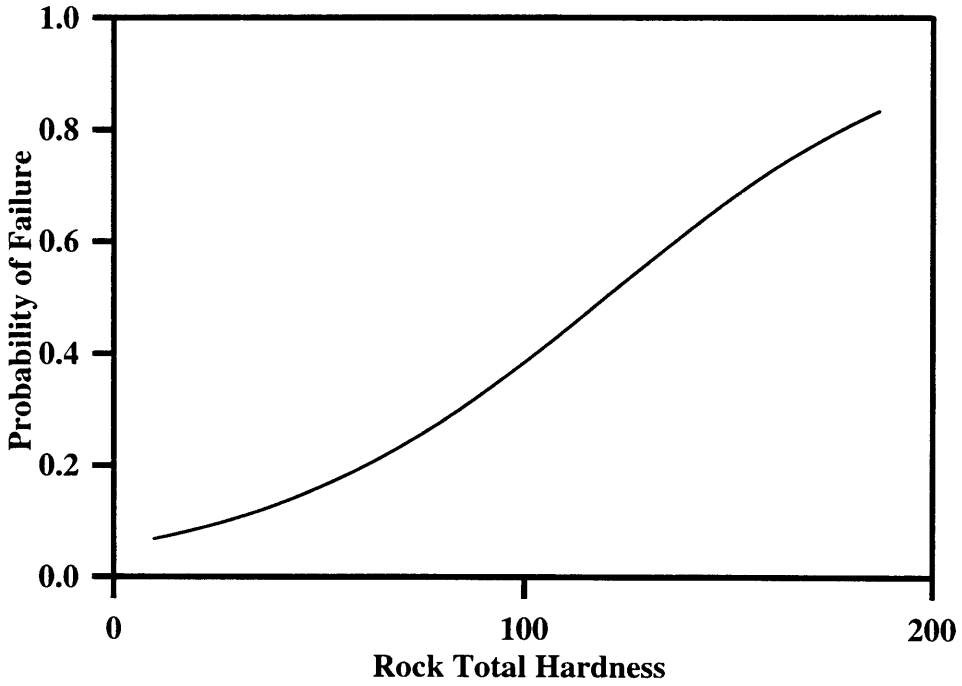

Figure 4.67: Probability of CU-element Failure Occurrence vs. Total Hardness

Figure 4.67 shows that the probability of failure increases as the total hardness increases. This result agrees well with the conclusions already reached about the total hardness impact on that failure category. The Chi-square test for non-zero coefficient values yielded the following:

- Chi-square statistic - 57.8;
- Prob > Chi-square - 0.0001.

Hence there is strong evidence for the conclusion that the total hardness is one of the most important factors influencing cutter performance.

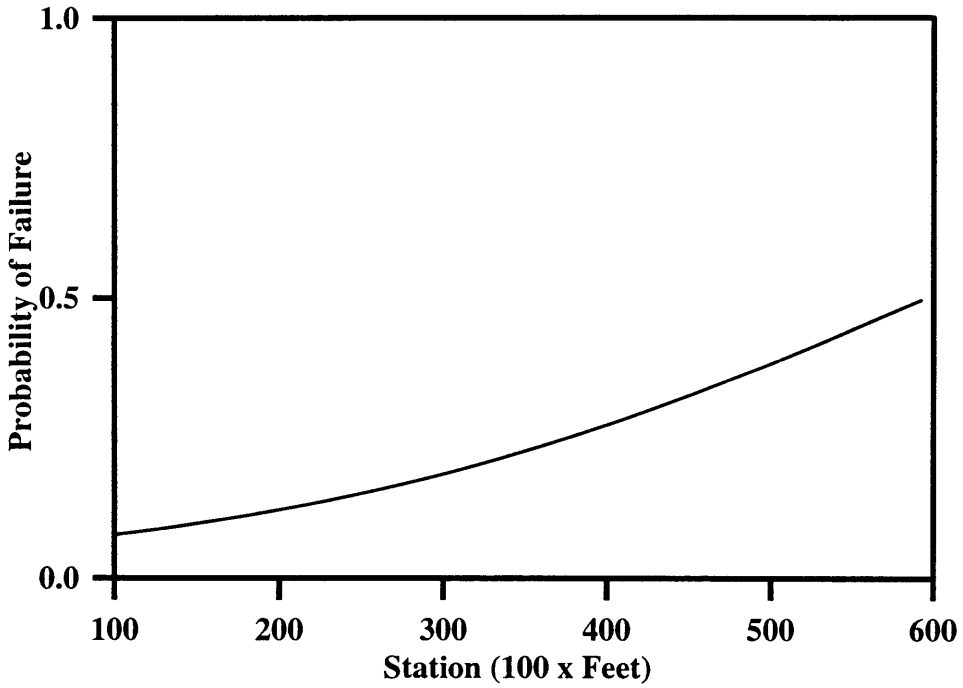

Figure 4.68: Probability of CU-element Failure vs. Station

Figure 4.68 illustrates the so called "fatigue" effect: probability of failure increases with the tunnel advance. Cutters wear out as they reach their "life time" limit. The regression parameters were as follows:

- Chi-square statistic for the coefficient - 70.72;
- Prob > Chi-square - 0.0001.

These parameters are evidence of a strong correlation.

At this point the question was raised what combined effect would hardness and location together have on the probability of cutter failure occurrence. The SAS System Logistic Procedure allows one to analyze more than one independent variable. The results are presented in Figure 4.69. And Table 4.10 presents the regression parameters.

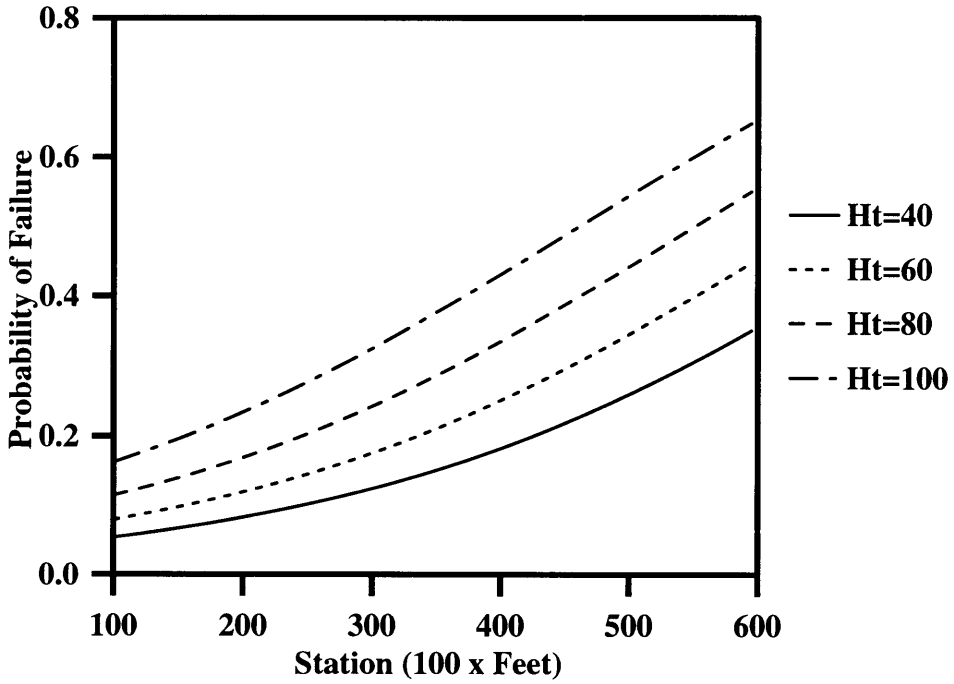

Figure 4.69: Combined Effect of Total Hardness And Location On Cutters Failure Probability Of Occurrence

Variable	Chi-Square-statistic	Prob > Chi-Square
Intercept	191.4607	0.0001
Hardness Coefficient	41.4431	0.0001
Station Coefficient	54.7963	0.0001

Table 4.10: Regression Parameters For Cutter Failure Combined Model

As a result of the combined effect of the rock total hardness and "fatigue" factor, the probability of the cutter related failure occurrence exponentially increases as shown on Figure 4.69. The impact that the total hardness and location have is thus substantial. The p-value is a strong evidence of that impact.

3. M-system failures

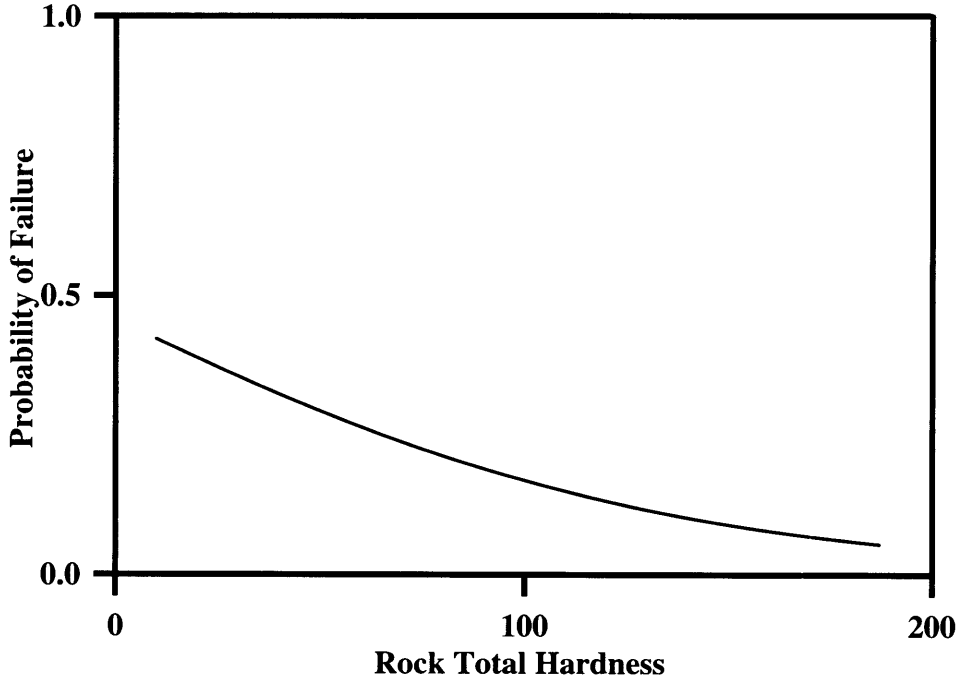

Figure 4.70: Probability of M-system Failure Occurrence vs. Total Hardness

The regression parameters were as follows:

- Chi-square statistic for the coefficient - 17.35;
- Prob > Chi-square - 0.0001.

Figure 4.70 is strong evidence in favor of the conclusion made earlier about the impact that the total hardness has on the muck removal system failures. The softer rock presents more uncertainty than the hard one. The p value of 0.0001 is evidence of a very strong impact. However, Figure 4.71 shows that the location does not have an impact on the M-system failure occurrence probability. The p value of 0.7324 supports this conclusion by suggesting that there is 73% chance that hardness coefficient is zero.

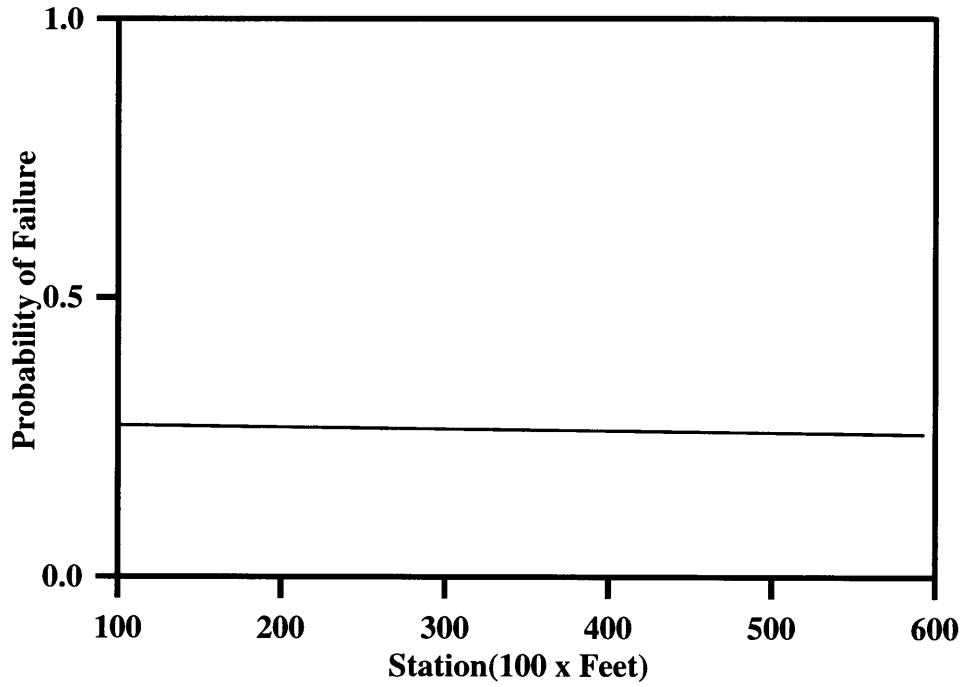

Figure 4.71: Probability of M-system Failure Occurrence vs. Station

4. Horizontal Conveyor Failures

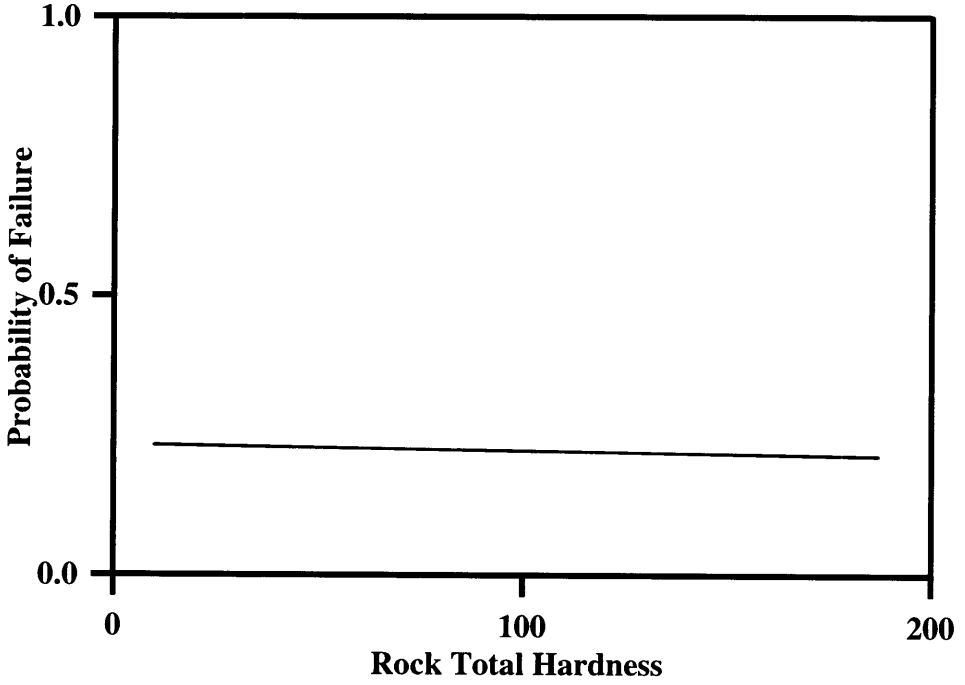

Figure 4.72: Probability of HZ-element Failure Occurrence vs. Total Hardness

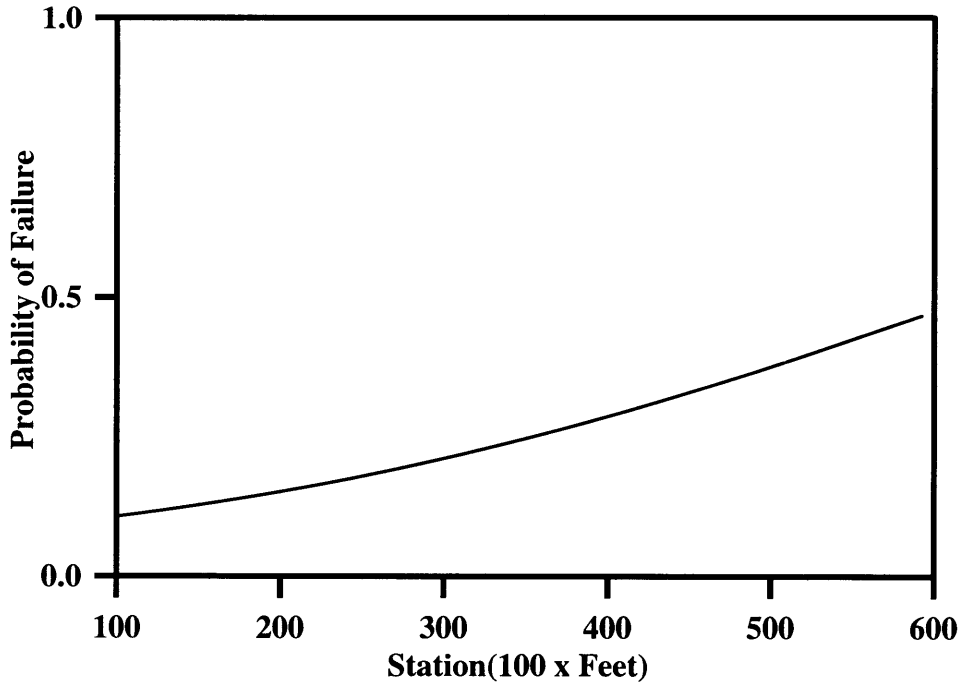

Figure 4.73: Probability of HZ-element Failure Occurrence vs. Station

The probability distribution of the horizontal conveyor failures (see Figure 4.72) supports the conclusions reached earlier in the chapter that this type of failure is independent of the rock properties, has a constant failure rate of 1 and a constant probability of 0.13. The regression parameters were as follows:

- Chi-square statistic for the coefficient - 0.0363;
- Prob > Chi-square - 0.8488.

The p-value of 0.8488 suggests that the impact of the total hardness is negligible. However, Figure 4.73 presents evidence in favor of the conclusion that the location has a great impact on the horizontal conveyor failure occurrence probability. Indeed, as tunnel progresses, the "fatigue" effect becomes more and more expressed. The regression parameters were as follows:

- Chi-Square - 52.3038;
- Prob > Chi-Square - 0.0001.

5. Support installation system failures

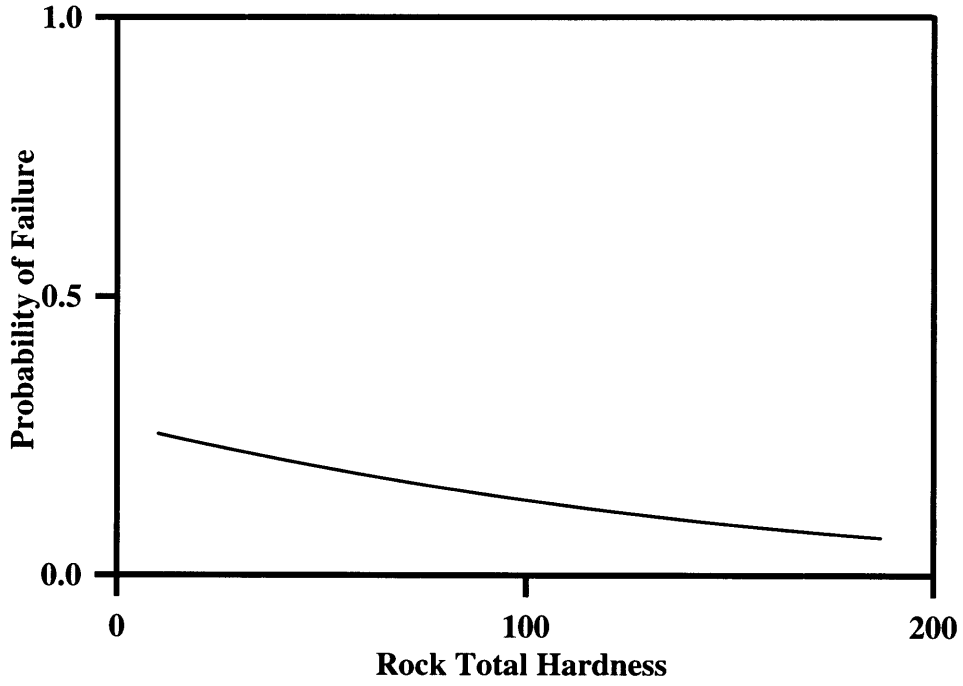

Figure 4.74: Probability of L-system Failure Occurrence vs. Total Hardness

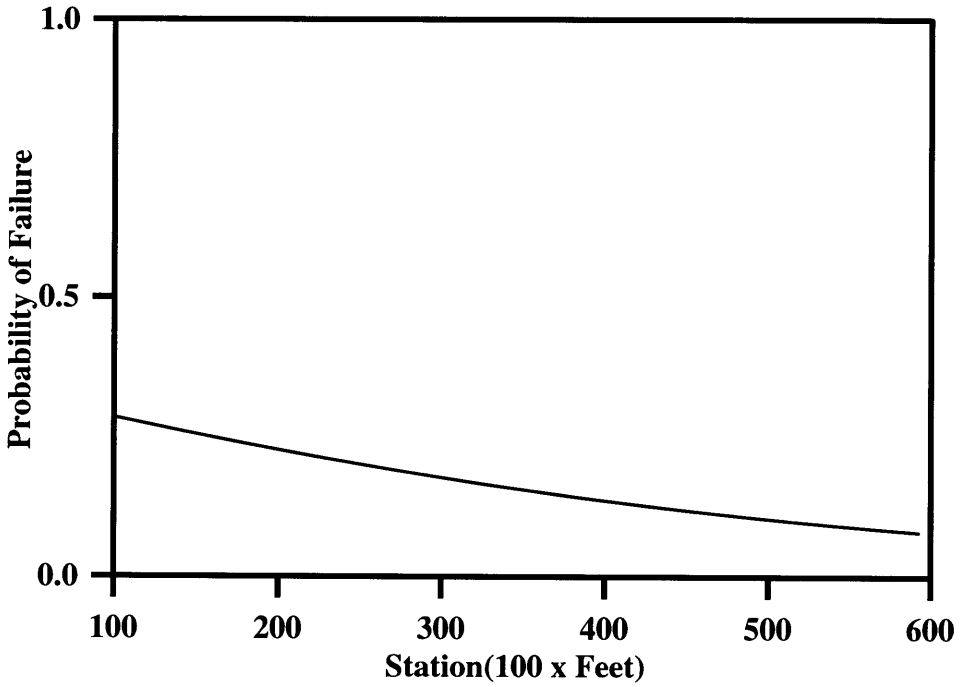

Figure 4.75: Probability of L-system Failure Occurrence vs. Station

Figures 4.74 and 4.75 show that both total hardness and location affect the L-system probability of failure. The p-values of the Chi-square test define the strength of these correlations. Table 4.11 presents the regression coefficients from two different models: one investigating the effect of the total hardness and the other investigating the effect of the location.

Variable	Chi-Square	Prob > Chi-Square
Total Hardness	5.3231	0.0210
Station	26.3775	0.0001

Table 4.11: Regression Parameters For L-system Failure Probability Models

The parameters suggest that the impact of the total hardness is much smaller than the impact of the location.

4.6 Comparison Of The Pre-Excavation And The Post-Excavation Data

Thus far, this chapter dealt with the total hardness values obtained as a result of the post-excavation exploration program. However, the entire bidding process is based on the somewhat limited pre-excavation data. It appeared interesting to conduct an analysis that would compare the two sets in terms of their predictive capabilities. To do that a code was written to do the following: create a data set that would combine the pre-excavation total hardness values and the post-excavation total hardness values using ID station as a merging criteria e.g., if ID station in the pre-excavation data set was 442.08, the closest one in the post-excavation data was used to obtain the total hardness. The SAS System Linear Regression procedure was executed relating pre-excavation total hardness and post-excavation total hardness. The ideal result if two were identical would be the 45 degrees line through the origin. The actual results were as follows:

Pre-excavation Hardness = 2.3565 + 0.9318*Post-excavation Hardness

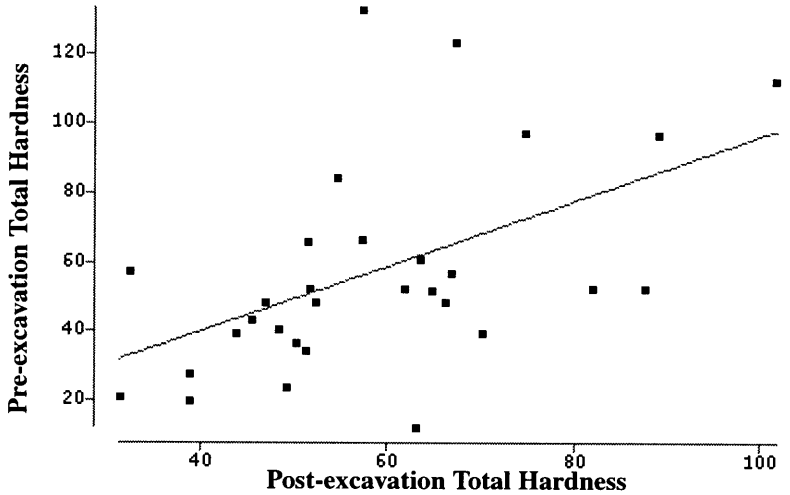

Figure 4.76: The Linear Regression Fitting Procedure on the Pre-excavation and the Post-excavation Total Hardness Data

The Student Residual Statistic was used to detect the observation that influences the regression the most. It was the (134.0, 57.4) pair, that was considered an outlier and taken

out of the analysis. Figure 4.76 shows the results of the initial regression analysis, and Figure 4.77 shows the resulting regression line after the detection of outlier, which is marked by "x".

Pre-excavation Hardness = -1.13 + 0.9452*Post-excavation Hardness

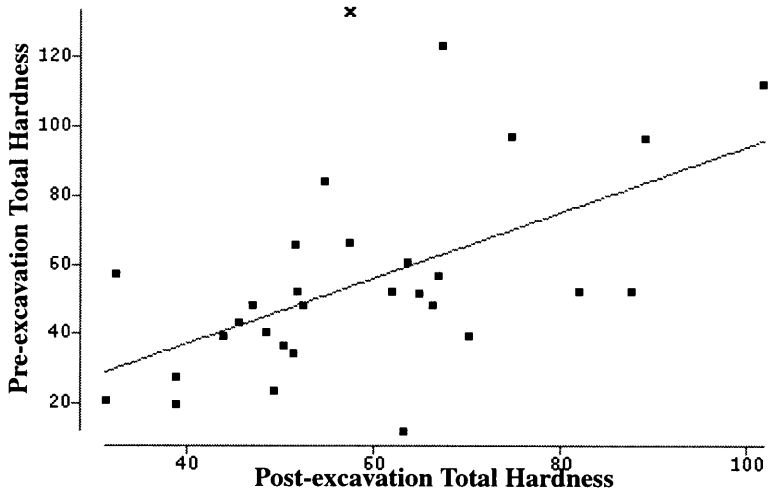

Figure 4.77: Modified Regression Model of the Post-excavation and the Pre-excavation Total Hardness

The goodness-of-fit test performed on both procedure runs yielded the following results:

Model	R-square	F-statistic	Prob > F
Unmodified	0.2652	10.1060	0.0036
Modified	0.3543	14.8181	0.0007

Table 4.12: Model Comparison Statistics

Table 4.12 presents an evidence in favor of the modified model i.e., both F-statistic and R-square values indicate the model improvement. As part of the SAS System Linear Regression procedure, the Student t statistic was computed for each of the regression parameters. The results are presented in Table 4.13:

Parameter	Estimate	T-statistic	Prob > |T|
Intercept	-1.1306	-0.0753	0.9405
Coefficient	0.9452	3.8494	0.0007

Table 4.13: Modified Model Parameter Statistics

Using the results of the T-test performed on the modified model one can conclude that there is 94% chance that the intercept is zero, and the coefficient of the regression is approximately one. If so, the post-excavation total hardness can be estimated using the pre-excavation exploration results.

4.7 Investigation of the Sample Size Effect

Pre-excavation exploration is usually limited by the number of borings that is feasible for a particular budget. For example, the post-excavation data set has 154 records, while the pre-excavation data set has 30 total hardness data points. To model this limitation, a code was written that implemented the following tasks:

- varying the sample size, subsample the data set i.e., if the sample size is 10, the number of such subsets would be 154/10 = 15;
- iterating one record by one, create as many such subsets as the total sample size would permit i.e., 154 divided by the sample size;
- for each subset, calculate the total number of failures for cutters and muck removal system failures using the theoretical models derived as a result of the regression procedure;
- for each sample size calculate mean (observed and theoretical), standard deviation (STD) and coefficient of variation (CV) of the number of failures (NF).

The results are presented in Table 4.14:

Sample Size	Numb. of subsets	Cutters Mean of NF (O)	Cutter Mean of NF (T)	Cutter STD of NF (T)	Cutter CV of NF (T)	Muck Mean of NF (O)	Muck Mean of NF (T)	Muck STD of NF (T)	Muck CV of NF (T)
10	15	257	229	1.54	10.09%	380	377	1.7	6.78%
20	8	254	229	2.65	9.23%	374	380	1.05	2.21%
30	5	257	230	2.17	4.71%	392	379	1.87	2.47%
40	4	258	230	2.72	4.73%	382	380	1.19	1.26%
50	3	257	230	3.28	4.28%	384	378	3.25	2.57%

Table 4.14: Sample Size Influence on Variance

Table 4.14 allows one to conclude that the magnitudes of the coefficient of variation are not large. Thus, smaller samples can, in fact, be representative of the entire population, in our case 154 records.

4.8 The Reliability Assessment of the TBM System

The investigation of the probability of failure discussed earlier in this chapter yielded the results allowing one to look at the question of the system reliability. The reliability of a system can be defined as its ability to perform i.e., it can be expressed as a probability of non-failure. It has been shown that the TBM system can be looked at as a series system consisting of the three major subsystems (the TBM mechanical system, the TBM muck removal system, and the TBM support installation system). Each TBM subsystem in turn can be viewed as a system of independent components, also "connected" in series. Therefore, the failure of the single component causes system failure. In a series system, if the probability of failure of component A is P(A), the probability of failure of component B is P(B), and the probability of failure of component C is P(C), then the probability of the system failure is:

$$P(sys) = P(A) + P(B) + P(C) - P(A) \times P[B] - P(A) \times P(C) - P(B) \times P(C) + P(A) \times P(B) \times P(C)$$

The reliability of the system is 1 - P(sys) (Dwass et al, 1970). This equation is based on the assumption that A, B, and C are independent events. Another assumption made for computation of the TBM system reliability is that the TBM mechanical system failure probability can be replaced by the cutter failure probability, and the TBM muck removal system failure probability can be replaced by the TBM muck removal system excluding the horizontal conveyor failure probability, as far as the total hardness influence is concerned. The system reliability is 1 - P(TBM system). Figure 4.78 presents the graphical representation of the total hardness influence on the TBM system reliability:

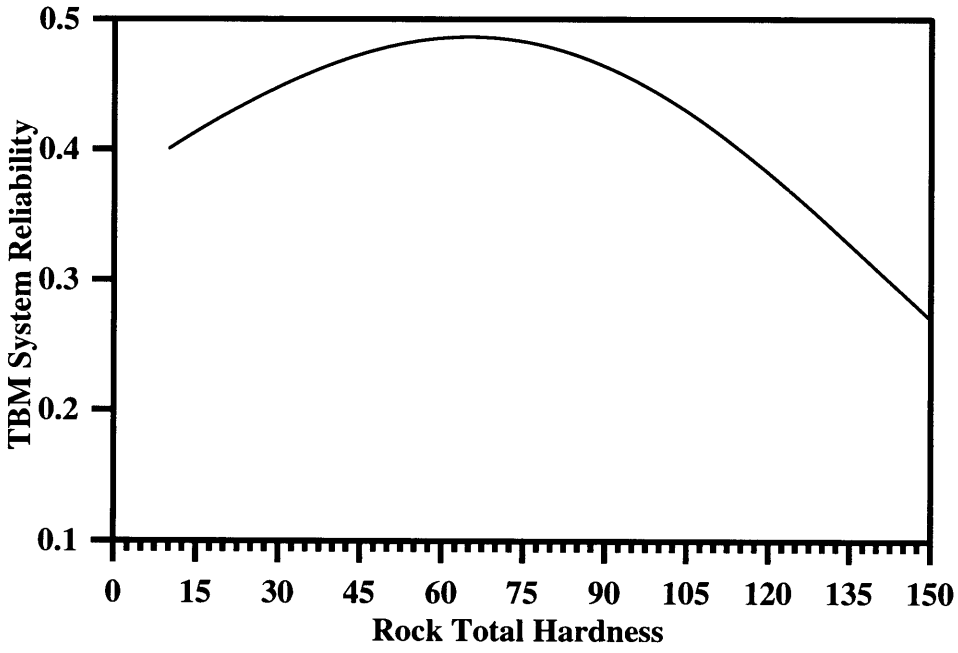

Figure 4.78: The TBM System Reliability as a Function of the Total Hardness

The reliability function reaches its maximum at the point of Ht~70, after which it decreases. This is evidence for the conclusion that, generally, the TBM system is more reliable in harder rock up to a point where the cutter failure becomes critical for the system

reliability. However, the cost and the time necessary for the cutter replacement are much less than the cost and the time to repair any other TBM subsystem. So, one can still say that as far as the time-to-complete-tunnel is concerned, the softer rock presents more problems. Also, as the technology advances, the possibilities to increase cutter "life" arise.

Chapter 5

Pre-bid Exploration Data Analysis

5.1 Introduction

It is hard to overestimate the importance of the pre-excavation exploration. Those data are the only available source for design and bidding. The obvious disadvantage of such a source is that very often the boring locations have a substantial offset from the alignment, both vertically and horizontally. One could ask a very legitimate question how well these data represent the actual rock mass conditions. The variability of the stratification can be substantial, and rock mass discontinuity may alter the general picture significantly. For the Outfall Tunnel pre-bid the exploration program was conducted by Metcalf & Eddy. The program was described in Chapter 2. The unique possibility to compare the results of the same analysis performed on both pre-excavation and post-excavation data was used and the results are presented in this Chapter 5. The subject of such a comparison are TBM downtime categories, defined in Chapter 2, namely T-system failures (drive motors, hydraulic and electrical subsystems), CU-element failures (cutters), M-system failures (muck removal system excluding the horizontal conveyor), HZ-element failures (horizontal conveyor), and L-system failures (support installation system). The linear regression procedure of the SAS System was used for CU-element related failures. Poisson regression was used for T-system failures, M-system failures, and L-system failures.

5.2 Results of the Regression Analysis

1. T-system, CU-element related failures:

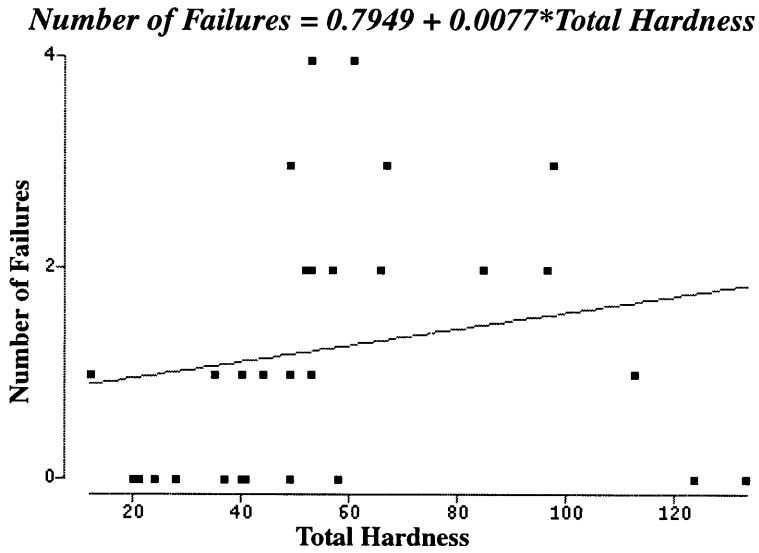

Figure 5.1: Results of the Regression Analysis of CU-element Failures (All Data)

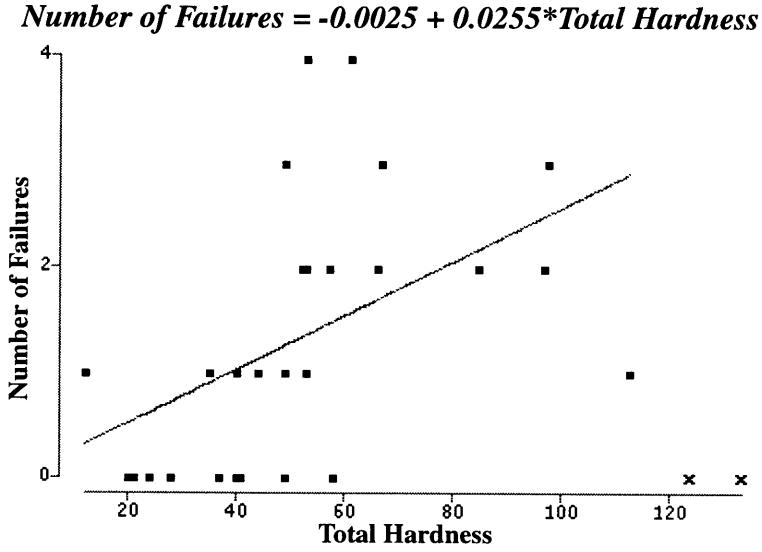

Figure 5.2: Results of the Regression Analysis of CU-element Failures (Truncated Data)

Truncated points are marked by "x".

The variance analysis statistics are shown in table 5.1:

Model:	Coefficient of Determ.	F-statistic:	Prob > F:
Unmodified	0.0346	1.0030	0.3252
Modified	0.2386	8.1473	0.0084

Table 5.1: Results of Goodness-of-Fit Test for Cutter Failures Linear Models

Figures 5.1 and 5.2 present the results of the regression analysis performed on CU-element data. There is strong correlation between the total hardness and number of failures, which agrees with the results of the corresponding analysis performed on the post-excavation data set. Figure 5.2 shows the same regression after the excluding of two outliers from the analysis. The difference in F-statistic for both models indicates that due to the relatively small sample size, data has become very sensitive: the elimination of two zero values changed the regression dramatically.

2. T-system Failures:

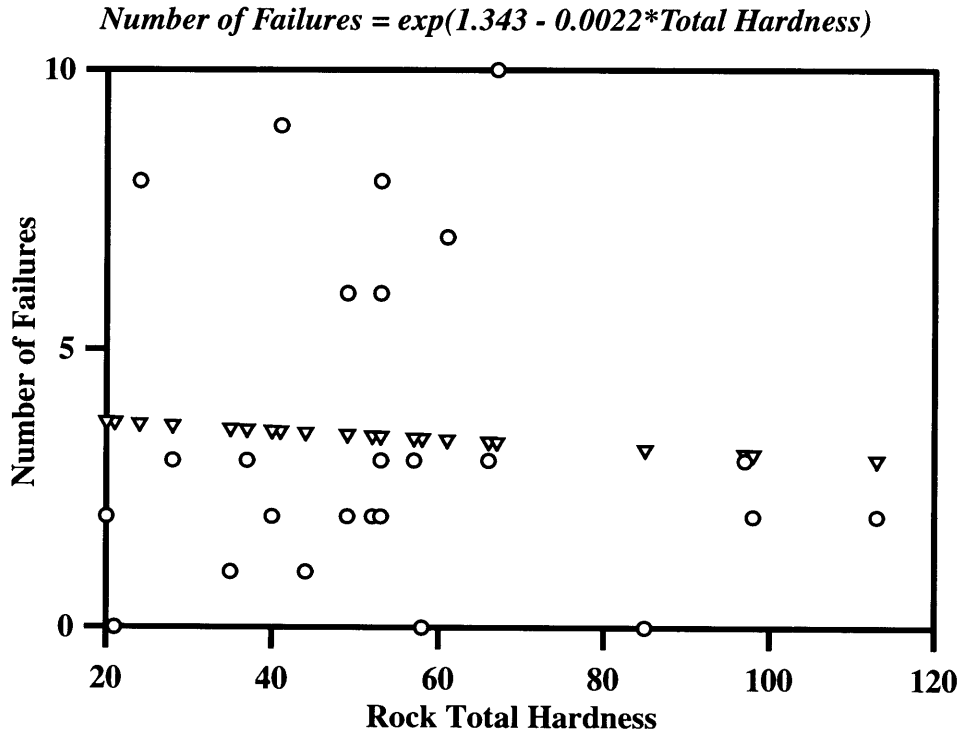

Figure 5.3: Actual and Predicted Values of T-system Failure Model
Circle markers denote actual values, inverted triangle markers denote predicted values.

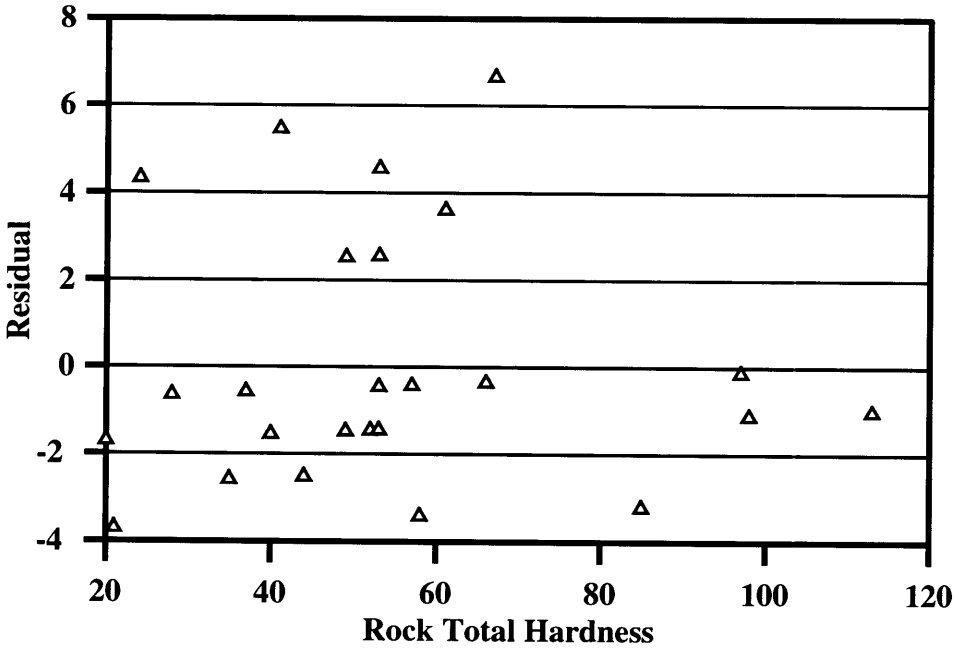

Figure 5.4: Residuals of the Predicted Values of T-system Number of Failures

The summary of the SAS analysis of the regression parameters is presented below:

Parameter	Estimate	Asymptotic	95% Confidence	95% Confidence
		Standard Error	Lower	Upper
Intercept	1.343	0.268	0.791	1.895
Hardness	-0.0022	0.0047	-0.0119	0.0075

Table 5.2: Regression Parameters for T-system Failure Model

Figure 5.3 shows almost no correlation between the total hardness and T-system number of failures. Since the true value of the coefficient for the total hardness lies between negative and positive number (see Table 5.2: upper and lower limits of the 95% confidence interval), one can consider an assumption of zero impact as reasonable. The corresponding analysis performed on the pre-excavation data set yielded similar results.

3. M-system related failures:

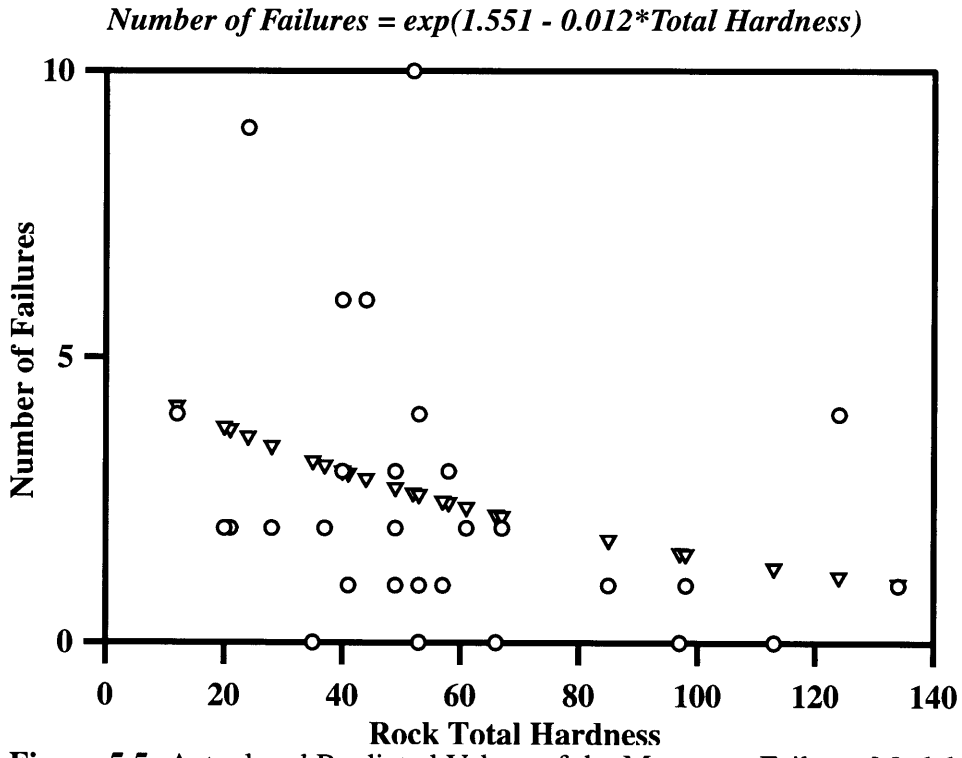

Figure 5.5: Actual and Predicted Values of the M-system Failures Model

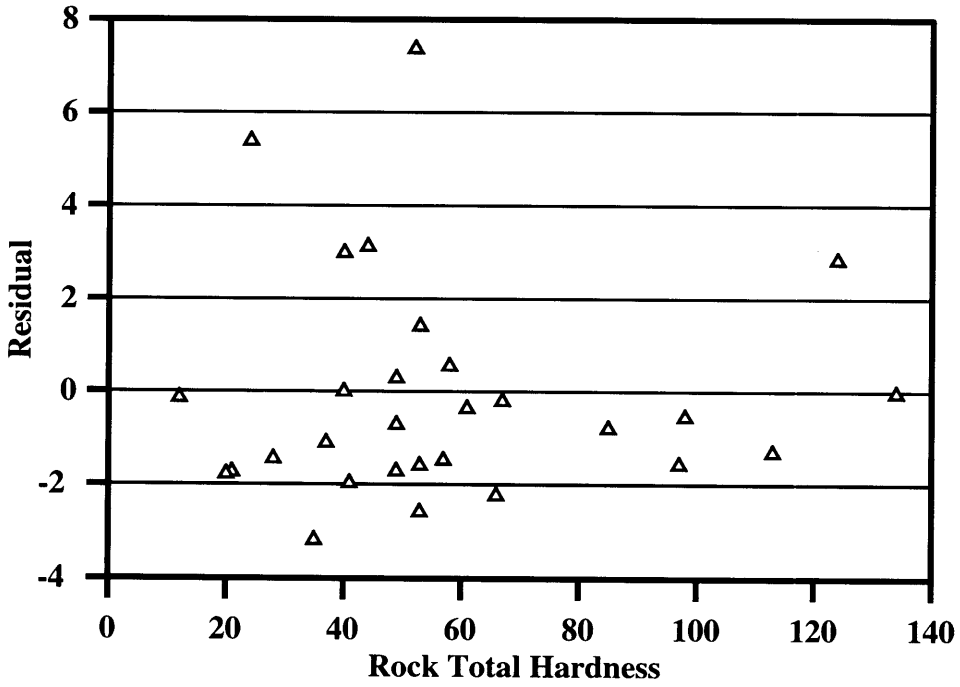

Figure 5.6: Residuals of the M-system Predicted Number of Failures

The summary of the SAS analysis of the regression parameters is presented below:

Parameter	Estimate	Asymptotic	95% Confidence	95% Confidence
		Standard Error	Lower	Upper
Intercept	1.551	0.25	1.0397	2.0627
Hardness	-0.0116	0.00458	-0.002098	-0.0002197

Table 5.3: Regression Parameters for M-system Failure Model

Figures 5.5 and 5.6 show a good correlation between the total hardness and M-system number of failures. There is an exponential decay function that describes the relationship, which agrees with the results obtained from the post-excavation data analysis. Another similarity observed is that the variance of the predictive model seems to decrease with increasing total hardness (see Figure 5.6). Table 5.3 shows the SAS System regression parameter estimation. The standard error for both intercept and coefficient has the same order of magnitude as the estimates.

4. L-system Failures:

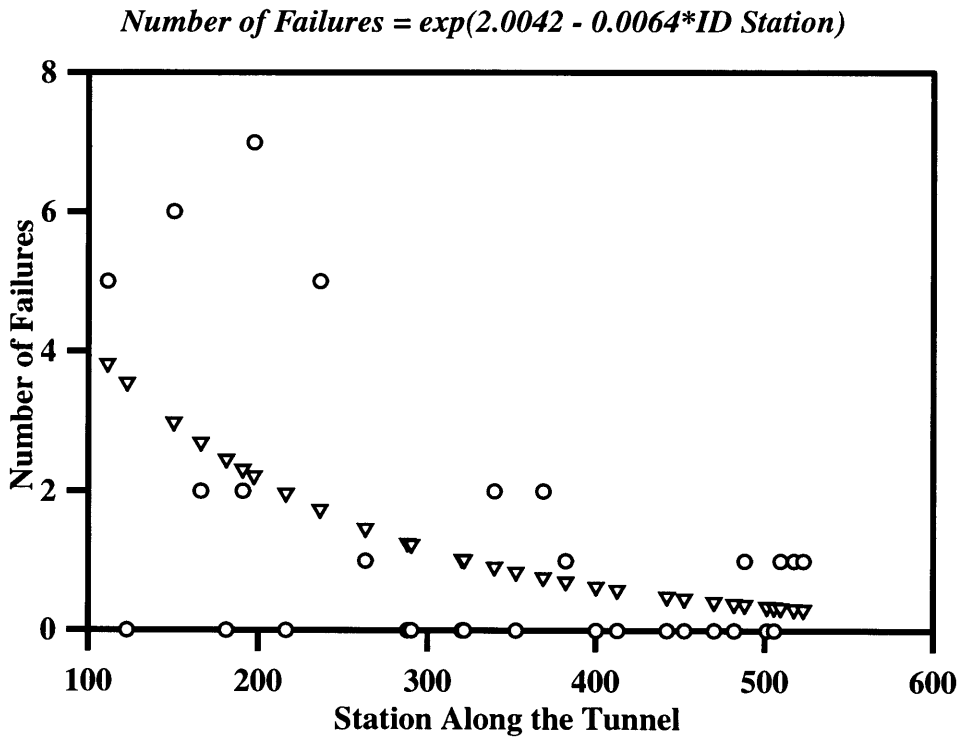

Figure 5.7: Actual and Predicted Values of the L-system Number of Failures

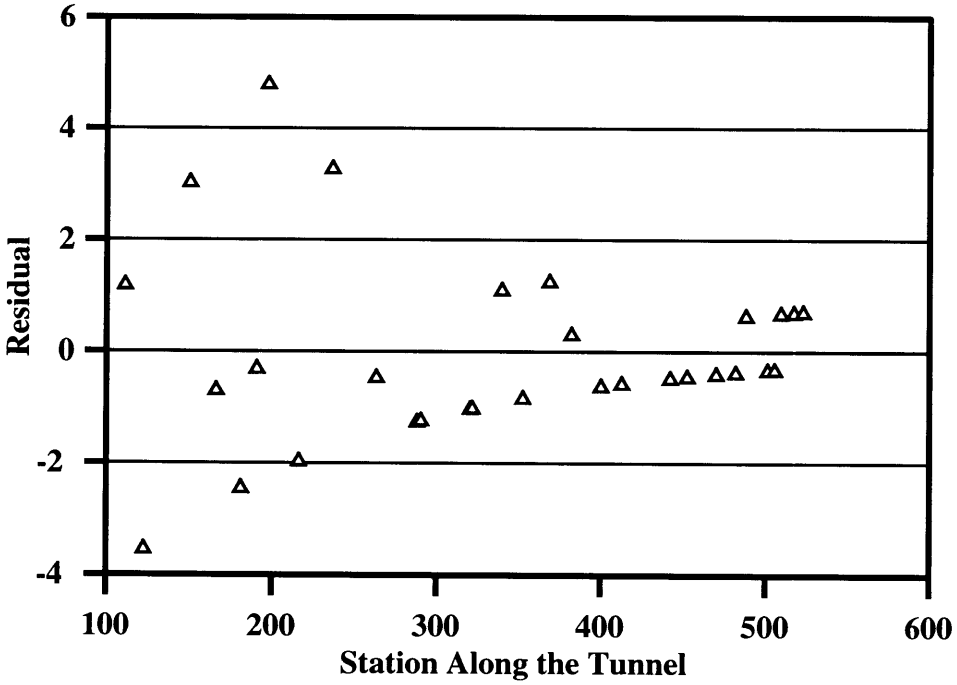

Figure 5.8: Residuals of the L-system Predicted Number of Failures

The summary of the SAS analysis of the regression parameters is presented below:

Parameter	Estimate	Asymptotic	95% Confidence	95% Confidence
		Standard Error	Lower	Upper
Intercept	2.0422	0.3842	1.2552	2.8293
Hardness	-0.00638	0.00145	-0.00936	-0.0034

Table 5.4: Regression Parameters for L-system Failure Model

Figures 5.7 and 5.8 indicate a strong correlation between the location and the L-system number of failures. The results agree well with the results of the corresponding analysis performed on the post-excavation data set. Residual values decrease to almost zero (see Figure 5.8) as the TBM advances. Table 5.4 shows that the standard error is not large.

5.3 Analysis of Failure Probability

The SAS System Logistic Regression Procedure was executed twice for two explanatory variables, namely the total hardness, and RQD - rock quality designation, a parameter introduced by Deer to account for the rock mass discontinuities. The RQD values used for the analysis were averaged over the tunnel height + - 25 feet. This average was entered into the data set. The results are presented below:

1. T-system failures

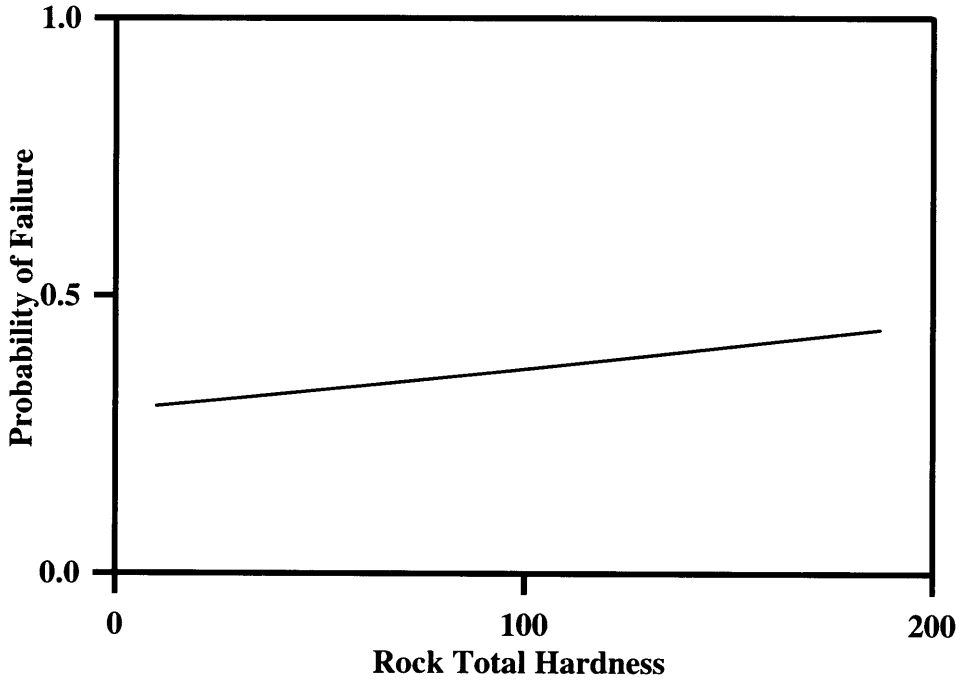

Figure 5.9: T-system Failure Probability vs. Total Hardness (Pre-bid Data)

The probability of T-system failure is essentially unaffected by the total hardness (see Figure 5.9), since the Chi-Square test performed to investigate the influence of the explanatory variable on the model yielded Prob > Chi-Square = 0.4817 (see Table 5.5). The results agree with the post-excavation data set analysis (see Figure 4.68).

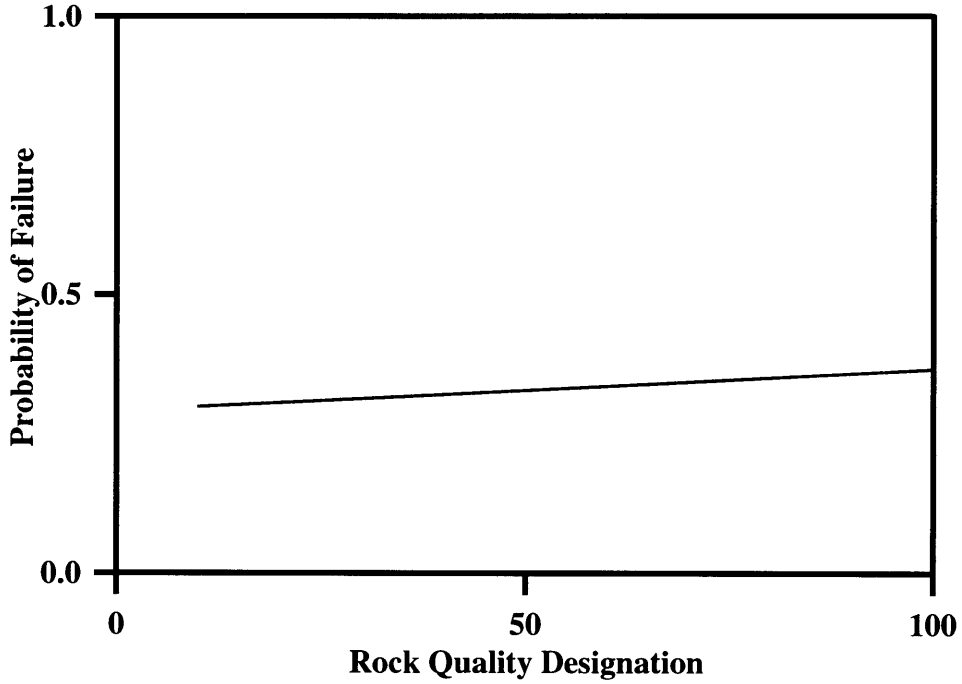

Figure 5.10: T-system Failure Probability vs. RQD (Pre-bid Data)

Figure 5.10 indicates that there is no correlation between the RQD and T-system number of failures. The results of the Chi-Square test (see Table 5.5) support that conclusion.

Failure Category	Prob > Chi-square for the Intercept (Hardness Model)	Prob > Chi-square for the Intercept (RQD Model)	Prob > Chi-square for the Coefficient (Hardness Model)	Prob > Chi-square for the Coefficient (RQD Model)
T-system	0.0053	0.1981	0.4817	0.6826

Table 5.5: The Results of the Chi-square Test for T-system Pre-bid Models

2. CU-element failures

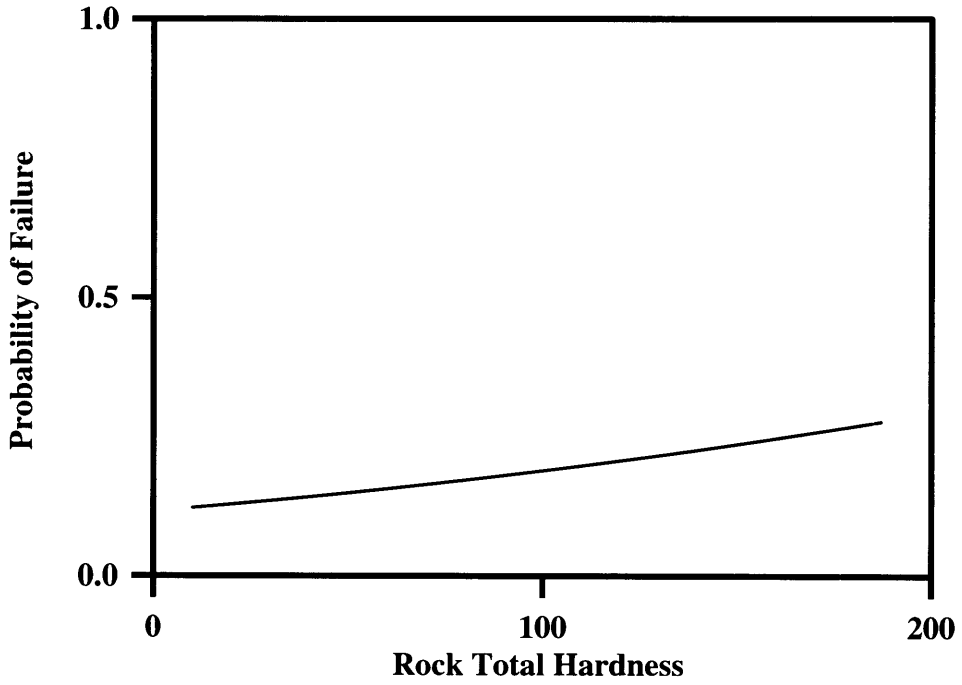

Figure 5.11: CU-element Failure Probability vs. Total Hardness (Pre-bid Data)

The cutter failure is an event that requires a one-to-one correspondence between the location of failure and the total hardness value at that particular location. The bore holes for the pre-excavation exploration program were located in some cases 1000 feet off the alignment. That is why the influence of the total hardness in the pre-excavation data analysis on the cutter number of failures is so small compared to the results of the post-excavation data analysis, although the general trend is indeed the same. One can still observe the increasing failure probability with the increasing total hardness (see Figure 5.11).

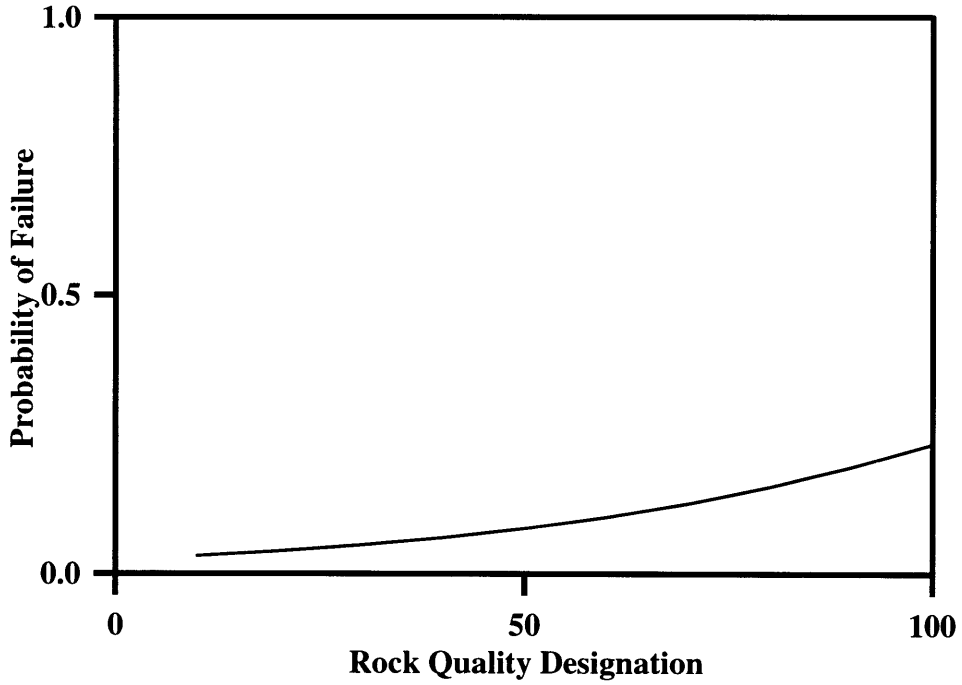

Figure 5.12: CU-element Failure Probability vs. RQD (Pre-bid Data)

Figure 5.12 presents an evidence in favor of the conclusion that the cutter failures are influenced not only by the total hardness, which is a property of the intact rock, but also by the RQD, which is a property of the rock mass. Logically, the smaller the RQD value, the easier it is to cut the rock. The Chi-Square test performed on the regression coefficients yielded the Prob > Chi-Square = 0.0652 (see Table 5.6), which is an evidence of a strong correlation.

Failure Category	Prob > Chi-square for the Intercept (Hardness Model)	Prob > Chi-square for the Intercept (RQD Model)	Prob > Chi-square for the Coefficient (Hardness Model)	Prob > Chi-square for the Coefficient (RQD Model)
CU-element	0.0001	0.0017	0.3387	0.0652

Table 5.6: The Results of the Chi-square Test for CU-element Pre-bid Models

3. M-system failures

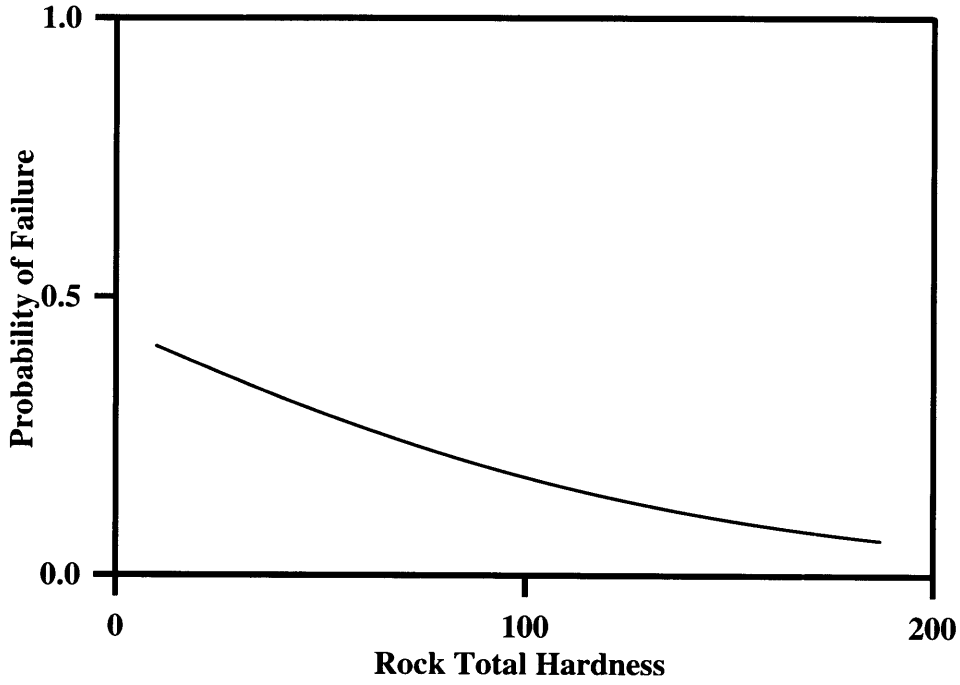

Figure 5.13: M-system Failure Probability vs. Total Hardness (Pre-bid Data)

Figure 5.13 clearly shows that the total hardness has an impact on the muck removal system number of failures. Both the shape of the curve and the probability values are identical to the result obtained from the post-excavation data analysis (see Figure 4.73). One could conclude that the correlation between the total hardness and the M-system failure probability is a rock mass property, even though the total hardness values were obtained from the intact rock testing.

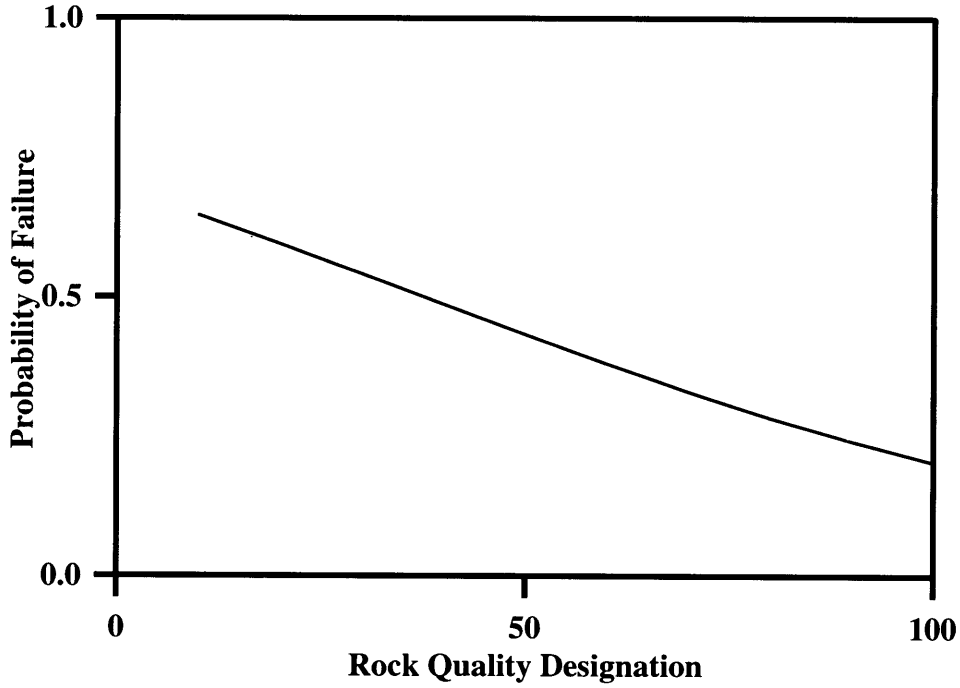

Figure 5.14: M-system Failure Probability vs. RQD (Pre-bid Data)

The correlation (see Table 5.7) between the rock quality designation (RQD) and the muck removal system (see Figure 5.14) failure probability is an evidence in favor of the conclusion that the rock mass discontinuities cause the non-uniformity and angularity of the muck fragments, which in its turn cause the conveyor failure.

Failure Category	Prob > Chi-square for the Intercept (Hardness Model)	Prob > Chi-square for the Intercept (RQD Model)	Prob > Chi-square for the Coefficient (Hardness Model)	Prob > Chi-square for the Coefficient (RQD Model)
M-system	0.5121	0.2238	0.0246	0.0100

Table 5.7: The Results of the Chi-square Test for M-system Pre-bid Models

4. HZ-element failures

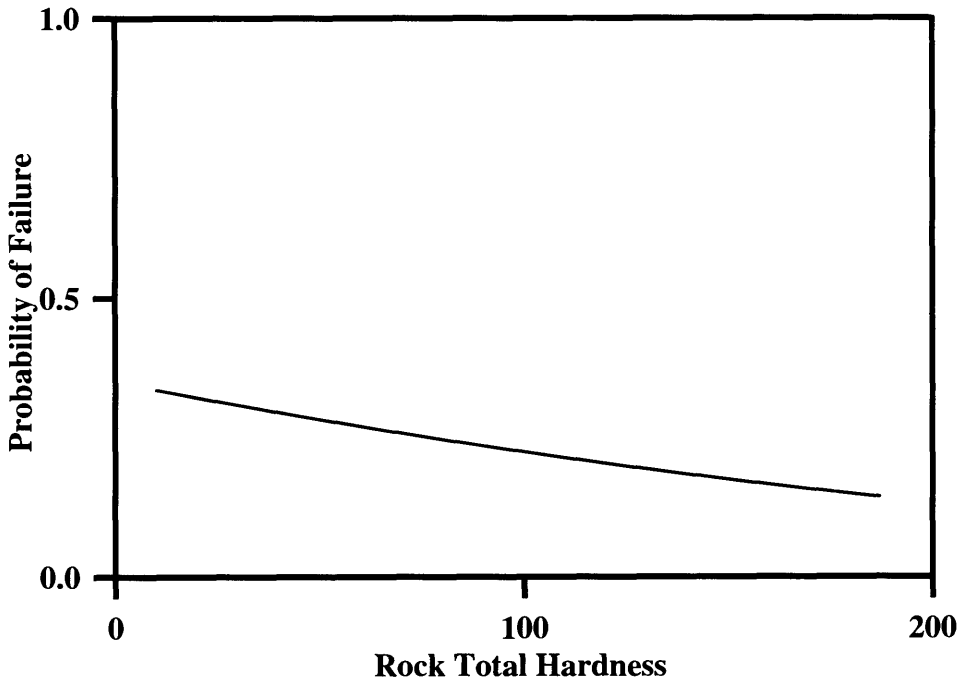

Figure 5.15: HZ-element Failure Probability vs. Total Hardness (Pre-bid Data)

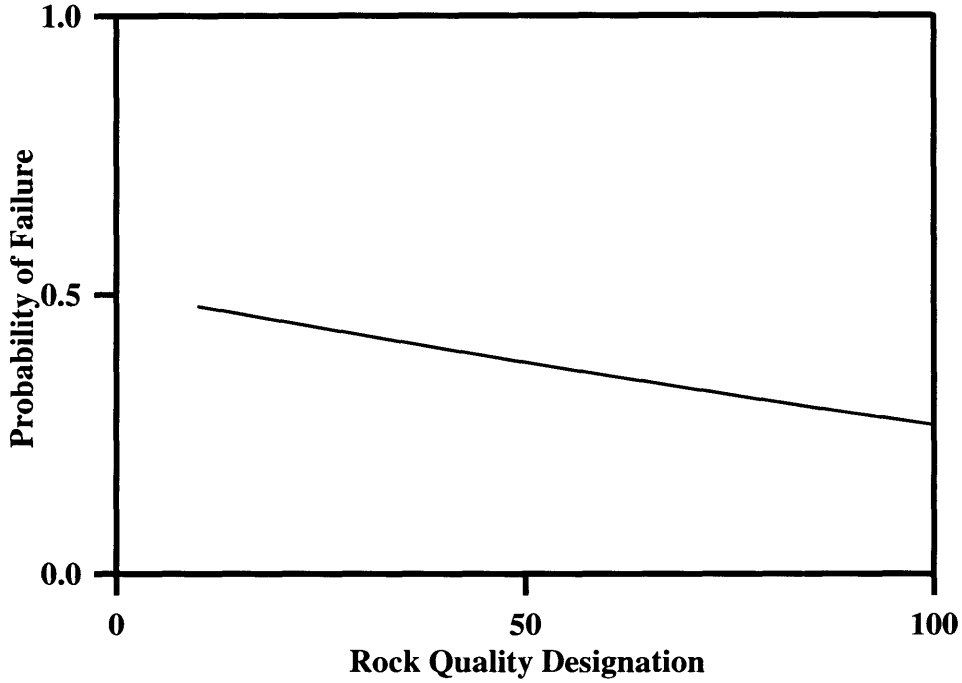

Figure 5.16: HZ-element Failure Probability vs. RQD (Pre-bid Data)

Figures 5.15 and 5.16 suggest that there is a very little correlation between the rock properties, namely the total hardness and the RQD, and the horizontal conveyor failure probability. The Chi-Square test for the coefficients yielded Prob > Chi-Square = 0.25 for the total hardness, and Prob > Chi-Square = 0.21 for the RQD (see Table 5.8), which supports the conclusion made above. It also agrees with the results obtained from the post-excavation data analysis (see Figure 4.75).

Failure Category	Prob > Chi-square for the Intercept (Hardness Model)	Prob > Chi-square for the Intercept (RQD Model)	Prob > Chi-square for the Coefficient (Hardness Model)	Prob > Chi-square for the Coefficient (RQD Model)
HZ-element	0.0628	0.9798	0.25	0.2114

Table 5.8: The Results of the Chi-square Test for HZ-element Pre-bid Models

5. L-system failures

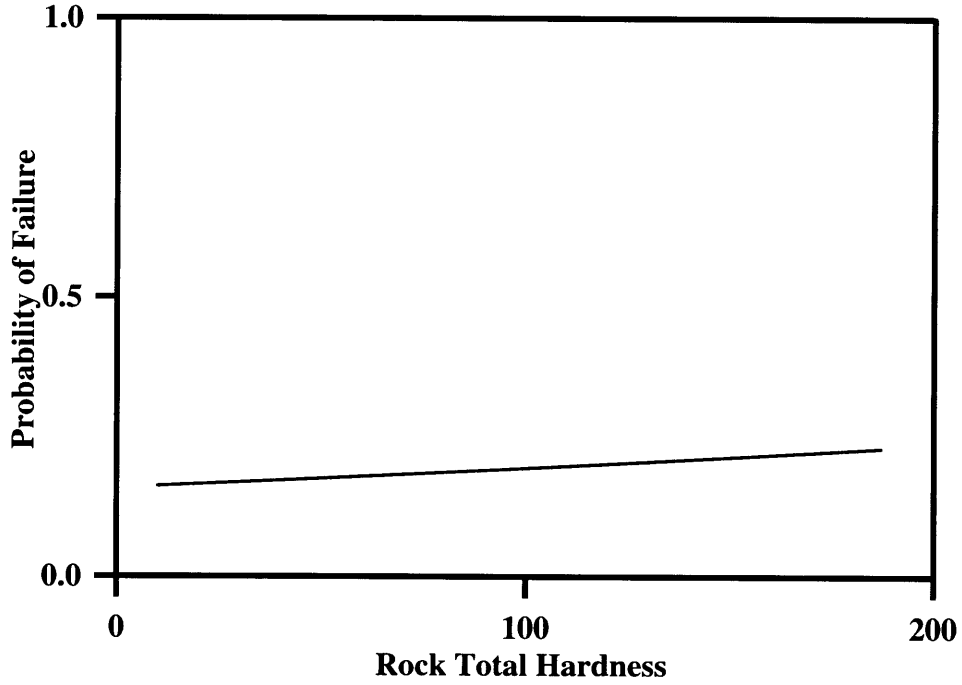

Figure 5.17: L-system Failure Probability vs. Total Hardness (Pre-bid Data)

Figure 5.17 and 5.18 as well as the results of the Chi-Square test (see Table 5.9) for the regression parameters suggest that both total hardness and RQD have no impact on the support installation system failure probability.

Failure Category	Prob > Chi-square for the Intercept (Hardness Model)	Prob > Chi-square for the Intercept (RQD Model)	Prob > Chi-square for the Coefficient (Hardness Model)	Prob > Chi-square for the Coefficient (RQD Model)
L-system	0.0001	0.1013	0.6736	0.6890

Table 5.9: The Results of the Chi-square Test for L-system Pre-bid Models

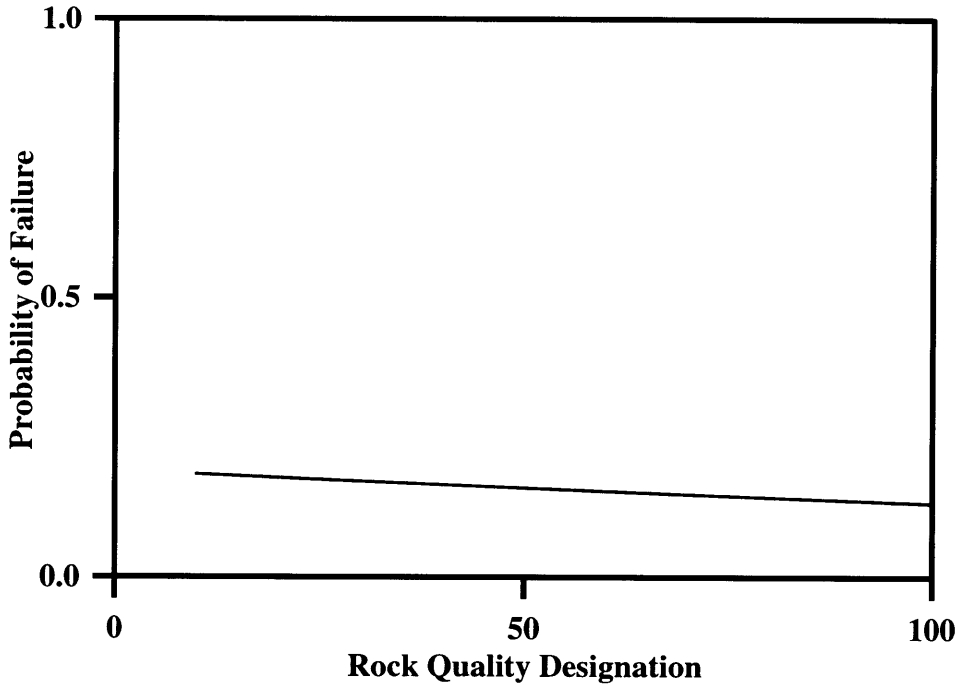

Figure 5.18: L-system Failure Probability vs. RQD (Pre-bid Data)

Chapter 6

Summary and Conclusions

6.1 Summary

The Tunnel Boring Machine (TBM) is a system consisting of three major subsystems, namely the TBM mechanical system (cutters, drive motors, electrical system, hydraulic system), the TBM muck removal system (transfer conveyor, boretec conveyor, TBM conveyor, horizontal conveyor, vertical conveyor), and the TBM support installation system (erector arm system, supply system). These subsystems are "connected" in series i.e., the entire system works only if all the subsystems work or, conversely, only if any of the subsystems does not fail. Two factors were found to have an impact on the failure occurrence, both in terms of the probability and in terms of the number of failures, namely the rock total hardness, and location.

The location impact was expressed as:

- the "fatigue" effect on cutters and horizontal conveyor, which are the components of the TBM mechanical system and the TBM muck removal system respectively. This effect is shown on Figure 6.1.
- the "learning" effect on the TBM support installation system. This phenomenon is presented on Figure 6.2.

The total hardness impact was observed for the following TBM components:

- cutters - both the number of failures and the probability of failure increase with increasing total hardness;
- muck removal system (except for the horizontal conveyor, effected only by location) - both the number of failures and the probability of failure decrease with increasing total hardness.

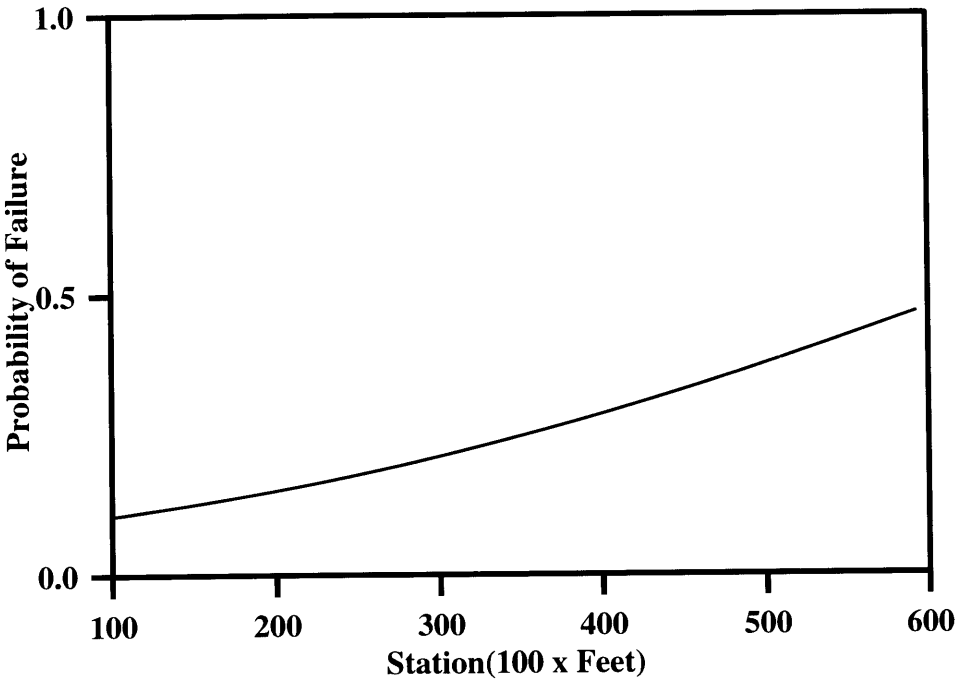

Figure 6.1: The Illustration of the "Fatigue" Effect: Horizontal Conveyor Failure Probability

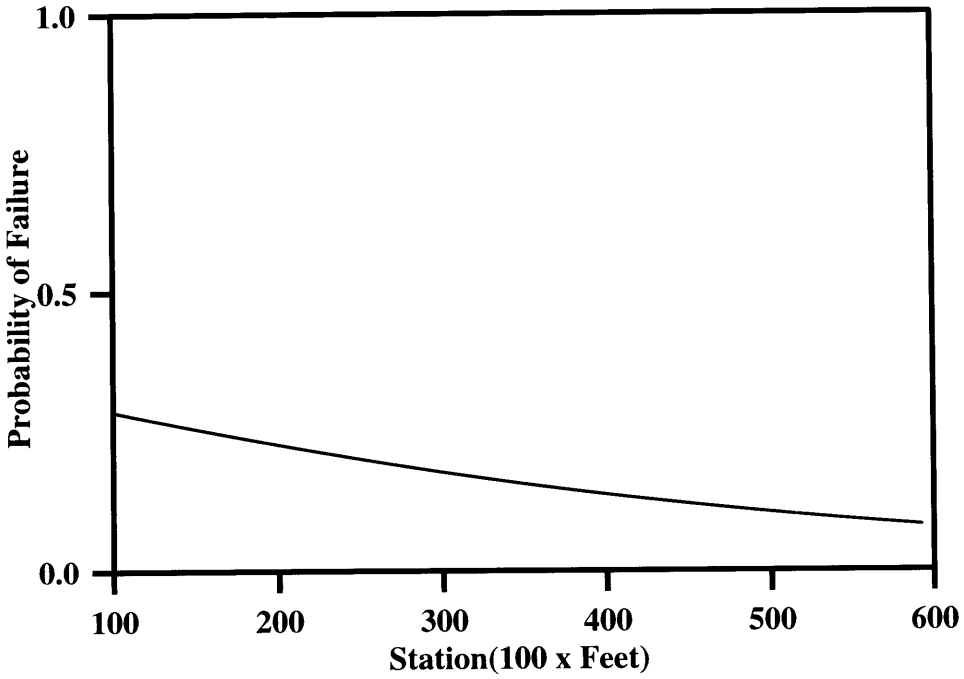

Figure 6.2: The Illustration of the "Learning" Curve: L-system Failure Probability

Another issue addressed in this thesis was the comparison of the pre-excavation and post-excavation data. The comparison of the total hardness values led to the conclusion that the pre-excavation total hardness data and the post-excavation total hardness data were very similar. The analysis of the sample size showed that the effect of the smaller pre-excavation sample was reasonably small (coefficient of variation in the order of 10%). However, the fact that the pre-excavation borings were horizontally offset from the tunnel alignment does influence the correlations. Figures 6.3, 6.4, 6.5. and 6.6 are examples of this influence.Figures 6.3 and 6.4 show the cutter related failure probability for both data sets. It is obvious that the offset effect is strong i.e., the curve flattened and the regression parameters indicate a weaker correlation for the pre-excavation data (see Table 6.1).

Parameter	Estimate	Chi-square statistic	Prob > Chi-square
Post-exc. Intercept	2.8476	171.15	0.0001
Pre-exc. Intercept	2.021	24.3952	0.0001
Post-exc. Hardness	-0.024	57.8	**0.0001**
Pre-exc. Hardness	-0.0057	0.9153	**0.3387**

Table 6.1: Regression Parameters Comparison for the Post-excavation and Pre-excavation Cutter Related Failure Probability Models

The evidence suggests that the pre-excavation data did not provide sufficient enough information about total hardness to capture the correlation between the total hardness and the probability of failure. Cutter failure is so location dependent that any variation in the total hardness values causes the correlation to weaken.

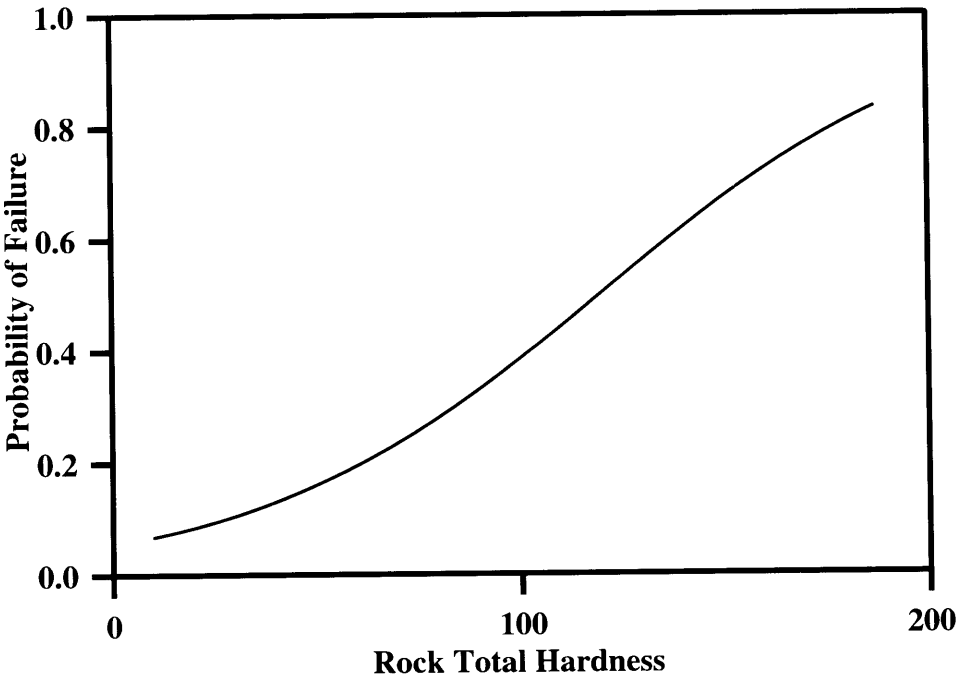

Figure 6.3: Cutter Failure Probability vs. Post-excavation Total Hardness

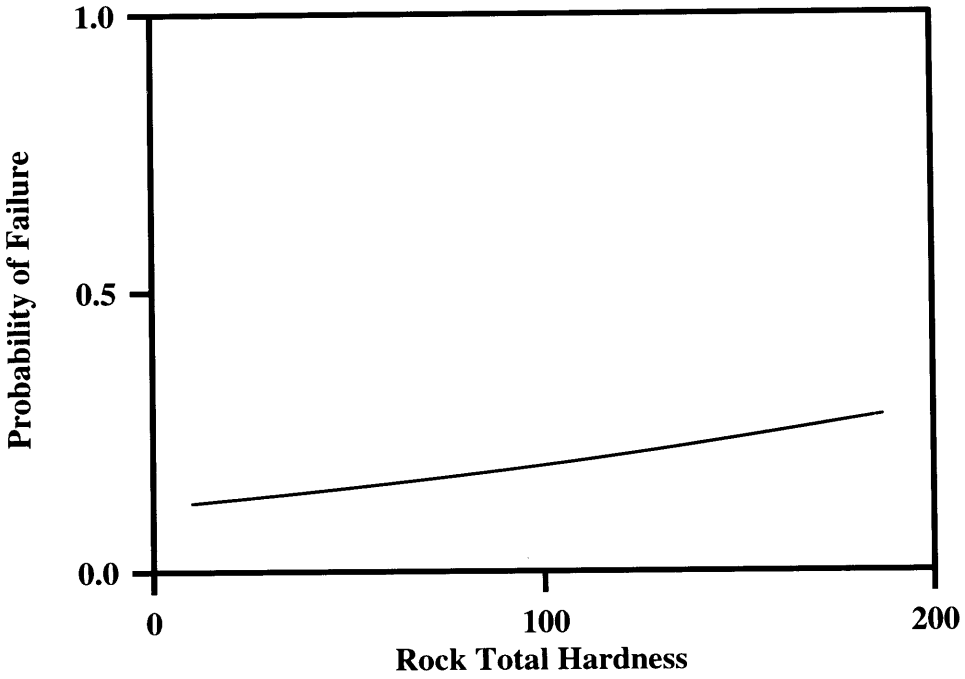

Figure 6.4: Cutter Failure Probability vs. Pre-excavation Total Hardness

On the other hand, the muck removal system failure probability analyses yielded almost identical results for the pre-excavation and pre-excavation total hardness (see Figures 6.4 and 6.5):

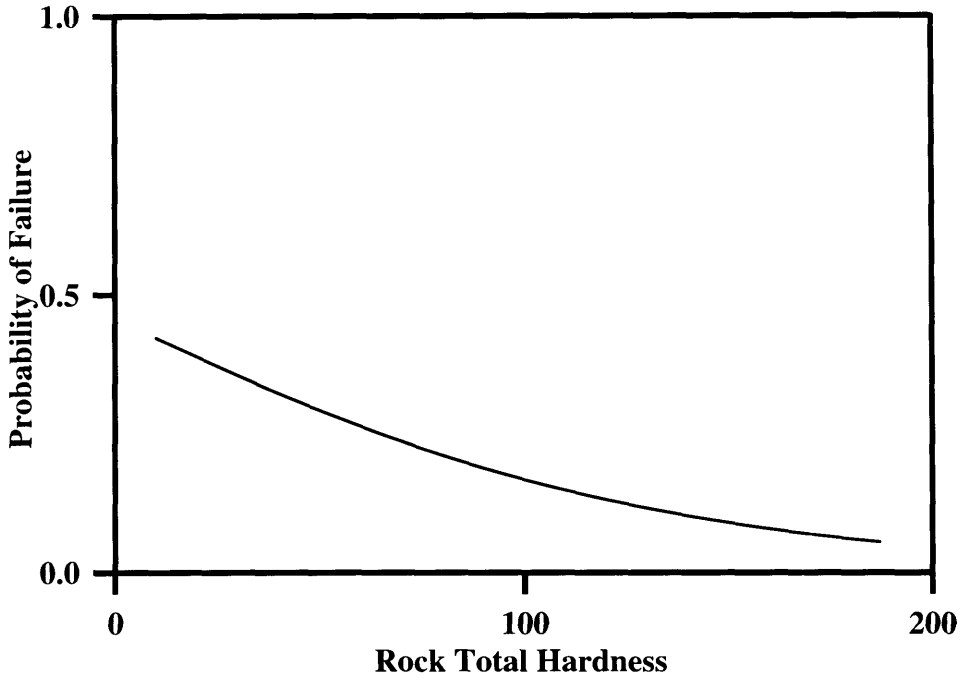

Figure 6.5: M-system Failure Probability vs. Post-excavation Total Hardness

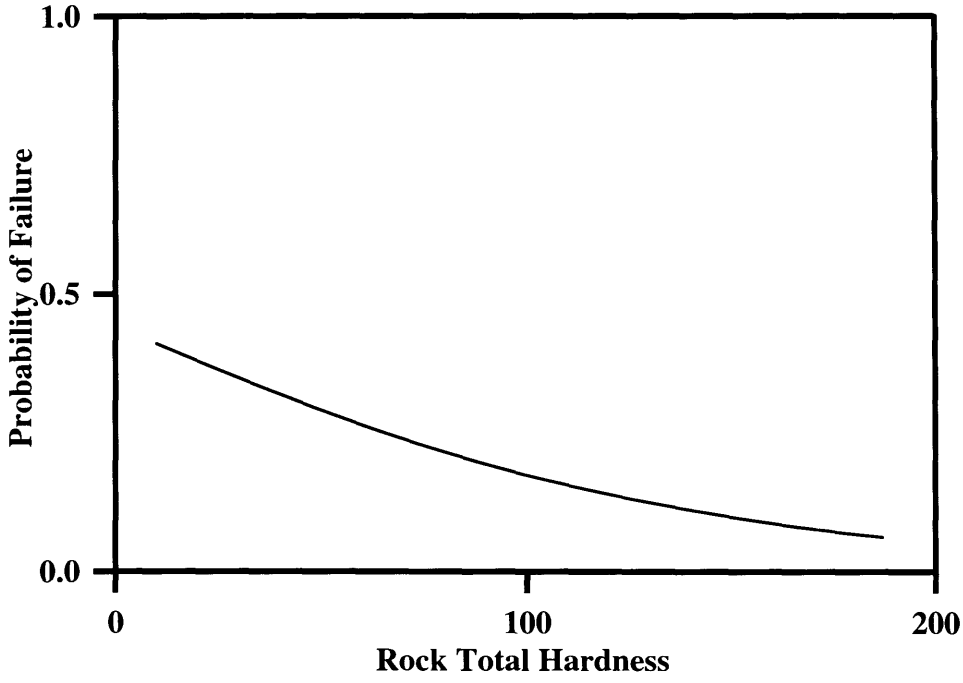

Figure 6.6: M-system Failure Probability vs. Pre-excavation Total Hardness

The regression parameters though indicate a weaker correlation for the pre-excavation data (see Table 6.2).

Parameter	Estimate	Chi-square statistic	Prob > Chi-square
Post-exc. Intercept	0.1693	0.6552	0.4179
Pre-exc. Intercept	0.2256	0.4297	0.5121
Post-exc. Hardness	0.0143	17.3504	**0.0001**
Pre-exc. Hardness	0.0132	5.0549	**0.0246**

Table 6.2: Regression Parameters Comparison for the Post-excavation and Pre-excavation M-system Related Failure Probability Models

Again, as in case of the cutter failures the bore hole offset weakens the correlation.

6.2 Conclusions

This results of this research allow one to draw the following conclusions:

- the Tunnel Boring Machine is a system, consisting of three major components (the TBM mechanical system, the TBM muck removal system, and the TBM support installation system), which are connected in series; this makes each component critical i.e., in the event of the single component failure, the system fails;
- total hardness influences failure occurrence of the following TBM systems and sub-systems: the cutters (CU-element of the T-system), and the muck removal system (M-system), excluding the horizontal conveyor (HZ-element of the M-system);
- another factor influencing the TBM component failures was the "fatigue" factor, which is a function of location; specifically, "fatigue" affects cutter and horizontal conveyor related failures;
- another factor that has a substantial impact on the probability of failure is RQD which is part of the pre-excavation data set: the cutter related failure probability increases with increasing RQD, and the muck removal system related failure probability decreases with increasing RQD, hence RQD affected the same failure categories as the total hardness, namely the cutters and the muck removal system. This allows one to conclude that both intact rock and rock mass properties are equally important in the TBM performance assessment;
- the "learning" effect, which is also location dependent, was observed on failures related to support installation, which shows the importance of the proper maintenance and repair programs;
- the analyses performed on the data sets containing the Argillite data yielded the same results as the data set containing Argillite and Diabase data i.e., the Diabase with the same total hardness as Argillite did not cause a higher number of failures.

The TBM system reliability investigation (see Figure 4.78) leads one to conclude that the TBM system seems to be performing better in harder and less fractured rock. Although the cutter related failures do become critical after a certain threshold (approximately Ht = 70 for this research), having replacement cutters in place, more durable cutters, as well as other maintenance improvements can minimize that effect.

6.3 Possible Extension and Application

The results discussed in this research allow one to better understand the origins of delay. This allows one to improve the existing models for TBM performance prediction. All the existing tunneling simulation programs schedule the delay occurrence based on theoretical probability density functions (Weibull, Exponential, Normal, Log-Normal, Uniform etc.) without any connection to the rock properties. The following technique establishes this connection:

1. Using the derived probability density functions, one can schedule failure occurrence as binary response variable i.e., 1 - failure; 0 - no failure.
2. Once the failure occurrence is scheduled, the number of failures can be estimated using the derived regression functions;
3. The total number of failures over the certain tunnel distance can then be computed and incorporated into the time-to-complete-tunnel estimation analysis.

Additional analyses could be performed to investigate the nature of the time-to-repair and time-between-failures distribution. Once established these can be incorporated as follows: (the total unscheduled delay time for a such and such failure category) = (the total number of failures for this category) x (mean-time-to-repair).

The final point is that any problem associated with the rock influence on the construction process should be solved using a probabilistic approach rather than a deterministic one, for one has to account for the numerous uncertainties that nature introduces.

Statistical Methods Used For The Analysis

A.1The Linear Regression

Let us define X and Y to be the predictor and the response, respectively, with observed values (x_i, y_i) of X and Y for i=1,2,...,n. Let us also define e_i to be the statistical error for the ith case, i=1,2,...,n. The simple linear regression model specifies the following: $y_i = \beta_0 + \beta_1 \times x_1 + e_i$, i=1,2,...,n with $E(e_i)=0$, $var(e_i)=\sigma^2$, $cov(e_i,e_j)=0$. In words, the model says that the observed value y_i can be determined from the value of x_i through the specific equation, except that e_i, an unknown random quantity, is added on. The three quantities β_0, β_1, and σ^2 are unknown. The e_i's are unobservable quantities introduced into the model to account for the failure of the observed values to fall exactly on a single straight line. Only the x_i's and the y_i's are observed and these data are used to obtain estimates of the unknown parameters, namely, β_0, β_1, and σ^2. The following figure presents the quantities used to compute β_0, β_1, and σ^2:

Quantity	Definition and Alternative Forms	Description
$\bar{x}$	$\sum x_i/n$	Sample average for the x_i's
$\bar{y}$	$\sum y_i/n$	Sample average for the y_i's
SXX	$\sum (x_i-\bar{x})^2 = \sum x_i^2 - (\sum x_i)^2/n$ $= \sum x_i^2 - n(\bar{x})^2$	Corrected sum of squares for the x_i's
SD_X^2	$SXX/(n-1)$	Sample variance of the x_i's
SD_X	$\sqrt{SXX/(n-1)}$	Sample standard deviation
SYY	$\sum (y_i-\bar{y})^2 = \sum y_i^2 - (\sum y_i)^2/n$ $= \sum y_i^2 - n(\bar{y})^2$	Corrected sum of squares for the y_i's: also called the total sum of squares
SD_Y^2	$SYY/(n-1)$	Sample variance of the y_i's
SD_Y	$\sqrt{SYY/(n-1)}$	Sample standard deviation
SXY	$\sum (x_i-\bar{x})(y_i-\bar{y})$ $= \sum x_i y_i - (\sum x_i)(\sum y_i)/n$ $= \sum x_i y_i - n\bar{x}\bar{y}$	Corrected sum of cross products
s_{XY}	$SXY/(n-1)$	Sample covariance
r_{XY}	$SXY/\sqrt{(SXX)(SYY)} = s_{XY}/s_X s_Y$	Sample correlation

Figure A.1: Definition of Statistical Symbols

The criterion function for obtaining estimators is based on the fitting errors or residuals, $\hat{e}_i = y_i - \hat{y}_i$, where $\hat{y}_i = \hat{\beta}_0 + \hat{\beta}_1 \times x_i$ is the value on the fitted line at $x=x_i$. The residuals

give the vertical distances between the fitted line and the actual y-values. The least squares estimators are those values $\hat{\beta}_0$ of β_0 and $\hat{\beta}_1$ of β_1 that minimize the function $RSS(\beta_0,\beta_1) = \sum[y_i - (\beta_0 + \beta_1 \times x_i)]^2$. When evaluated at $\hat{\beta}_0$, $\hat{\beta}_1$, it is called the residual sum of squares, or just RSS. The least squares can be derived as follows: $\hat{\beta}_1 = (SXY)/(SXX)$, and $\hat{\beta}_0 = \bar{y} - \hat{\beta}_1 \times \bar{x}$.

The analysis of variance provides a convenient method of comparing the fit of two or more models to the same set of data. The sum of squares due to regression is defined by SSreg=SYY-RSS. If SSreg is large, then the simple regression model $y_i = \beta_0 + \beta_1 \times x_1 + e_i$ should be a significant improvement over the model given by $y_i = \beta_0 + e_i$. This is equivalent to saying that the additional parameter in the simple regression model β_1 is different from zero. To formalize this notion, "large" has to be defined. This is done by comparing the regression mean square (SSreg divided by its degree of freedom, which for simple regression is 1) to the residual mean square. This ratio is called F. $F = \frac{(SSY - RSS)/1}{\hat{\sigma}^2}$. Formally, we can consider testing the null hypothesis (NH) against the alternative hypothesis (AH)

NH: $y_i = \beta_0 + e_i$ i=1,2,...,n

AH: $y_i = \beta_0 + \beta_1 \times x_1 + e_i$ i=1,2,...,n

The p-value is the conditional probability of observing a value of the computed statistic (here, the value of F) as extreme or more extreme (here, as large or larger) than the observed value given that the NH is true. A small p-value provides evidence against the NH. Confidence intervals and tests of the parameter estimates can be based on the t distribution: $t = \frac{\hat{\beta}_0 - \beta^*_0}{\hat{\sigma}(1/n + \bar{x}^2/(SXX))^{1/2}}$,

NH: $\beta_0=\beta^*$, β_1;

AH: $\beta_0 != \beta^*$.

A.2 Logistic Regression

Suppose that for each individual or experimental unit, the response, Y can take only one of two possible values, denoted 0 and 1. We may write $pr(Y_i=1) = \pi_i$; $pr(Y_i=0) = 1 - \pi_i$ for the probabilities of "failure" and "success" respectively. To investigate the relationship between the response probability π and the covariate vector $(x_1,x_2,...,x_n)$ it is convenient to construct a formal model thought capable of describing the effect on π of changes in $(x_1,x_2,...,x_n)$. We suppose therefore that the dependence of π on $(x_1,x_2,...,x_n)$ occurs through the linear combination $\eta = \sum_{j=1}^{p} x_j \times \beta_j$ for unknown coefficients $\beta_1,...,\beta_n$. The logistic function links the response probability and the unknown coefficients $\beta_1,...,\beta_n$:

$$g(\pi_i) = \log\{\pi_i/(1-\pi_i)\} = \eta_i = \sum_{j=1}^{p} x_{ij} \times \beta_j ; \text{ i=1,...,n.P}$$

To estimate the parameters the likelihood function is introduced. The responses $y_1,...,y_n$ are assumed to be the observed values of independent random variables $Y_1,...,Y_n$ such that Y_i has the binomial distribution with index m_i and parameter π_i.The log likelihood may be written in the form

$$l(\beta;y) = \sum_i \sum_j y_i \times x_{ij} \times \beta_j - \sum_i m_i \times \log\left(1 + \exp \sum_j x_{ij} \times \beta_j\right).$$

The likelihood equations for the parameters β are as follows $(\partial l)/(\partial \beta) = X^T \times (Y - \mu)$ when written in matrix notation. In addition, the diagonal matrix of weights is in a form $W = diag\{m_i \times \pi_i \times (1-\pi_i)\}$. Maximum likelihood estimates satisfy the equation: $X^T \times W \times X \times \hat{\beta} = X^T \times W \times Z$, where $z_i = \hat{\eta}_i + \frac{y_i - m_i \times \hat{\pi}_i}{m_i} \times \frac{d\eta_i}{d\pi_i}$. The revised estimate is $\hat{\beta}_1 = (X^T \times W \times X)^{-1} \times X^T \times W \times Z$ (McCullagh et al, 1989).

A.3 Poisson Regression

The Poisson distribution is the nominal distribution for counted data in much the same way that the Normal distribution is the bench-mark for continuous data. Such counts are assumed to take the values 0,1,2,... without an upper limit. The maximum likelihood estimates of the parameters β in the linear predictor η can be obtained by iterative weighted least squares. In this regression the dependent variable is not y but z, a linearized form of the link function applied to y, and the weights are functions of the fitted values μ [for the Poisson Regression $\eta = \sum_{j=1}^{p} x_j \times \beta_j$, and $\mu=\exp(\eta)$]. The process is iterative because both the adjusted dependent variable z and the weight W depend on the fitted values, for which only current estimates are available. The quadratic weight is defined by $W^{-1}{}_0 = \left(\frac{d\eta}{d\mu}\right)_0^2 \times V_0$, where V_0 is the variance function evaluated at μ_0.

References

[1] Barosh, P.J., Kaye, A.C., Woodhouse, D. "Geology of the Boston Basin & Vicinity", Civil Engineering Practice, Spring 1989;

[2] Brocard, D.N., Van Wheele, B.J., Williamson, C.A. "The New Boston Outfall", Civil Engineering Practice, Spring 1994;

[3] Dilorio, F.C. "SAS Application Programming", Duxbury Press, Belmont, CA 1991;

[4] Dwass, M. "Probability Theory and Applications", W.A. Benjamin Inc., New York 1970;

[5] Freud, R.J., Wilson, W.J. "Statistical Methods", Academic Press, London 1997;

[6] Jaffe, J.A. "Mastering the SAS System", International Thomson Computer Press, Boston 1996;

[7] Knezevic, J. "Reliability, Maintainability and Supportability", McGraw Hill Co., London 1993;

[8] McGullagh, P., Nelder, J.A. "Generalized Linear Models", Chapman and Hall, New York 1983;

[9] Nelson, P. "Tunnel Boring Machine Performance in Sedimentary Rock", The Cornell University, Ph.D. Thesis 1983;

[10] Nelson, P. "Tunnel Boring Machine Project Data Bases and Construction Simulation", The University of Texas at Austin, Geotechnical Engineering Report 1994;

[11] Parsons Brinckerhoff Quade & Douglas, Inc. "Geotechnical Design Summary Report", MWRA Contract, Boston 1990;

[12] Parsons Brinckerhoff Quade & Douglas, Inc. "Geotechnical Interpretive Report", MWRA Contract, Boston 1989;

[13] SAS Institute "SAS/STAT User's Guide", Volume 2, SAS Institute Inc., Cary, NC 1990;

[14] Sinha, R.S. "Underground Structures: Design and Construction", Elsevier, Oxford 1991;

[15] Tarkoy, P.J. "A Study of Rock Properties and Tunnel Boring Machine Advance Rates in Two Mica Schist Formations", Proceedings of the 15th US Symposium on Rock Mechanics, Custer State, SD 1975;

[16] Tarkoy, P.J. "Predicting Tunnel Boring Machine Penetration Rates and Cutter Costs in Selected Rock Types", Proceedings of the 9th Canadian Rock Mechanics Symposium, Montreal 1973;

[17] Weisberg, S. "Applied Linear Regression", Wiley, New York 1985;

[18] Woodhouse, D. "Tunneling Projects in the Boston Area", Civil Engineering Practice, Spring 1989.